Review
Article

phys. stat. sol. (a) **204**, No. 7, 2129–2184 (2007) / **DOI** 10.1002/pssa.200622520

Review Article

Hydrogen blistering of silicon: Progress in fundamental understanding

Bernard Terreault*

Institut National de la Recherche Scientifique–Energie, Matériaux et Télécommunications, Université du Québec, 1650 boul. Lionel-Boulet, Varennes (Québec) J3X 1S2, Canada

Received 27 October 2006, revised 2 March 2007, accepted 2 May 2007
Published online 3 July 2007

PACS 61.72.Qq, 61.72.Tt, 61.82.Fk, 85.40.–e

When silicon is implanted with a sufficient concentration of H ions, at low to moderate temperature, and subsequently annealed at high temperature, dome-shaped gas-filled blisters and/or craters of exploded blisters appear on the surface. Under particular conditions, blistering can be produced by plasma hydrogenation as well. The phenomenon is another facet of hydrogen behaviour in silicon, a question with both fundamental and applied implications. Blistering is at the origin of the "ion-cutting" process for the fabrication of silicon-on-insulator and other heterostructures; this process is particularly useful whenever atomically sharp interfaces between layers are required. The novelty and vast potential of this process has spurred since the mid-1990's a burst of experimental activity on blistering. The purposes of those works were either to improve or extend the ion-cut process, or to clarify its underlying mechanisms. In "mechanisms", the plural is used to convey the fact that it is a multi-step phenomenon. Because of this complexity, the theoretical work, in comparison, is far less abundant. Hydrogen blistering of silicon is qualitatively understood in broad terms: H being insoluble in Si, it tends to segregate into cavities which grow and coalesce at high temperature, and the H_2 pressure in the cavities finally deforms the surface. In fact, our understanding of the microscopic mechanisms has progressed much beyond that level thanks to the sophisticated work that has been carried out using techniques such as transmission electron microscopy, Rutherford backscattering in the channelling mode, infrared spectroscopy of local vibrational modes, stress and strain measurements, and others. The effects of n- or p-doping, He ion coimplantation, and isotope substitution have also greatly helped in discriminating between different hypotheses. After a review of the most relevant experimental facts, the blistering mechanisms that have been proposed in the literature will be discussed and their conformity with the data assessed. Finally an attempt will be made to identify the key questions and suggest a few avenues for future work.

Contents

* e-mail: terreault@emt.inrs.ca, Phone: +1-450-929-8111, Fax: +1-450-929-8102

List of acronyms

AFM	Atomic force microscopy	MV	Multivacancy
CVD	Chemical vapour deposition	NRA	Nuclear reaction analysis
Cz-Si	Silicon crystal grown by the Czochralski process	PECVD	Plasma-enhanced chemical vapour deposition
ERD(A)	Elastic recoil detection (analysis)	PAS	Positron annihilation spectroscopy
FZ-Si	Silicon crystal grown by the float-zone process	RBS/C	Rutherford backscattering in the channelling mode
HRTEM	High resolution transmission electron microscopy	RSS	Raman scattering spectroscopy
		SIMS	Secondary ion mass spectrometry
IBA	Ion beam analysis	SOI	Silicon-on-insulator
IRAS	Infrared absorption spectroscopy	TEM	Transmission electron microscopy
KLMC	Kinetic lattice Monte-Carlo	TDS	Thermal desorption spectroscopy
LACBED	Large angle convergent beam electron diffraction	XRD	X-ray diffraction
		XTEM	Cross section transmission electron microscopy
LVM	Local vibrational mode		
MBE	Molecular beam epitaxy		

1 Introduction

1.1 Scope and emphasis of this review

When silicon is implanted with a sufficient concentration of H ions (several H at%), usually at room temperature but occasionally at cryogenic temperature or at a few hundred Celsius, and subsequently annealed at high temperature (e.g. at ~400–500 °C for 10 min to an hour), dome-shaped blisters as well as craters of exploded blisters appear on the surface, as first reported in 1976 by Ligeon and Guivarc'h [1]. Typical blisters and craters are shown in Fig. 1 [2]. This takes place for ion energies as low as 2 keV [3] and as high as 1 MeV [4]. Under particular conditions, blisters can be produced by plasma hydrogenation as well [5]. Blistering has also been observed on many other semiconductors: Ge [6, 7], SiC [7, 8], GaAs [7, 9, 10], InP [11], and insulators: diamond [6], Si_3N_4 [11], $SrTiO_3$ [7, 12], $LaAlO_3$ [13], $LiNbO_3$ [11]. Helium ion implantation can also induce blistering in silicon, but only at very high doses (concentrations in the tens of at%), a situation reminiscent of helium blistering of metals [14, 15]. (GaAs, in contrast, is more easily blistered using He ions [9, 16].)

Light ion blistering is indeed a very common phenomenon, and it is qualitatively understood in broad terms. H and He are hardly soluble in most materials, therefore they tend to segregate into cavities which grow and coalesce at high temperature, and the gas pressure in the cavities finally deforms the surface. If this makes sense thermodynamically, by what path, under what conditions, and how fast does it happen – if it happens at all before the gas is reemitted through the surface – varies enormously. From the evidence, it is unlikely that there exists a single, general, microscopic mechanism: this is true not only when H and He blistering are compared [16], but also when H blistering of supposedly similar semiconductors like Si and Ge are compared [7]. For fundamental as well as practical reasons, hydrogen blistering of silicon has received the bulk of the attention. Only in this case have there been enough experimental studies using sophisticated probes to make real progress in understanding the underlying, atomic scale, mechanisms. Silicon is also the subject of most of the theoretical work. Consequently, this review, whose objective is to give an overall picture of "where do we stand" and "what are the still open questions" in our understanding of blistering, must less ambitiously limit its scope to hydrogen in silicon. Understanding blistering means establishing a scenario, based on fundamental physics, for the evolution leading to it, because it involves a number of successive steps: the creation of defects by implantation or otherwise, the interaction of H with these defects during implantation, then the high temperature evolution of the H-defect complexes into presumed blister precursors such as the "(001) platelet" [17], and finally the pressure-driven crack propagation and elastic (and eventually plastic) deformation giving rise to micron sized blisters. In the author's opinion, there is as yet no totally convincing detailed scenario of blister

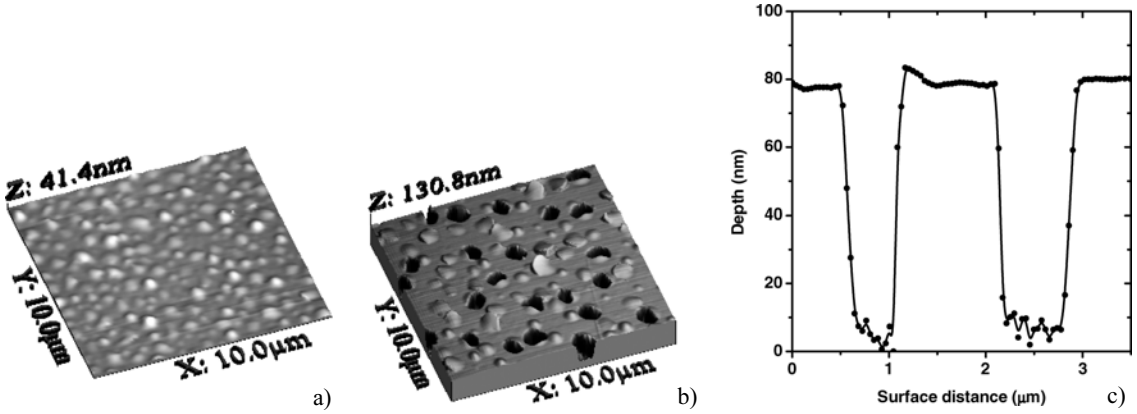

Fig. 1 Atomic force micrographs (AFM) of Si(001) surfaces showing blisters produced by 2×10^{16} H/cm^2 (a), and craters produced by 4×10^{16} H/cm^2 in 3D view (b) and in cross section (c); the crater depth of ~75 nm roughly corresponds to the mean projected range of the 5 keV ions (from Giguère et al. [2]).

nucleation. An attempt will be made to identify key questions and suggest a few avenues for future work. Once a clear and credible scenario has been established for H in Si, the analogies and differences found in other ion-material combinations will hopefully help in understanding those other cases as well.

1.2 Blistering and the question of hydrogen interactions with defects in semiconductors

The blistering phenomenon is but another facet of hydrogen behaviour in silicon, a question with both fundamental and applied implications that will not be detailed here, because it has been the subject of numerous and authoritative reviews since the mid-1980's [18–22]. Hydrogen can be incorporated at many steps in silicon device processing. Sometimes this happens adventitiously, unwillingly or unknowingly, though this rarely causes the type of damage we will talk about. Other times, hydrogen compounds are used in processing, as in surface conditioning with acids or hydroxides or as in chemical vapour deposition from a precursor like silane: here H introduction may not be the goal but it happens all the same. Finally, it can be injected deliberately by ion implantation or plasma exposure. The way by which H enters Si determines the type and extent of damage. Exposure to molecular H_2 at high temperature and pressure results in little measurable damage, although infrared spectroscopy clearly shows hydrogen presence in the lattice [23]. On the other hand, exposure to atomic hydrogen, even from a remote plasma, produces a peculiar type of defect, the {111} platelet, a nanometer size disc-shaped cavity decorated with, and stabilized by, adsorbed hydrogen, and lying in {111} planes [24–27]. Finally, if energetic H ions are implanted, an abundance of diverse defects is produced. The ion's collisions with lattice atoms produce point defects (vacancies, V, and self-interstitials, I) [28, 29]. At room temperature these are mobile in Si, and so are the H atoms that have just been implanted; the three species (V, I, H) migrate until either H reacts with a dangling bond, or V and I annihilate, or V's or I's form clusters, or they disappear at sinks including the surface. Many aspects of these processes have already been clarified as discussed in the cited reviews [18–22]. But they are still being studied in earnest, in particular in relation with blistering, but also in connection with other important questions such as defect passivation and dopant inactivation. It must be added that H atoms are very reactive not only with the dangling bonds provided by V's and I's, but also with almost any impurity (O, C, metals) and with common dopants (B, P, As, Sb).

1.3 Application of blistering: ion-cutting in microtechnology

Silicon blistering was considered a nuisance and attracted only sporadic attention for nearly two decades. Indeed, investigators of H behaviour in Si generally used subthreshold H doses and avoided the complications due to blistering. However, as we shall see, blistering-related work has contributed valuable insights into H–Si interactions. The burst of activities that has taken place since the mid-1990's springs directly from the perspectives opened by Bruel's invention of *ion-cutting* [30]. It is not our purpose to discuss in detail this technological use of blistering for silicon-on-insulator (SOI)[1] fabrication: This has been reviewed by Bruel [31] in 1998 and Celler and Cristoloveanu [32] in 2003, and more recent progress was reported at the ECS Symposium on SOI [33]. Ion cutting is in fact a generic process applicable not only to the now commercial fabrication of SOI, but also to the creation of a wide variety of heterostructures composed of semiconductor and/or insulator layers [11]. It is particularly useful whenever atomically sharp and defect-free interfaces between layers are required. Briefly, in its original form [30], the process works as follows: (1) A "donor" Si wafer "*A*" is given a thin thermal oxide or else its surface is cleaned and made hydrophilic; (2) wafer *A* is implanted with a dose of several 10^{16} H/cm^2 at a typical energy of tens of keV; (3) a "handle" wafer "*B*" with a thick, high quality, thermal, CVD or PECVD oxide is bonded hydrophilically to wafer *A* (this involves a mild anneal to strengthen the bond and improve the interface quality [34]); (4) the bonded pair is annealed up to the blistering temperature; the presence of wafer *B* on top of wafer *A* prevents the *A* surface from deforming and, instead, the gas pres-

[1] A list of acronyms is given at the beginning of the paper.

sure drives lateral crack propagation parallel to the surface over the whole wafer area; a thin layer of Si from *A* (typically hundreds of nm) thus remains attached to *B*: A SOI structure results. The transferred layer can be further thinned and smoothed by standard means.

2 Phenomenology of H blistering of Si

At the outset it is important to note that a multitude of parameters can possibly influence blistering. Therefore, if not specified otherwise, the results presented from hereon pertain to room temperature (RT) implantation of the most standard material, low-doped or undoped Cz-grown Si(001) crystals with resistivity of 1 Ω cm or more. Note that amorphous Si does not blister, although both H_2 [35, 36] and platelet-like configurations [37] have been detected in a-Si; presumably its structure accommodates isolated H_2 or small bubbles or platelets which do not coalesce.

2.1 Dose window giving rise to blistering

Blistering is a threshold phenomenon and the minimum ion fluence or H concentration giving rise to blisters would seem to be one of the most fundamental quantities for any microscopic theory. Nevertheless, the threshold dose has not been the object of much precise and systematic work (presumably because it is tedious work and the prospect of a really accurate theory appears remote). One would also have to define precisely the threshold (scattered blisters or near complete surface coverage?). Most of the literature concerns work done with ion energies in the tens of keV and doses above 4×10^{16} H/cm^2, and the threshold is around that value at those energies. Explicit results [3, 38–42] are shown in Fig. 2 (lower border of shaded area). Since the fundamental parameter is presumably the H concentration, the ion fluence was converted into the H concentration at its peak, using numerical simulations performed with the code SRIM [43]. It is seen that the threshold is approximately 5 at%. Less well known is the existence of a maximum dose. At low energy (≤10 keV) there is definitely an upper limit [3], as shown in Fig. 3 for 5 keV: there are no more blisters or craters for 6×10^{16} and 1×10^{17} H/cm^2 (compare with 2×10^{16} and 4×10^{16} H/cm^2 in Fig. 1). The width of the blistering window increases with the energy. At a higher energy of 40 keV, Liu et al. [38] also found a maximum blistering dose, their cut-off being somewhere between 8×10^{16} and 1.6×10^{17} H/cm^2, probably nearer to the upper end of this range, since several authors [39–41] found blisters for 1×10^{17} H/cm^2 at comparable energies. The available information on the maximum blistering doses are summarized in Fig. 2.

Two other features appear in the AFM pictures of Fig. 3, obtained by 5 keV H implantation into a trench defined lithographically in a polymethylmetacrylate mask. At high dose (≥6×10^{16} H/cm^2), the implanted region swells uniformly, even at room temperature, instead of blistering. The line scans of

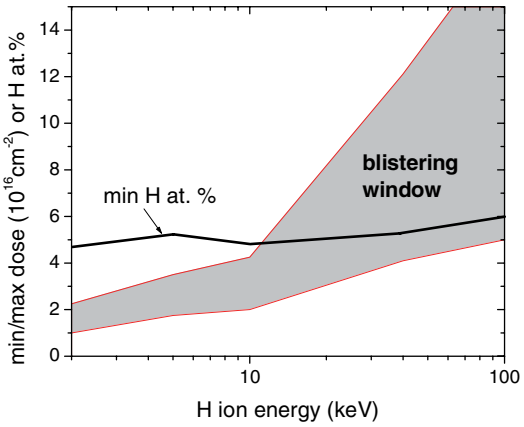

Fig. 2 (online colour at: www.pss-a.com) Threshold and maximum H doses or concentrations for blistering of implanted and annealed lightly doped Si(001). Shaded area: blistering window; solid line: threshold H atom concentration. Data from Moutanabbir et al. [3], Liu et al. [38], Huang et al. [39], Höchbauer et al. [40], Aspar et al. [41] and Bedell & Lanford [42].

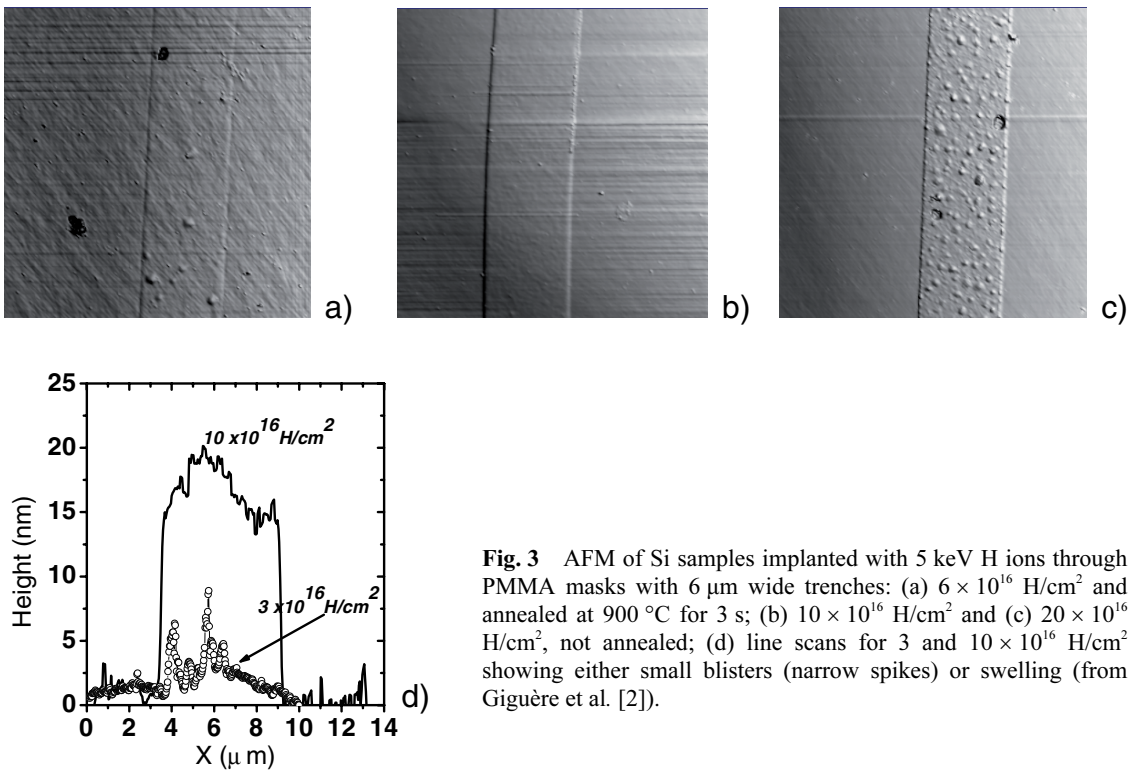

Fig. 3 AFM of Si samples implanted with 5 keV H ions through PMMA masks with 6 μm wide trenches: (a) 6×10^{16} H/cm^2 and annealed at 900 °C for 3 s; (b) 10×10^{16} H/cm^2 and (c) 20×10^{16} H/cm^2, not annealed; (d) line scans for 3 and 10×10^{16} H/cm^2 showing either small blisters (narrow spikes) or swelling (from Giguère et al. [2]).

Fig. 3(d) illustrate the contrast between the low dose (3×10^{16} H/cm^2, blistering) and high dose (1×10^{17} H/cm^2, swelling). This is consistent with the explanation offered in Ref. [44] for the high dose blister absence: At high dose, the cavity-rich region becomes thick, i.e. not small compared to the ion range, and the stress is rather uniform over this whole thickness. Moreover, the compressive stress generated in its neighbourhood by a gas-filled cavity will tend to close up other nearby cavities: the result is a decrease in the average compressive stress [40]. So, a modest expansion of the numerous small cavities, resulting in swelling, can relieve the stresses. The other interesting point is that blisters reappear at very high dose (2×10^{17} H/cm^2, Fig. 3(c)), but this time at RT during implantation.

2.2 Blister morphology and dimensions; fracture mechanics

When they first appear, hydrogen-induced blisters are roughly circular and shaped like a dome (Fig. 1(a)), as if produced by elastic deformation of a pressurized thin plate. The absence of dislocations in cross section transmission electron microscopy (XTEM) observations tends to indicate that plastic deformation is not involved [45]. Other simple observations are the following: (i) Although the packing is dense, the blisters do not appear to form a pattern on the surface. This suggests random nucleation of blisters and absence of long-range interactions between them. (ii) The diameter (D) and height (h) distributions are narrow with, e.g., standard deviations of ~15% and ~30% respectively [46]. These facts suggest again that the blisters are nucleated at randomly located weak spots, from which point they extend in a circle whose radius is determined by the depth at which they are located, and imply a one-to-one relationship between depth and radius, in agreement with the mechanics of plate deformation. Perhaps related is the fact that when H is implanted in trenches that are narrower than the normal blister size, the blisters remain circular, though they are quite smaller, instead of conforming to the straight walls of the trenches [2]. Note that the aspect ratio h/D is small (few percent) so that h is practically

unmeasurable on plan view optical or scanning electron micrographs; even with atomic force microscopy, it is difficult to be precise because of the uncertainty on the reference level or true location of the undeformed surface. Under the assumption of a spherical shell, the elastic strain is $\varepsilon = (8/3)\,(h/D)^2 \sim 10^{-3}$: This value confirms that the yield stress should not have been reached.

There are relatively few quantitative data even for the diameters, or estimates of the gas pressure ($P \sim 1$ GPa [4]), contrary to He blisters on metals [14, 15]. Figure 4 shows the available measurements [1, 2, 4, 39, 44, 46] for the average D as a function of the mean H implantation depth R. One must mention that the depth in the data of Huang [39] does not always correspond to the implantation energy: the measurements at the depths of 80 and 300 nm were obtained by implanting at higher energy (19 and 45 keV/atom) through a 150 nm oxide that was removed after implantation; their dose was high (1×10^{17} H/cm^2), corresponding to peak H concentrations in the 15–20 at% range. The trend, as expected, is that the blister diameter increases with the implant depth. One can see that a power law fit ($D \sim R^n$) to the data of Huang gives a rather slow increase, i.e. $n \sim 0.35$ (dashed line). It must be said that the diameters are commonly observed to vary with ion dose and anneal temperature (see, e.g. the three points for $R = 75$ nm). If we use the other data obtained at more typical doses (dot-dash line), we get $n \sim 0.5$.

Some authors have attempted to use the D vs. R relation to infer blistering mechanisms or material properties. If the blister is viewed as a spherical shell formed by plastic deformation, one can obtain the following equation [47, 48]:

$$D = (16hR\sigma_Y/P)^{1/2}\,, \tag{1}$$

where σ_Y is the material's yield stress. Although this formula was derived in the context of He blistering of metals it is very general. But h and P must be derived from other arguments. If the ratio h/P were constant one would indeed find $D \sim R^{1/2}$. However, h certainly increases with R, while it is not clear for P, which may result in a higher power n. Referring specifically to H blistering of Si, Huang [39] considered blistering as resulting from cavity enlargement due to crack propagation instead; in this case the relevant material parameters are the surface energy γ, Young's modulus E and Poisson's ratio v; the relation

$$D = 4(\gamma E R^3/9\alpha(1 - v^2)\,P^2)^{1/4} \tag{2}$$

is found, with α a geometrical constant of order 1; thus $n = 3/4$ if P is assumed constant. Since the experimental value of n is substantially smaller than 0.75, it suggests that the required pressure is increas-

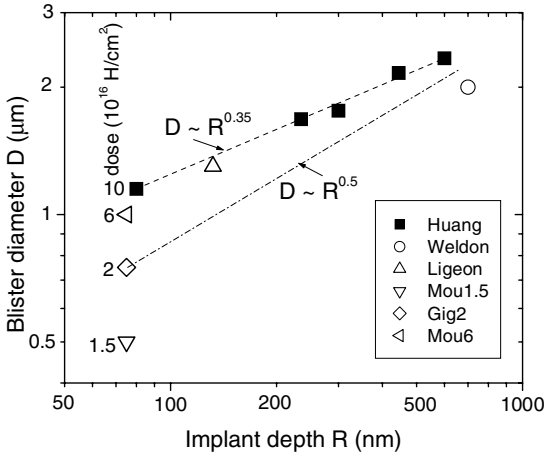

Fig. 4 Log–log plot of mean blister diameter D as a function of implant depth R. The data are from Huang et al. [39], Weldon et al. [4], Ligeon & Guivarc'h [1], Moutanabbir et al. [44, 46], and Giguère et al. [2]. The depths R are those given by Huang, or else those calculated by SRIM-2003. The different doses used in the measurements at 75–80 nm are also indicated.

ing with the thickness of the layer to be deformed. Although the *D* vs. *R* data may look closer to the plastic model, other evidence favours the elastic model, as mentioned earlier. This point is important since it implies no loss of H_2 by blister rupture at this stage. One should add a caveat: It is known that blisters pop up suddenly (within 2 s [39] and probably less) and at that stage they have a narrow size distribution, but if heating is continued they grow further [e.g. 41]. Since the literature generally does not state precisely at what stage the data were acquired, the published diameters may actually represent overestimates. In addition, at higher doses, not only the yield stress but the ultimate strength of the silicon can be overcome and craters appear (Fig. 1(b), (c)).

Since there is no reason to doubt the validity of fracture and deformation mechanics, the real challenge for theory will be to predict the amount of gas that segregates into the cavities and the ensuing pressure. In this connection, Henttinen et al. [49] found a way to partly decouple the pressure and mechanical strength effects: Two wafers, one of them H-implanted, were bonded as in SOI fabrication but, instead of annealing them at high temperature, a sharp blade was inserted edgewise at the interface after a mild, subthreshold, anneal. If the implanted zone is weaker than the wafer-to-wafer bond, then delamination will occur at the implanted depth. From plate mechanics, the separation energy can thus be determined in a situation in which the gas pressure, though probably present, is not the trigger of the delamination. They found the following. (i) The measured strength decreases precipitously with temperature in the 270–300 °C range, reflecting the microscopic transformations that are taking place. (ii) The strength depends strongly on crystal orientation, e.g. 0.7, 1.5 and 2.3 J/m^2 for (001), (111) and (110), respectively, at 290 °C (these correspond to 0.65, 1.2 and 1.5 eV/atom on the (001), (111) and (110) surfaces respectively). (iii) Heavy boron doping reduces the strength.

The blister cover thickness (or equivalently the crater depth) is very close to the peak in H concentration or the peak in radiation damage; since these quantities differ by less than 10% [43], only very precise work using ion-beam analysis (IBA) and/or secondary ion mass spectrometry (SIMS) and cross section transmission electron microscopy (XTEM) allows a distinction between the two. This point will be discussed in Section 3.7. Whatever the case, the H localization near its mean range indicates trapping in irradiation-induced defects.

2.3 Thermodynamics

2.3.1 Activation energies

The effective activation energy for blistering certainly reflects its underlying mechanism. This energy is usually obtained by isothermally annealing a number of identical samples at different temperatures until they blister, as observed visually under a microscope or through a drop in the specular reflectivity. Then

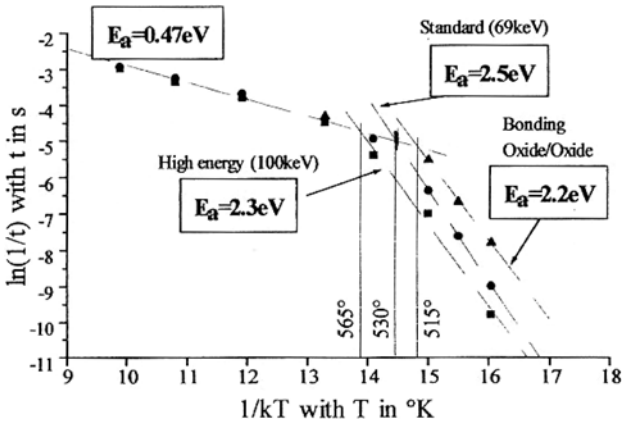

Fig. 5 Arrhenius plot of the inverse blistering time vs. inverse absolute anneal temperature (from Aspar et al. [41], by permission).

the slope of the Arrhenius plot of the blistering time vs. the inverse temperature provides an activation energy, E_a. Early on, the Grenoble group [31] found that there is no single slope: the data showed a high value of E_a (~2 eV) at temperatures $T < 500$ °C, then a break and a low value (~0.5 eV) at high temperature (Fig. 5 [41]). They interpreted this as meaning that the limiting step at lower temperature was the breaking of Si–H bonds to liberate H atoms and form H_2 to fill the nascent blisters, whereas, at higher temperature, the diffusion rate of H atoms from the surrounding region into the cavities was the only limitation. Alternatively, Tong et al. [50] interpreted the high E_a as the energy necessary to break Si–Si bonds and induce crack propagation. In both models, the orders of magnitude of the bond energies are right. However, these simple pictures became foggy with the finding that the "high E_a" decreased monotonically with the implanted dose [41, 42]. Figure 6 summarizes the data [4, 41, 42, 50, 51]. In addition, the decrease is confirmed very precisely by the deuterium data of Bedell and Lanford [42] (that could not be shown on the same graph because of an unknown conversion factor). In the framework of the Si–Si bond breaking model, if that energy is identified with the surface energy in Eq. (2), the weakening of E_a could be explained by the increased presence of adsorbed H atoms on the platelet internal surfaces. On the other hand, within the Si–H bond breaking scenario it was proposed instead that the average bond energy decreased with dose because the deepest traps are filled first [41].

Relatively little work has been done with wafers of orientation other than (001) but there is clear evidence that Si(110) crystals do not blister as easily as Si(001) and Si(111), requiring higher doses, temperatures or anneal times. Zheng et al. [52] found the same activation energies (high E_a of 1.7 eV and low E_a of 0.7 eV) for all three orientations, but the kinetic prefactor was almost an order of magnitude larger for (001) than for (111), and similarly for (111) compared to (110). This was tentatively explained in terms of the density of Si–Si bonds to break. Note that this is the same ranking as found above in Section 2.2 for the ease of purely mechanical splitting of implanted Si. However, the link between these two measurements is not straightforward since the effect in thermally induced blistering involves only the kinetics whereas the effect in mechanical splitting apparently involves the energetics. Recently Bourdelle et al. [51] found the same ranking but also a significant difference in the E_a values ($T < 480$ °C): 1.45 eV for the (001) orientation and 1.9 eV for the two other ones.

2.3.2 H_2 thermal desorption

Gas release is also a probe of the thermal evolution of H-implanted Si. Weldon et al. [4] reported a burst of H_2 "coinciding with blistering" and amounting to ~1/3 of the implanted H. It was implied that this amount represented the contents of the blisters, although it is not evident that the gas in the blisters should have escaped, even in part, since that implies blister rupture. Figure 7 shows the H_2 desorption rates as a function of temperature during ramp annealing (0.33 K/s), for two samples implanted at 5 keV

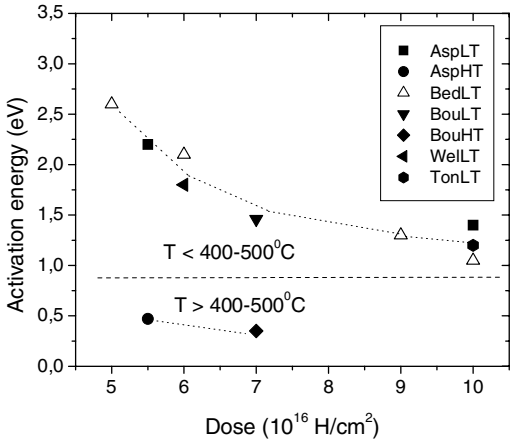

Fig. 6 Activation energies for blistering of lightly doped Si(001). The data from Aspar et al. [41], Bedell and Lanford [42], Bourdelle et al. [51], Weldon et al. [4] and Tong et al. [50] form two distinct groups (LT and HT) depending on whether the temperature is below or above 400–500 °C.

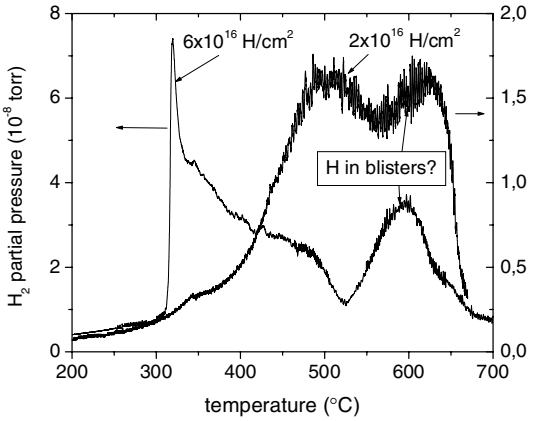

Fig. 7 H_2 release rate measured by TDS for 2×10^{16} H/cm^2 and 6×10^{16} H/cm^2 at 5 keV (from Moutanabbir et al. [44]).

with 2 and 6×10^{16} H/cm^2, respectively [44]. Cerofolini et al. [53] also reported a non vanishing desorption at 200 °C and a strong rise in the desorption rate around 400 °C. The lower dose sample of Fig. 7 blistered at ~475 °C, so indeed an important release of gas took place while the blisters appeared and grew. These blisters did not seem to be ruptured (similar to Fig. 1(a)), although the AFM may not be able to detect very small (~nm) cracks. In any case, it is impossible to say if the gas comes from the blisters or happens to be released from the lattice at about the same time as the blisters appear. Finally, the remaining H_2 is desorbed around 600 °C; this suggests that the "600 °C peak" (~30% of total) is partly or totally made up of the blister contents. Note, however, that there is also some H_2 released at lower temperature, especially at the higher dose. (That large burst of gas at ~325 °C is possibly related to the small implant depth in that experiment: a gas permeable layer extending almost to the surface may be created at high dose. Such an effect was observed in He implantation of metals [15]). There are admittedly many uncertainties in the interpretation of desorption spectra but it remains true that: (i) desorption peaks coincide in temperature with other events measured by other techniques; and (ii) the blister gas contents appears to be no greater than 1/3 of the implanted dose, i.e. the equivalent of $\leq 5 \times 10^{15}$ H/cm^2 only at low keV energies or less than 4 monolayers of SiH_2 on {100}. Under the standard conditions mentioned so far, the greater part of the implanted hydrogen is thus "wasted". This fact suggests that different and possibly more effective ways of using hydrogen may be found: this is the approach dubbed here *hydrogen engineering* and which will be discussed in Section 4.

2.4 Are there significant differences between blistering and ion-cutting?

Ion-cutting requires crack propagation over an area (~10^2 cm^2) approximately 10^{10} times larger than blistering (~10^{-8} cm^2), it is thus not surprising that it requires longer times than simple blistering [41, 50]. The comparison can hardly be precise since, during isothermal annealing, scattered blisters first appear, followed by blister growth [11], so there is some arbitrariness in defining a "blistering time". Tong et al. [50] found a typical factor of 10 in splitting times, a small price to pay for a factor of 10^{10} in area. This demonstrates that blistering and wafer splitting take place in "catastrophic" fashion (it generates an audible sound [41]). More importantly, Tong et al. showed that the activation energies for both phenomena are identical (E_a of 1.2 eV for a dose of 1×10^{17} cm^{-2}, data included in Fig. 6). This gives confidence that the physics and chemistry of the two phenomena are the same, except perhaps for the very final purely mechanical step. This has led many to assume that basic studies on blistering of unbonded wafers can be used to quickly explore process improvements or new materials for ion-cutting. This is generally confirmed by comparative studies. At least one counter-example has been found, however. It concerns the maximum blistering dose. Ion-cutting has the same threshold dose of ~1.75×10^{16} H/cm^2 as blistering at 5 keV, but it has no upper limit [54]. This is of course fortunate for technology, and may help in understanding why there is an upper limit in blistering. With a bonded wa-

fer on top, there is no alternative, except splitting, to relieve the stresses. This shows the importance for blistering of the boundary conditions imposed on the stress and strain fields. In this particular case, blistering experiments have led to overly pessimistic prospects on ion-cutting, especially because higher doses give smoother surfaces at those low energies [54].

3 Mechanistic investigations using microscopic probes

3.1 Transmission electron microscopy of extended defects; platelets

It is natural to look for extended structures buried under the surface as the nuclei of blisters. Romani and Evans [17] and many others afterward [4, 11, 40, 41, 51, 55–59] indeed found in H-implanted Si planar structures with (001) or {111} habit planes using TEM, both in plan view and in cross section. Actually, the {111} variety had been found earlier in plasma hydrogenated Si [24], and it is the thermodynamically favoured structure [60, 61]. The (001) platelet, on the other hand, is dominant in implanted Si(001) [40, 51, 56, 58].

3.1.1 As-implanted material

A high resolution (HR) XTEM micrograph of a platelet is shown in Fig. 8 [57]. As implied by its notation – (001), not {100} – it is located in a plane parallel to the surface. This is of course no coincidence, the compressive stress obviously favours separation of (001) planes and overcomes the normally lower free energy of {111} platelets. In Fig. 8 the flatness and smoothness of the parted planes is to be noted. Similarly, the surrounding lattice is remarkably undisturbed. This is confirmed by the weakness of the strain contrast in TEM [17, 56]. The typical (001) platelet diameters are ~10 nm (at RT) and their thickness ~1 nm, with a volume of $\sim 10^3\ \Omega$ (atomic volumes). The less numerous and smaller {111} platelets tend to be located deeper into the crystal, beyond the peaks in hydrogen and damage, in a region of lower stress [56, 58]. In addition, some unlikely "vertical" {100} platelets, this time accompanied by strain contrast, have been observed [59]. In Si(111), (111) platelets unsurprisingly dominate [51]. The case of Si(110), which is the least prone to blistering, is interesting: a mixture of {111} and {100} platelets, which cannot be parallel to the surface, is found [51]. These observations all confirm the role of the compressive stress in their nucleation. Moreover, the platelet-forming tendency naturally explains the differences in mechanical strength found for the different orientations (Section 2.2), since platelets obviously weaken the crystal, and also explain the differences in splitting kinetics (Section 2.3.1).

Many investigators have noted the close connection between the (001) platelets and hydrogen. First, the underfocus/overfocus contrast indicates a low electron-optical density, consistent with H decoration

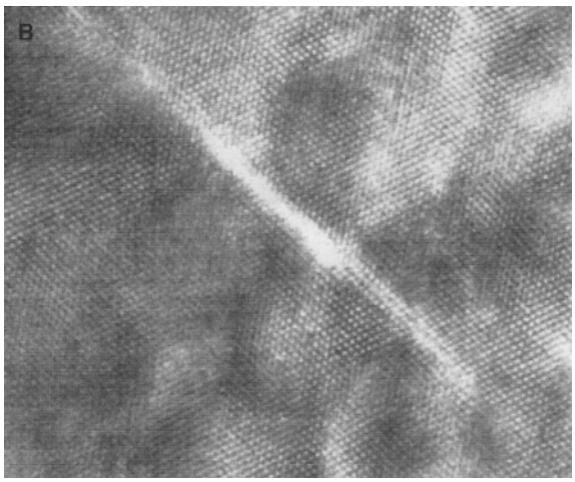

Fig. 8 HRXTEM of (001) platelet; the ⟨001⟩ direction points "North-East" (from Bruel [57], by permission).

of the platelets [53, 56, 58]. Second, their depth distribution is rather similar to the H distribution and even tends to be narrower [40, 55, 56]. The internal surfaces of the (001) platelet, just like free (001) surfaces, are expected to adsorb H exothermally (~2 eV/atom). Unfortunately, they have not received so far as much theoretical attention as the {111} platelets [60].

3.1.2 Thermal evolution of platelets

Under annealing, platelets grow while their number decreases [41, 55, 56, 62]. The free energy of a platelet of radius R and thickness t may be written:

$$G = \pi R^2 t(n\,\Delta G_C + pV) + 2\pi R^2\gamma + 2\pi R(t\gamma + T_d \ln(D/b)) \,. \quad (3)$$

In this equation, the first term is the chemical potential for H in a platelet (with respect to H in solution, $\Delta G_C < 0$); the second is the pressure term if gaseous H_2 is present; the third and fourth terms are the surface energies of the faces and the perimeter; and the fifth term is the strain energy, modeled as a dislocation loop [28], T_d being the line tension, b the Burger's vector and D the extent of the elastic disturbance. Aspar et al. [56] found that the {111} platelets actually do not grow under annealing; only the (001) kind, which are the most numerous and the most centrally located, do so. Figure 9 shows the results of isothermal annealing at 450 °C on those [62]. The total cavity volume displayed here is a quantity equivalent to the total defect area because the platelet thickness is constant. We see that the total volume is constant. This type of growth is called Ostwald ripening and implies random exchange of atoms between the platelets. If we consider the free energy of the ensemble of all the platelets, we see from Eq. (3) that the third term $2\pi R^2\gamma$ is constant but the last two decrease during growth; thus, even without net H influx into the platelet system, the total energy decreases. (And if there is an H influx, the chemical energy gain is of course much larger than the pressure term.) During growth the platelet depth distribution was also observed to become narrower. If one assumes for simplicity that each platelet internal surface is dihydride-passivated (normal RT configuration since the {100} surface has two dangling bonds), and with a surface density of 6.8×10^{14} Si/cm^2, the data of Fig. 9(b) actually correspond to a total of 5×10^{15} H/cm^2. We see that we are close to the minimum cavity H contents necessary for blistering, as estimated from thermal desorption in Section 2.3.2. An interesting question is what is the nature of the atoms being exchanged between the platelets during the Ostwald-type phase of the growth (prior to the final crack propagation phase). Of course cavity growth implies exchange of Si atoms or Si vacancies between the platelets. However, the high temperature at which it occurs suggests that its kinetics are limited by another factor, e.g. H atom transport. This is understandable because chemisorbed H is necessary to stabilize the platelets and probably also to weaken Si–Si bonds and lead to platelet enlargement

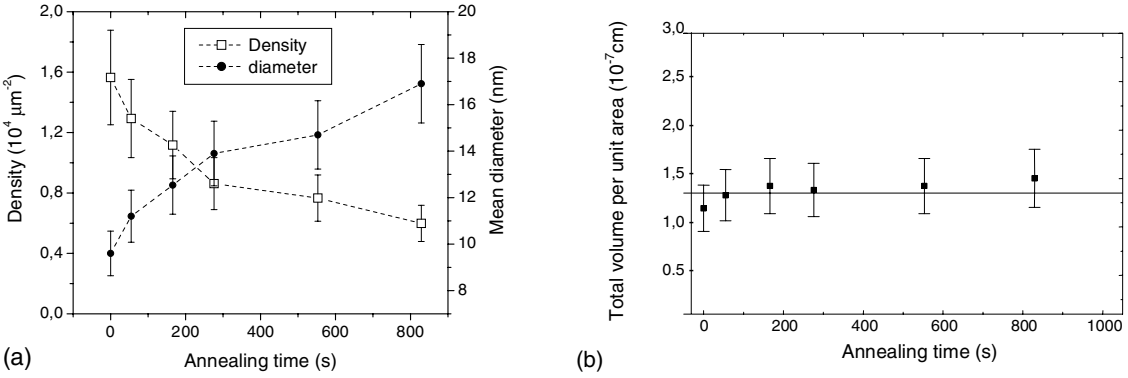

Fig. 9 Thermal evolution of (001) platelets in H-implanted Si (70 keV, 6×10^{16} H/cm^2) under isothermal annealing at 450 °C: mean diameter and density (a) and total volume (b) (from Grisolia et al. [62], by permission).

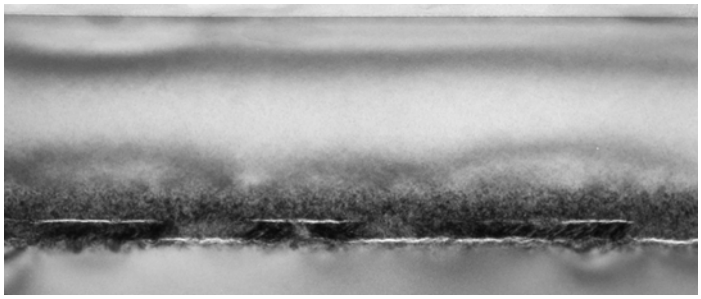

Fig. 10 XTEM view of microcracks in Si implanted with 7×10^{16} H/cm^2 at 40 keV and annealed at 600 °C for 30 min. In this particular case microcracks appear at two different characteristic depths (from Höchbauer et al. [40], by permission).

[45]. In turn, H transport is limited by retrapping. Actually, the nucleation phase is not always complete at RT: For a dose of 3.5×10^{16} H/cm^2, an increase in the number of platelets, then followed by Ostwald ripening, was observed in the first few minutes of the anneal [56], whereas for 6×10^{16} H/cm^2 the nucleation was apparently complete at RT [62]. Facets with {100} and {111} orientations have been seen on some [58].

At high dose under prolonged annealing, continuous microcracks parallel to the surface appear [4, 11, 40, 56, 58, 63]. In some cases, the microcrack follows an apparently continuous but zigzag path [58, 63]; in one instance, the large (001) platelets were reported to be connected by smaller {111} platelets [4], but this seems surprising in view of the physical separation between the zones occupied by each type. An example of microcracks is shown in Fig. 10 [40]: a typical microcrack diameter is a fraction of a micron, that is an order of magnitude larger than a platelet (Fig. 9) and an order of magnitude smaller than a blister (Fig. 4). It is then natural to consider that microcracking constitutes an intermediate step before blistering. One question is when does the transition from Ostwald-type ripening to explosive growth take place. Another is whether the growth is fueled by absorption of gas from the lattice, leading to a reduction in free energy (ΔG_C term in Eq. (3)), and if so, at what stage(s). It is also to be mentioned at this point that there are dissenting voices [53, 64]: basically these authors attribute the precursor role to smaller H_2-filled cavities. These will be discussed again later.

3.2 H depth profile evolution

Hydrogen depth profiles have been measured after implantation and after annealing by secondary ion mass spectrometry (SIMS) [65, 66], ^{1}H(^{11}B,α)^{8}Be [1] and ^{1}H(^{15}N,αγ)^{12}C [42] nuclear reaction analysis (NRA), and elastic recoil detection (ERD) [65–68]. Such measurements also give the total H contents [4], which can be correlated with the thermal desorption results (Section 2.3.2). A key feature of the H evolution was already observed in 1976 [1], namely a narrowing of the depth distribution under annealing, with the loss occurring mostly on the shallow side. This has been confirmed by others [42, 66, 68] and it is well illustrated by the NRA profiles of Bedell and Lanford [42] for 5×10^{16} H/cm^2 at 100 keV, shown in Fig. 11. At 400 °C, the profile is narrower and more peaked than at lower temperatures, and at 500 °C, the sample, which is now blistered, has lost an appreciable fraction of its H. Similarly, Weldon et al. [4] found no decrease in total H contents below 400 °C, for both 2×10^{16} H/cm^2 and 6×10^{16} H/cm^2 at 75 keV. For a subthreshold dose of 2×10^{16} H/cm^2 (at 42 keV), high precision measurements combining SIMS and ERD show no enhanced peaking at 350 °C; the small H loss occurs mostly on the surface side [66]. Those results are qualitatively consistent with the release of H_2 shown in Fig. 7 (2×10^{16} H/cm^2), but a quantitative comparison cannot be made due to the disparity in implantation energies (hence proximity to the surface).

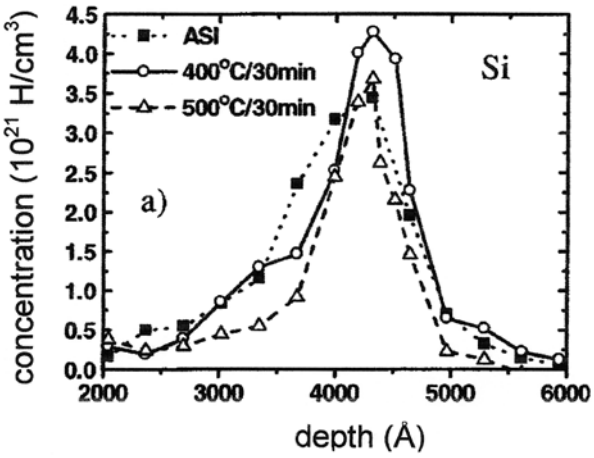

Fig. 11 H depth profiles (100 keV, 5×10^{16} H/cm^2), obtained using NRA, as implanted (ASI) and after 30 min anneals at 400 and 500 °C; note that a 5000 Å sacrificial oxide was removed before measurement (from Bedell & Lanford [42], by permission).

3.3 Defect creation and evolution probed by ion channelling

Rutherford backscattering in the channeling mode (RBS/C) is a powerful technique to detect disorder in a lattice and measure its depth profile. It may be useful to recall that the enhancement in backscattering yield includes two components. First, in the heavily damaged region, atoms displaced from their lattice positions (self-interstitials or interstitial impurities) can directly scatter the channelled ions at backward angles. Second, ions may simply be deflected slightly out of the channel, so that their probability of being backscattered later, deeper inside, becomes that of an ion in a "random" trajectory; this is called dechannelling and is visible as a deep tail in the backscattering yield. The backscattering yield can be converted into an equivalent "density of displaced atoms". However, that density should not be interpreted too literally as if all due to displaced atoms embedded in an ideal lattice, because the relaxation of the lattice around any kind of defect also gives rise to enhanced scattering [69].

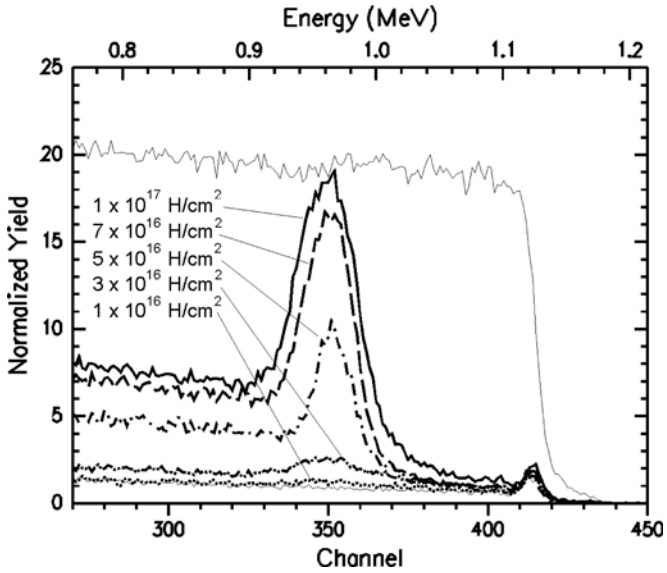

Fig. 12 Backscattering spectra for 2 MeV ^{4}He particles channelled in the ⟨001⟩ direction in Si(001) implanted with $1-10 \times 10^{16}$ H/cm^2 at 40 keV. The ordinate is the backscattering yield normalized to the same number of incident ions; the top abscissa is the energy of the backscattered α's (1.125 MeV corresponds to the surface). The thin solid line is the random yield (from Höchbauer et al. [40], by permission).

3.3.1 Dose dependence

Both components of backscattering can be seen in the ^{4}He backscattering spectra of Fig. 12 [40], i.e. displacement damage in the 0.9–1.0 MeV energy range, and dechannelling below 0.9 MeV. Several authors [40, 42, 44, 65] have studied the dose dependence of the damage by RBS/C with similar results. The peak value of the yield increases non-linearly with dose: at subthreshold doses ($\leq 3 \times 10^{16}$ H/cm^2) the level is very low; around the blistering threshold ($\sim 5 \times 10^{16}$ H/cm^2) it increases super linearly (although it is not blistered at RT); and at the highest doses ($\geq 7 \times 10^{16}$ H/cm^2) it saturates. This indicates that the H atoms and the point defects generated by ion implantation are reacting non linearly to create the complexes that are detected as atomic displacements. It has been known for a long time [18] that H and defects interact synergistically in Si and stabilize defects that would otherwise simply anneal out during RT implantations. (This becomes obvious when H and He implantations are compared: paradoxically, H ions result in much higher damage levels than He [53, 61, 70].) In Fig. 12, the displacement density actually reaches the "random" level for 1×10^{17} H/cm^2, although TEM shows that the crystal is in no way amorphized. This illustrates the fact that naïve interpretation of RBS/C spectra overestimates the real level of disorder [69].

3.3.2 Dependence on temperature: reverse annealing

Pioneering work [1] showed the effect of high temperature annealing after low temperature implantation, i.e. a dramatic increase in both backscattering and dechannelling called *reverse annealing*. This effect was rediscovered in the 1990's [42, 55]. This is shown in Fig. 13 for the displacement field and it is equally true for dechannelling. The reverse annealing is occurring in the same temperature range as the platelet growth. This unusual temperature dependence makes it unlikely that the backscattering is due, in

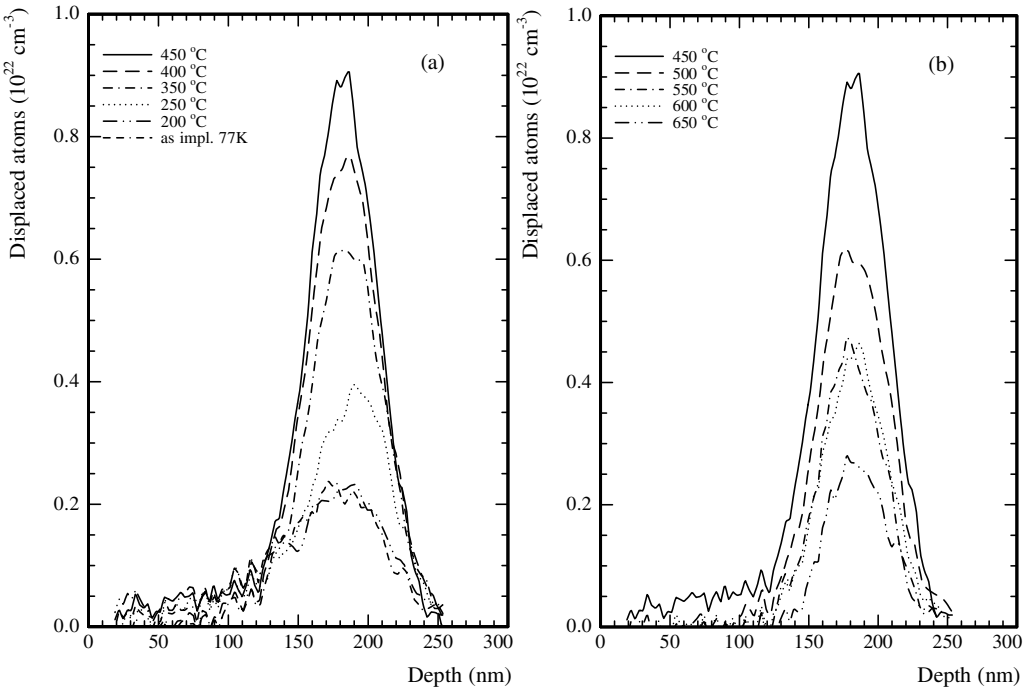

Fig. 13 Evolution of the displacement field in implanted Si (1.6×10^{16} H/cm^2, 15.5 keV) under annealing for 2 h at 200 to 450 °C (a) and 450 to 650 °C (b) (from Cerofolini et al. [55], by permission).

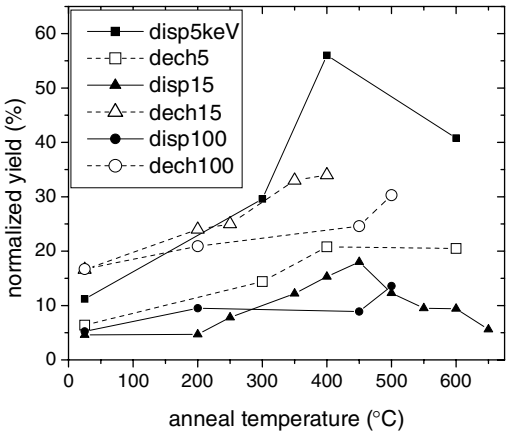

Fig. 14 Peak atomic displacement densities and dechannelling yields as a function of the annealing temperature. Full symbols and solid lines refer to displacements, open symbols and dashed lines to dechannelling; the data are also labelled by the H ion implantation energy. The yields are normalized to the random yield (5 and 100 keV) or the Si atom density (15.5 keV). Data from Moutanabbir et al. [71] (5 keV, 2×10^{16} cm^{-2}, ramp anneal at 0.33 K/s), Cerofolini et al. [53, 55] (15.5 keV, 1.6×10^{16} cm^{-2}, 2 h anneals) and Bedell & Lanford [42] (100 keV, 2×10^{16} cm^{-2}, 30 min anneals).

"classic" fashion, to interstitials. Rather, it suggests that it is caused by a lattice deformation. In Fig. 14 is shown a compilation of available measurements on this subject [42, 53, 55, 71]. The maximum in displacements occurs at 400 °C to 500 °C; note that the annealing times were different in the different experiments, so exact agreement is not expected. The 5 keV data set corresponded to a blistering dose, the other two to subthreshold doses. This last fact results in great differences in the absolute levels of displacement damage that are explained by the highly non-linear dependence on dose (Fig. 12).

Looking closely at Fig. 13, one notices that the peak shifts in depth at 250 °C and then back towards the surface at higher temperature; the same two shifts occur, and more markedly, in Ref. [71]. In Refs. [42] and [67], only the shift in depth at intermediate temperature is observed. The shift in depth is suggestive of a movement from the peak in damage energy deposition to the peak in H concentration, indicating a change in the nature of the defect responsible for backscattering [71]. The identification of this or these defect(s) will be discussed again in Section 3.7. The opposite shift towards the surface at the highest temperatures was seen in the most evident fashion by Tonini et al. [72] in the case of coimplantation of He and H. This is visible in Fig. 15. Starting at 400 °C, when the first blisters appear, the yield in channels 290 to 340 increases significantly; at 500 °C and above the increase is dramatic and the yield in these channels is flat and of the order of 50% of the random yield, which is just equal to the fraction of

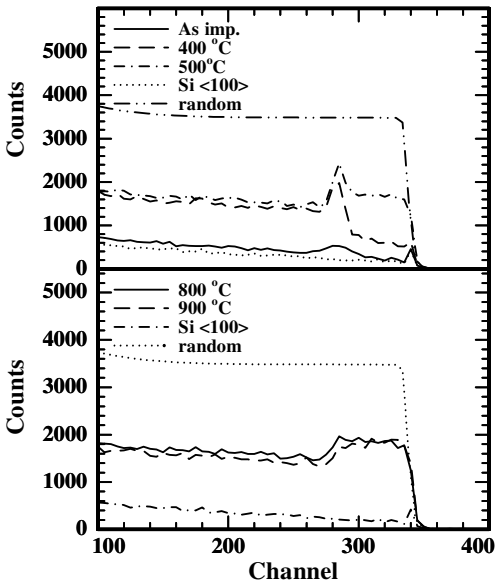

Fig. 15 RBS/C spectra in samples coimplanted with He and H (1×10^{16} cm^{-2} each). The peak around channel 285 corresponds to the implant depth, the high but flat yield seen in channels 290–340, at 500 °C and above, is due to a lattice deformation of the surface layer (from Tonini et al. [72], by permission).

the surface that is covered by blisters. Indeed, those ^{4}He ions that happen to impinge on blister domes are not aligned with the ⟨001⟩ axis and they are never channelled. The near surface enhancement in RBS/C is thus connected with blistering and can even constitute a measure of its extent.

3.4 H-defect interaction and evolution probed by IR spectroscopy

The frequencies of the local vibration modes of the Si–H bonds are highly sensitive to their environment. For instance the stretch modes alone cover the wave number range from $k \sim 1820\ \mathrm{cm}^{-1}$ to $k \sim 2240\ \mathrm{cm}^{-1}$ (Fig. 16). Most of the lines within this range have been identified with specific configurations thanks to their symmetry properties, using polarized light at different angles, by applying uniaxial stress, by correlation with the bending modes, and by H/D isotope substitution [4, 64, 73–78]. Table 1 lists those assignments that are most relevant in the context of blistering. Note that some k values may differ slightly between authors, due to two factors: (i) the frequencies can vary with temperature (cryogenic vs. RT measurements); (ii) the lines can also be shifted and broadened by the proximity to other defects (low H vs. high H concentration measurements). Some complexes present more than one vibration mode and show up or not depending on the geometry or the technique used, i.e. IR absorption spectroscopy (IRAS) or Raman scattering spectroscopy (RSS). So, both IRAS [4, 41, 70, 79, 80, 85] and RSS [64, 78, 81–84] have been highly useful to pinpoint the specific H-related defects present and monitor their thermal evolution.

3.4.1 Thermal evolution of Si–H stretch modes: isochronal (or ramp) annealing

The first IR work specifically applied to the blistering problem is that of Weldon et al. [4]. Their basic results are displayed in Fig. 16. This series of plots of IR absorption as a function of wave number, ob-

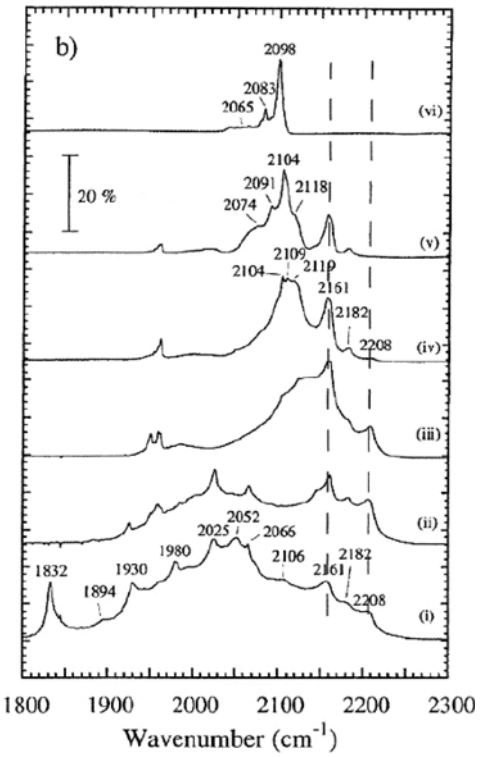

Fig. 16 IRAS spectra of Si–H stretch modes for a sample implanted with 6×10^{16} H/cm^2 at 75 keV, at RT (i), and after annealing for 30 min at 300 °C (ii), 425 °C (iii), 500 °C (iv), 550 °C (v) and 650 °C (vi) (from Chabal et al. [76], by permission).

Table 1 Assignments of different local stretch modes of the Si–H bond to different defect complexes.

wave number (cm^{-1})	identification	Ref.
2068	VH	Bech Nielsen [74]
2022		Lavrov [78]
2121, 2144	VH_2	Bech Nielsen [74]
2166, 2191	VH_3	Bech Nielsen [74]
2155, 2180	V_2H_6	Chabal [76], Lavrov [78]
2222, 2258	VH_4	Bech Nielsen [74]
2205, 2234		Lavrov [78]
1939, 2025	$V_2H_{1,2}$	Weldon [4]
~1950–2050 broadband	monohydride multivacancies	Weldon [4]
1987, 1990	IH_2	Budde [75]
1957		Weber [64]
1960	4th overtone, Si optical phonon	Heyman [25]
1838, 2062	H_2^*	Holbech [73]
1998	H_{BC}^+	Budde [77]
~2060–2120	Si–H on internal surfaces, including:	Weldon [4], Chabal [76]
2084	reconstructed 1 × 1Si(111):H	
2088–2099	reconstructed 2 × 1Si(001):H	
2098	Si(001):H	
2100–2120	perturbed Si(001):H	

tained by implantation at 75 keV with 6×10^{16} H/cm^2, a dose comfortably above the blistering threshold, contains an enormous amount of information. After implantation (bottom curve) a dozen discrete modes show up superimposed on a dominant broadband. The discrete modes are associated with small isolated defect complexes. It can be noticed that interstitial defects are not abundant, only IH_2 is seen although interstitials and vacancies are produced in equal numbers by the atomic collisions. This discrepancy has been noted before [21] and is plausibly due to the compressive stress that surrounds an interstitial and repels H atoms. (This argument neglects electrostatic effects, which do not seem to play a large role in blistering). This seems like a nice subject for theory which has treated so far only the energetics of the defects and their vibrational properties [21]. Particularly important here are the following:

– The low wave number broadband ("LWNBB") delimited by $k < 2050$ cm^{-1}, thought to be due to monohydride-terminated multivacancies V_nH_m, $m \leq n$.

– There is also a non negligible background at high k that is not well understood.

– The peaks at 2161 and 2182 cm^{-1}: VH_3 and/or V_2H_6. These two are hardly distinguishable experimentally and theoretically, but the peaks have been shown to be actually due to V_2H_6 in H-implanted Si [78]).

– The hump with some peaks in the range from ~2060 to ~2120 cm^{-1}: diverse modes of Si–H on internal surfaces (some reconstructed), mostly {100} and henceforth labelled Si(001):H, and some shifted and broadened by the imperfection of these internal surfaces.

The figure displays the evolution of the IR spectra after annealing for 30 min at the successively higher temperatures given in the caption. At 300 °C (Fig. 16 (ii)), we see a general attenuation of the LWNBB while the high wave number region shows more and more structure. At 425 °C (iii), the LWNBB is further reduced with V_2H_6, VH_4 (2208 cm^{-1}) and a shoulder around 2100 cm^{-1} emerging. At 500 °C (iv), the spectrum is composed of only two features: V_2H_6 and Si(001):H. Further annealing leads to blistering and the appearance of sharper lines, characteristic of Si–H stretch vibrations on smoother surfaces. Note that throughout the process there was a net loss of bound hydrogen starting somewhere below 300 °C, while negligible loss of total H was found by ERD. The Si(001):H complexes are of course identified with the (001) platelets observed by TEM. The survival of the complex at

2161 cm^{-1} while VH_4 (2208 cm^{-1}) has disappeared constitutes additional evidence that the 2161 cm^{-1} peak consists of V_2H_6 alone, since the totally passivated V_2H_6 is obviously more stable than VH_3 and plausibly more so than VH_4 because its dissolution would require more atomic rearrangements.

Similar scenarios have been reported by Aspar et al. [41], Moutanabbir and Terreault [81], Weber et al. [64], and Düngen et al. [84], although minor differences are observed. In Weldon's data, at 425–550 °C the intensity around 2100–2120 cm^{-1} and that of V_2H_6 definitely increase substantially above their RT values, suggesting a transfer of H from multivacancies into these high-*k* complexes. Only a modest increase is seen in Aspar's data, and in Moutanabbir's, Weber's and Düngen's spectra the 2100–2120 and V_2H_6 peaks only seem to emerge from a fading background, accompanied by a narrowing of the lines: it is by no means clear that these modes are fed by the disappearance of other defects. Another difference is in the behaviour of V_2H_6 at the highest temperatures after the onset of blistering: it disappears in Weldon's and Düngen's data but not in the others'; in any case its stability looks comparable to that of Si(001):H.

3.4.2 Thermal evolution of Si–H stretch modes: isothermal annealing

While isochronal annealing has been used in a majority of the fundamental studies, the simpler isothermal annealing is the technique of choice for practical applications. Moreover, it gives complementary information on basic mechanisms. Personnic et al. [85] measured the IRAS spectrum at several times during isothermal annealing leading to blistering. In the results, shown in Fig. 17(a), the time scale is normalized by the total time (10 min) required for blistering at that temperature (450 °C). It is seen that a major part of the depletion in Si–H modes takes place during the first 10% of the annealing time; the depletion concerns essentially the multivacancy region. Let us recall that this early time corresponds to the platelet nucleation phase, whereas the long later phase corresponds to Ostwald ripening of the platelets (Section 3.1.2). Small increases are also observed in the V_2H_6 and VH_4 modes during the first minutes, and in the Si(001):H modes after ~30% of the annealing time. These observations indicate that a small fraction of the H atoms liberated by multivacancies is captured by monovacancies, and later by internal surfaces. The conclusion that logically follows from this experiment is that the rate-limiting step in blistering is the Ostwald ripening of the platelets (which is possibly mediated by the transport of hydrogen between the platelets). This type of experiment is promising. First, by performing several IR measurements during the "first 10%", the Si–H dissociation kinetics could be established with precision; and secondly, by studying the platelet growth kinetics during the "remaining 90%" (as in Fig. 9) at several different temperatures, the activation energy for Ostwald ripening could be determined. The activa-

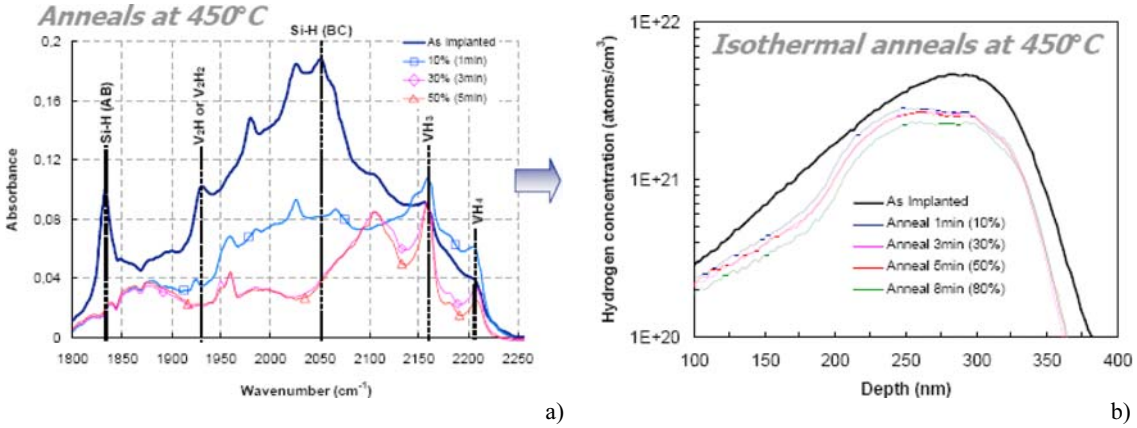

Fig. 17 (online colour at: www.pss-a.com) (a) IRAS spectra of Si–H stretch modes, as implanted and after annealing for 1, 3 and 5 min, corresponding to 10%, 30% and 50% of the thermal budget for fracture at 450 °C; (b) SIMS H profiles in the same experiment; note the log scale (from Personnic et al. [85], by permission).

tion energies of both the dissociation step and the Ostwald ripening step could be compared with the effective E_a for blistering and to those of basic processes such as I, V and H diffusion and Si–Si and Si–H bond breaking.

3.4.3 Dose dependence

The spectrum of Fig. 18 was obtained in the same conditions as that of Fig. 16, but for a subthreshold dose, 2×10^{16} H/cm^2 [4]. At low temperature, the differences between low and high doses are not blatant, except that the LWNBB is relatively weaker at low dose, indicating less clustering of the multivacancies. The thermal evolution also starts similarly; however, the Si(001):H complexes never really develop, only the V_2H_6 emerge clearly. These facts of course reinforce the assumption that the Si(001):H associated with the platelets are the essential precursors of the blisters. (They also led to the suggestion that the release of H atoms from the H reservoir in the multivacancies was important for eventual blistering.)

While the intensity of the LWNBB increases with dose at low dose, it saturates at very high dose. The RSS spectra for 5 keV implantation are compared in Fig. 19 [44] for three doses: a subthreshold dose of 1×10^{16} H/cm^2, a blistering dose of 2×10^{16} H/cm^2 and a very high dose of 7×10^{16} H/cm^2. The high dose spectrum is characterized by a quasi absence of sharp lines at RT, an indication of high damage, as expected; however its maximum is not at low k-values, it is right around the $k = 2120$ cm^{-1} value characteristic of perturbed hydrogenated internal surfaces. This observation suggests that high H and damage

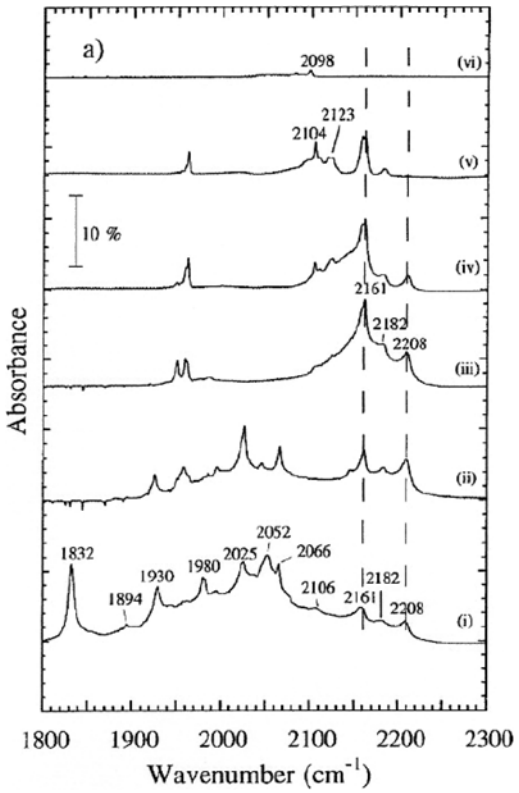

Fig. 18 IRAS spectra of Si–H stretch modes for a sample implanted with 2×10^{16} H/cm^2 at 75 keV, at RT (i), and after annealing for 30 min at 300 °C (ii), 425 °C (iii), 500 °C (iv), 550 °C (v) and 650 °C (vi) (from Chabal et al. [76], by permission).

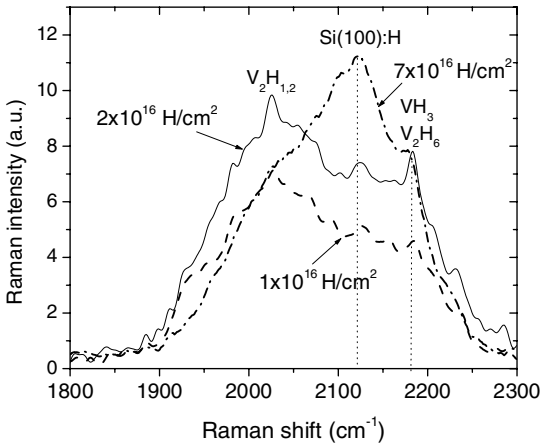

Fig. 19 Raman spectra of Si–H stretch modes at RT for samples implanted with different doses of 5 keV H ions (from Moutanabbir et al. [44]).

densities generate conditions favourable to internal surface creation. Under annealing these complexes would become less defective and transform into *bona fide* Si(100):H and V_2H_6 characterized by sharp lines. Indeed at high temperature the high dose sample evolves rapidly towards the stage depicted in Fig. 16, i.e. a pure dominance of Si(001):H and V_2H_6. This shows that the H reservoir of the multivacancies is not necessary for blistering and constitutes a waste of hydrogen.

3.4.4 Molecular hydrogen

Contrary to IRAS, RSS can detect H_2 molecules. Three stretch modes are known, gaseous H_2 at 4158 cm^{-1}, H_2 in the interstitial T_d site at 3601 cm^{-1} [23, 86] and H_2 in multivacancies such as V_2, V_6 and V_{10} at 3820 cm^{-1} [82, 83]. $H_2(T_d)$ has never been seen in H-implanted Si, only in plasma hydrogenated Si [86], likely because there are stronger traps such as dangling bonds in implanted Si [53]. Both Aspar et al. [11] and Düngen et al. [84] succeeded in detecting gaseous H_2 by focusing their exciting laser microbeam precisely on blisters, see Fig. 20(a). However, they failed to see it in the spaces between blisters or at low or intermediate temperature. It is thus natural to interpret this line as due to gas filling the blister cavities. As for the "V_n(3820)" complex, it has been clearly identified at RT by Weber et al. [64], Düngen et al. [84] and Moutanabbir et al. [71]. Actually, Kilanov et al. [79] have quantified their IRAS data in terms of absolute numbers of H atoms and they claim that the Si–H absorbance accounts for only 60–70% of the implant dose, the rest presumably being in the form of H_2 in multivacancies. Both Düngen and Moutanabbir also studied the thermal behaviour of the V_n(3820) complex, as shown in Fig. 20(b). We see that the H_2 in V_n's disappears above 200 °C, in agreement with Ref. [83], and consistent with the disappearance of the multivacancy defects in the Si–H Raman modes. Therefore it has nothing to do, at least directly, with the H_2 that pressurizes the blisters that show up at quite higher temperature.

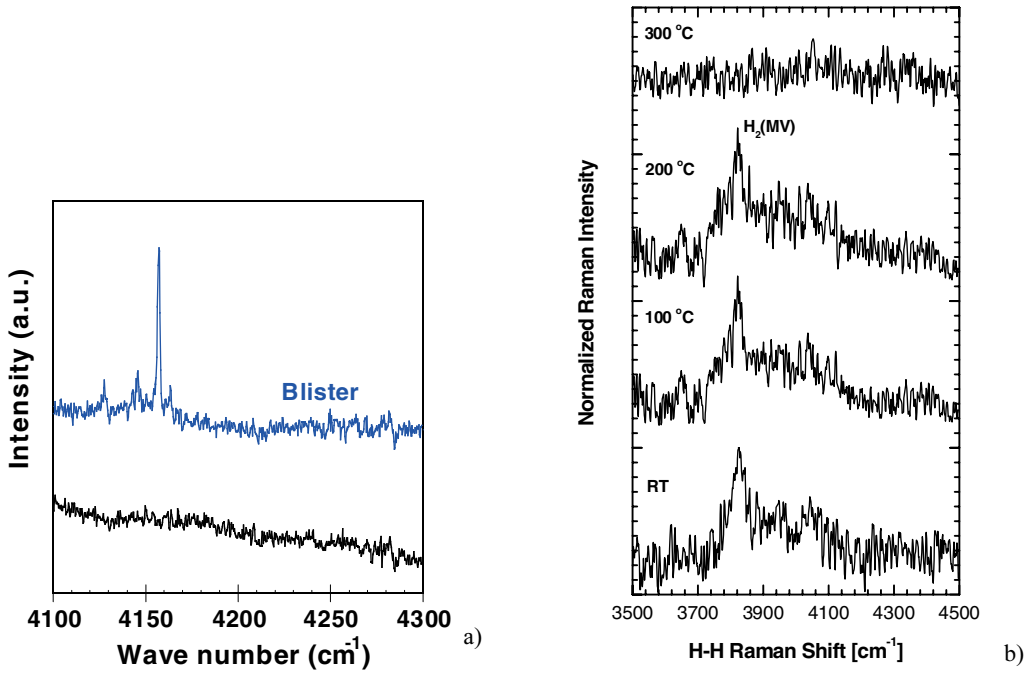

Fig. 20 (online colour at: www.pss-a.com) Raman spectra of H_2 stretch modes: (a) the top curve shows the Raman line of gaseous H_2 at 4158 cm^{-1} when the laser microbeam is focused on a blister, while the bottom curve shows no line when the beam is focused elsewhere (from Aspar et al. [11], by permission); (b) 3820 cm^{-1} line of H_2 in multivacancies as implanted and after annealing at the indicated temperatures (from Moutanabbir et al. [71]).

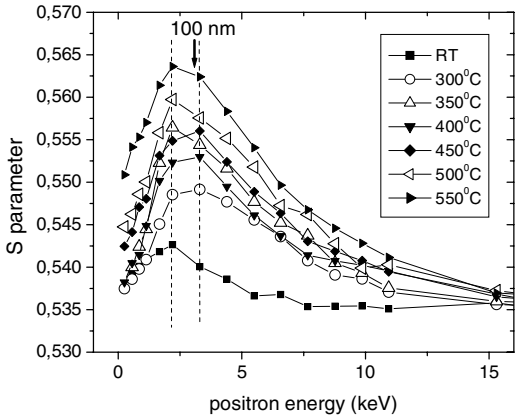

Fig. 21 *S*-parameter as a function of positron energy for 2×10^{16} H/cm^2 at 5 keV, at RT and after annealing as indicated; the relation between e^+ energy and depth is not linear, a 100 nm marker is shown (from Moutanabbir et al. [71]).

3.5 Open volume evolution probed by positron annihilation spectroscopy

In positron (e^+) annihilation spectroscopy (PAS), the line shape of the γ-ray is determined by the electron momentum distribution. In regions distant from atomic nuclei, such as vacancies or voids, the line has no high momentum tail. The *S*-parameter is a mathematical measure of the sharpness of the line, so it takes higher values in vacancies and cavities. For instance, the silicon divacancy yields an *S*-parameter of 1.045 times the value of virgin silicon [87]. By varying the incident e^+ energy, its penetration depth is changed, and a depth profile of cavities can be deconvoluted. The early work of Brusa et al. [88], although it was carried at a subthreshold dose, nevertheless revealed an important fact for the interpretation of PAS spectra, namely that the *S*-parameter of H-passivated vacancies reverts to virgin-like values, so they are practically PAS-invisible. With pulsed beams, the positronium lifetimes can also be measured and Fujinami et al. [89] showed that cavities display longer lifetimes.

Figure 21 shows PAS spectra of the *S*-parameter vs. the e^+ energy from a recent study at a blistering dose [71]. At high e^+ energy (large depth), the expected well-known value for virgin Si is obtained. In the implanted region (~100 nm) an enhancement is observed, indicating the presence of cavities already at RT. At 300 °C, the PAS signal has increased in intensity and more strongly so at 350 °C, consistent with an increase in cavity volume. It dips slightly at 400 °C, which may be rationalized by the final collapse of the multivacancies and/or a capture of H by cavities, because H adsorption will reduce the *S*-parameter, as mentioned. Finally, at and above 450 °C, the *S*-parameter increases rapidly, in accord with the growth of the blisters. The peak S value obtained at 550 °C is ~1.05 times larger than the value for virgin silicon, which imposes a lower limit on the size of the positron-trapping defects of at least 4 vacancies. However it is likely that the positron trapping defect is larger than V_4, since the measured value of $S = 1.05$ represents a weighted average of trapped and untrapped positrons. Another feature of interest is that the depth of the peak shifts in a way similar to the RBS/C peaks (Section 3.3.2). At 300 °C it is deeper than at RT, then it moves towards the surface at 350 °C, then deeper again at 400–450 °C, and finally back towards the surface at 500–550 °C. This may seem erratic but the "shallow peak" is

Table 2 Temperatures of occurrence of shifts in depths of peak values of RBS/C yield or void volume measured by the *S*-parameter [71].

quantity	temperature range	
	shift in depth	strong shift to surface
RBS peak yield	300 to >400 °C	~600 °C
S-parameter peak	300–450 °C	>500 °C

Table 3 Values of the perpendicular tensile strain ε found in different experiments; either the maximum value at the peak is given, or else an average value.

ion energy (keV)	implant temperature	H dose (10^{16} /cm^2)	ε (%)		Ref.
			RT	high temperature	
15.5	<100 °C	2.0	0.5 (max)	–	[65]
15.5	LN_2	1.6	0.5 (av)	1.2 (300 °C) 0.5 (500 °C)	[58]
40	LN_2	5.0	0.65 (max)	–	[91]
40	RT	5.0	1.25 (max)	–	[91]
42	LN_2	3.0	0.35 (max)	–	[90]
64.5	RT	5.0	0.033 (rms)	0.053 (500 °C)	[64]
76	RT	8.0	2.9 (max)	"weak" (350 °C)	[92]

always associated with higher S values. The shifts are summarized in Table 2. The shifts in depth at intermediate temperature are interpreted as a move of the void volume from multivacancies to the platelets. The "larger cavities" ($>V_4$) only show up at ~475–500 °C and their shift towards the surface together with the shift in the RBS/C profile identifies them with blistering.

3.6 Stress and strain

The presence of cavities is expected to be accompanied by an in-plane stress, σ, and a perpendicular strain, ε. Strain measurements have been done using X-ray diffraction [64, 65, 90–92], and large angle convergent beam electron diffraction (LACBED) [58]. In some cases, an ε profile was obtained from these data, in other cases an average value only. From the ε values, an in-plane stress could be deduced, using the standard values of Young's modulus and Poisson's ratio for Si. The depth-integrated or average stress has also been obtained by the thin sample curvature method [40, 52]. While all agree on the existence and the sign of the strain or stress, there is a rather wide range of absolute values in the literature: this is shown in Tables 3 (strain) and 4 (stress). One can surmise that the deconvolution of absolute strain values is fraught with difficulties, but we will continue the discussion assuming that relative values within the data of one group using the same apparatus in similar conditions are at least qualitatively instructive.

Table 4 Values of the in-plane compressive stress σ found in different experiments; either the maximum value at the peak is given, or else an average value.

ion energy (keV)	implant temperature	H dose (10^{16} /cm^2)	σ (MPa)		Ref.
			RT	high temperature	
15.5	LN_2	1.6	1000 (max)	3000 (300 °C) 1000 (500 °C)	[58]
40	LN_2	7.0	325 (av)	–	[40]
		10.0	100 (av)	–	
40	RT	8.0	225 (av)	–	[52]
64.5	RT	5.0	60 (rms)	10 (500 °C)	[64]
76	RT	8.0	1900 (max)	"weak" (350 °C)	[92]

3.6.1 Effect of temperature

Inspection of the strain data of Refs. [90, 91] in Table 3 shows that (i) the strain increases with dose, and (ii) it increases markedly with the implantation temperature. In fact, as shown by Lee et al. [91], the strain depth distribution follows precisely the trend of the displacement damage (Section 3.3): both distributions are considerably more peaked for RT implantation than for cryogenic implantation. This suggests a close connection between the strain and whatever defects cause the backscattering. Moreover, the results of Tables 3 and 4 show that, around 300 °C, at the same time as the defects observable by TEM, RBS/C or IR spectroscopy start evolving, the stress and the strain increase, showing again the connection between stress/strain and the huge enhancement in RBS/C yield. When the blisters appear at somewhat higher temperature, the stress is expectedly relieved, though not entirely; this behaviour is again similar to the RBS/C evolution (Figs. 13 and 14). These facts are of great importance concerning the stress and strain but they are based on few data unfortunately.

The power of LACBED is that the defect concentration and the relaxation volume around these defects can be deduced from the 2-D intensity maps of the Bragg contours. Using LACBED measurements, Frabboni [58] calculated the product of these two quantities, which gives the total defect "volume". This is displayed in Fig. 22 (converted in our units), together with the RBS/C data obtained at the same ion energy and dose [53] (which is part of the data of Fig. 14). One can see that, with increasing temperature, as the defect relaxation volume (a) increases, the defect concentration (b) decreases. Note that the increase in the relaxation volume can be simply due to an increase in H_2 contents and the concomitant pressure enhancement, rather than to a growth in the size of the clusters themselves. The total defect volume (c) has a maximum at 300 °C and then decreases at higher temperature. We are now familiar with this type of temperature dependence: it is very similar to the backscattering yield (d). In addition, Frabboni points out that the defects are too numerous and too small to be platelets, and too large to be interstitials; he assumes the defects to be H_2 pressurized vacancy clusters.

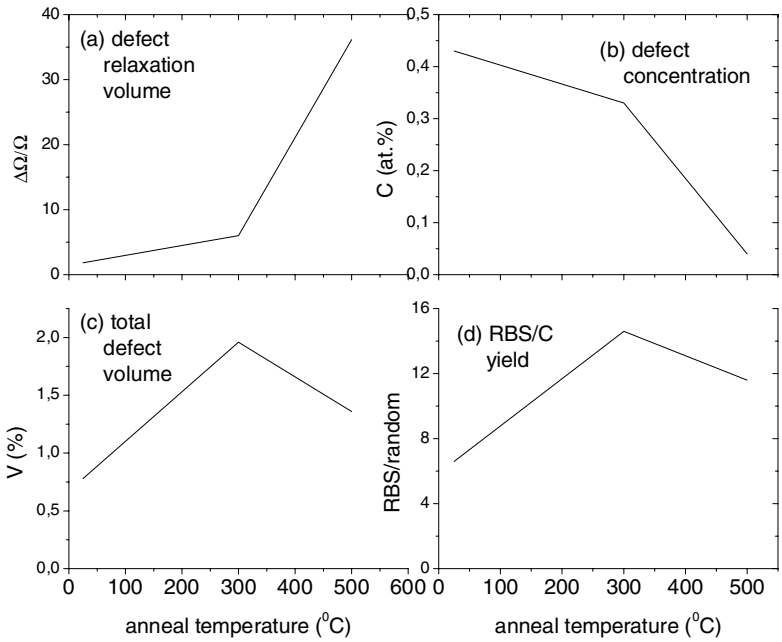

Fig. 22 Defect relaxation volume normalized to atomic volume (a), defect density normalized to atomic density (b), defect volume as % of total (c), and maximum RBS/C yield as % of random yield (d), for 1.6×10^{16} H/cm^2 at 15.5 keV (adapted from Frabboni [58] and Cerofolini et al. [55]).

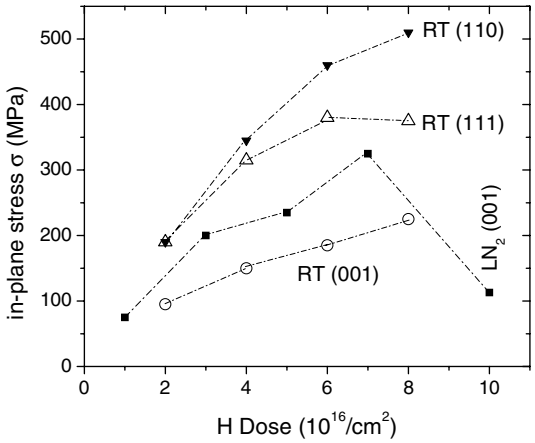

Fig. 23 In-plane compressive stresses measured by the wafer curvature method as a function of implanted dose and crystal orientation at 40 keV. The labels RT and LN_2 refer to the RT implants of Zheng et al. [52] and the cryogenic implants of Höchbauer et al. [40].

3.6.2 Dose and crystal orientation effects

The dose and orientation dependences of the RT stress were studied by Höchbauer et al. [40] and Zheng et al. [52], both at 40 keV. Figure 23 is a compilation of their measurements. The stress increases and then saturates at increasing dose; and one of the experiments gives a drastic reduction of σ for doses above 7×10^{16} H/cm^2. The difference in implantation temperatures (RT for Zheng, LN_2 for Höchbauer) possibly explains the difference in the two data sets for Si(001), both obtained by the same method in the same laboratory. Unfortunately, this interesting result is based on a single datum, but it correlates with other evidence that will be discussed in the next section. The figure also shows that the stress depends markedly on the crystal orientation, the ordering being $\sigma(110) > \sigma(111) > \sigma(001)$. This is the order of the mechanical bond strengths at intermediate temperature (Section 2.2), and the inverse order of the kinetics of splitting (Section 2.3). Zheng et al. hypothesize that the lower stress for Si(001) is due to the higher abundance of platelets, which leads to stress relief. A somewhat different ordering was found in another strain measurement, using X-rays, namely $\varepsilon(111) > \varepsilon(110) > \varepsilon(001)$ [92]. The authors explain it in terms of bond angles: the smaller the angle between the bond direction (always {111}) and the interface normal (⟨111⟩, ⟨110⟩, or ⟨001⟩), the higher the strain.

It is worth noting at this point that while platelet formation, stress and strain, and "ease of blistering" vary substantially depending on crystal orientation, on the contrary the defects measured by either IR spectroscopy or backscattering/channelling are qualitatively and quantitatively similar whatever the orientation [52].

3.7 Spatial correlations; the depth of splitting

Several authors have noted unsurprising similarities in the depth distributions of H, of "damage" measured by RBS/C, of platelets, of positron annihilation and of strain, and in the depth at which the substrate splits, either by blistering or ion-cutting. The Los Alamos group has endeavoured to put these similarities on a quantitative basis [40, 67, 68, 70, 90, 91]. It was first found in Ref. [67] that, in their conditions (5×10^{16} H/cm^2 at 175 keV), the depth of splitting coincided precisely with the peak in the backscattering yield and not to the peak in H concentration, which is ~7% deeper; the cut was not at the center of the platelet distribution either. Further work [90] investigated also the strain distribution, using a subthreshold dose of 3×10^{16} H/cm^2 at 42 keV. The results are shown in Fig. 24. Displacement density, strain and platelets all peak at the same depth within 10 nm, some 50 nm shallower that the peak in H. We notice that the strain profile is narrower that the displacement profile, and the platelet profile even narrower. That last fact is understandable, since platelets are suspected to require a minimum H concentration, their distribution is a sort of convolution of the damage and H distribution. For the strain it is not as clear but it could indicate an influence of the hydrogen, as claimed by others [53, 58].

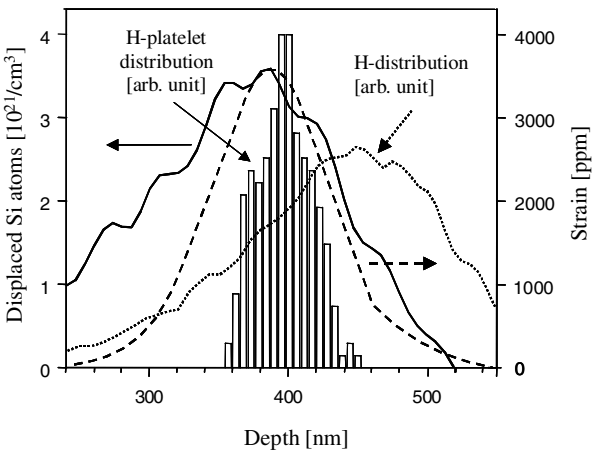

Fig. 24 Depth distributions of H (dotted line), atomic displacements (solid line), strain (dashed line), and platelets (histogram), for 3×10^{16} H/cm^2 at 42 keV (from Nastasi et al. [90] by permission).

On the basis of their observations, Nastasi et al. argue that mobile vacancies are drawn into the region of maximum perpendicular tensile strain (and in-plane compressive stress) and so facilitate platelet nucleation and growth. Moreover these processes are favoured energetically as we saw in Eq. (3). Since H capture by platelets, either adsorbed on the walls or in the gas phase, is exothermal, H atoms are drawn into the platelets. Growing platelets are thus fed with hydrogen. At high temperature, these processes are presumably accelerated and the pressure drives crack formation and blistering. Unfortunately, the thermal evolution of the strain profiles was not investigated to confirm this picture. In their model, the compressive stress is assumed to be due to the same defects that are responsible for the displacement field. It is argued very sensibly that these defects have to be clusters, but also that they are unrelated to hydrogen. This is opposite to the view of Cerofolini [53] and Frabboni [58]. It is indeed hard to understand how clusters unrelated to H would be so abundant and cause such a high backscattering yield, when He implantation produces so little damage. Moreover, the huge increase in the displacement field at intermediate temperature is even more difficult to understand in this framework, particularly as we see the multivacancies and the interstitial defects disappearing in the IR spectra. So, the question of the displacement field, its origin, and its role in blistering is still perplexing.

A different situation arises at very high dose. For instance, for 1×10^{17} H/cm^2 at 40 keV, microcracking occurs at the peak of the H distribution; and for 7×10^{16} H/cm^2, microcracks can be observed at both the peak in backscattering yield and the peak in H [40]. This is nicely illustrated in Fig. 10. This TEM observation and similar ones for 5×10^{16} and 1×10^{17} H/cm^2 are confirmed by AFM line scans in the craters of ruptured blisters. Let us recall that the authors had found (Fig. 23) the maximum in the stress at 7×10^{16} H/cm^2 and a strong reduction for 1×10^{17} H/cm^2. They suppose the stress relief to have proceeded by radiation-enhanced defect migration, which would naturally occur above a certain defect concentration. With a lower stress, the mechanism described in the preceding section would be less powerful of course and splitting could occur at the depth of the H maximum, the more so since the H concentration is very high. Actually, contrary to low dose, for 1×10^{17} H/cm^2 the platelet depth distribution becomes very wide and it shows two peaks, one located at the peak in H and the other somewhat shallower than the peak in RBS/C-damage (Fig. 25) [68]. Since the shift in splitting depth is already initiated at 7×10^{16} H/cm^2, for which the stress is maximum, another factor must also intervene. Höchbauer et al. [40] hypothesize that it is an enhancement in fracture toughness at high damage levels [93] which prevents microcracking at the peak damage depth.

3.8 The *Elusive hydrogen*

The question to be addressed here is probably the most puzzling one in relation with the evolution of implanted hydrogen. It deserves a careful and exhaustive examination, which is not straightforward be-

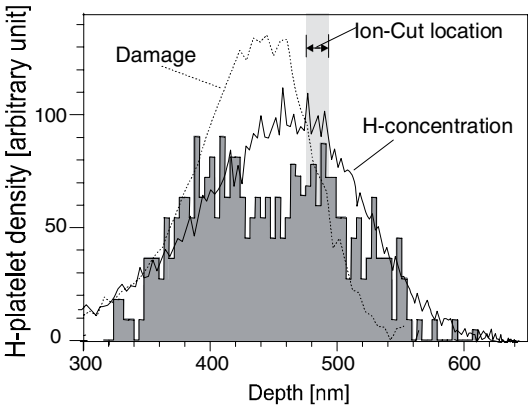

Fig. 25 Histogram (shaded) of the depth distribution of platelets at high dose: 1×10^{17} H/cm^2 at 50 keV; the damage and H depth profiles are also shown (from Höchbauer et al. [68], by permission).

cause the evidence comes from different experiments with, e.g. different H doses and different annealing protocols. We saw in Section 3.4.1 that the Si–H modes, especially the low-*k* ones, start disappearing progressively above 250 °C, while the total H contents measured by IBA (Section 3.2) or thermal desorption spectrometry (Section 2.3.2) remain high up to >400 °C. In isothermal annealing, more than half of the low-*k* Si–H are lost during the first 10% of the annealing time (Section 3.4.2). We show in Fig. 26 the quantitative comparison made between the integrated amount of bound H measured by IRAS of Si–H modes and the net H retention measured by ERD [76]. ERD, like other IBA techniques, is the least prone to artefacts, but very similar results were obtained using RSS and TDS [44]. The Si–H depletion at relatively low temperature (or in the first few minutes under isothermal annealing) is confirmed by Refs. [41, 64, 80, 81, 84, 85], and the nearly total retention, almost until blisters appear, is also confirmed by NRA [42] and ERD [66]. To that bound H must be added the H_2 molecules trapped in multivacancies, which also disappear at relatively low temperature [71, 84]. It has been generally assumed that the freed H took the form of IRAS-invisible H_2 [4]. This H_2 could be for instance at the source of the displacement field through the stress or pressure it would necessarily cause [53].

The problem with the above assumption is that those H_2 molecules are nowhere to be seen until quite higher temperature. To demonstrate this without using disparate experiments, the data of Düngen et al. [84] are shown in Fig. 27. We see that the low-*k* multivacancies (MV's) start to decrease at 350 °C, that the 3628 cm^{-1} line of H_2 in MV's also vanishes at 350 °C, but that the 4162 cm^{-1} line of gaseous H_2 does

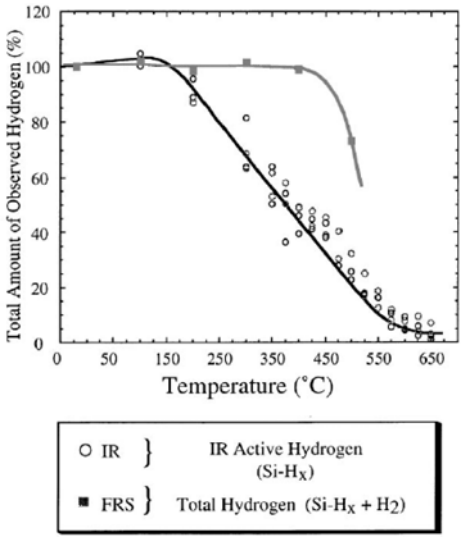

Fig. 26 Comparison of integrated bound hydrogen (Si–H stretch modes) with total H retention measured by ERD (here called FRS), for 6×10^{16} H/cm^2 at 75 keV (from Chabal et al. [76]).

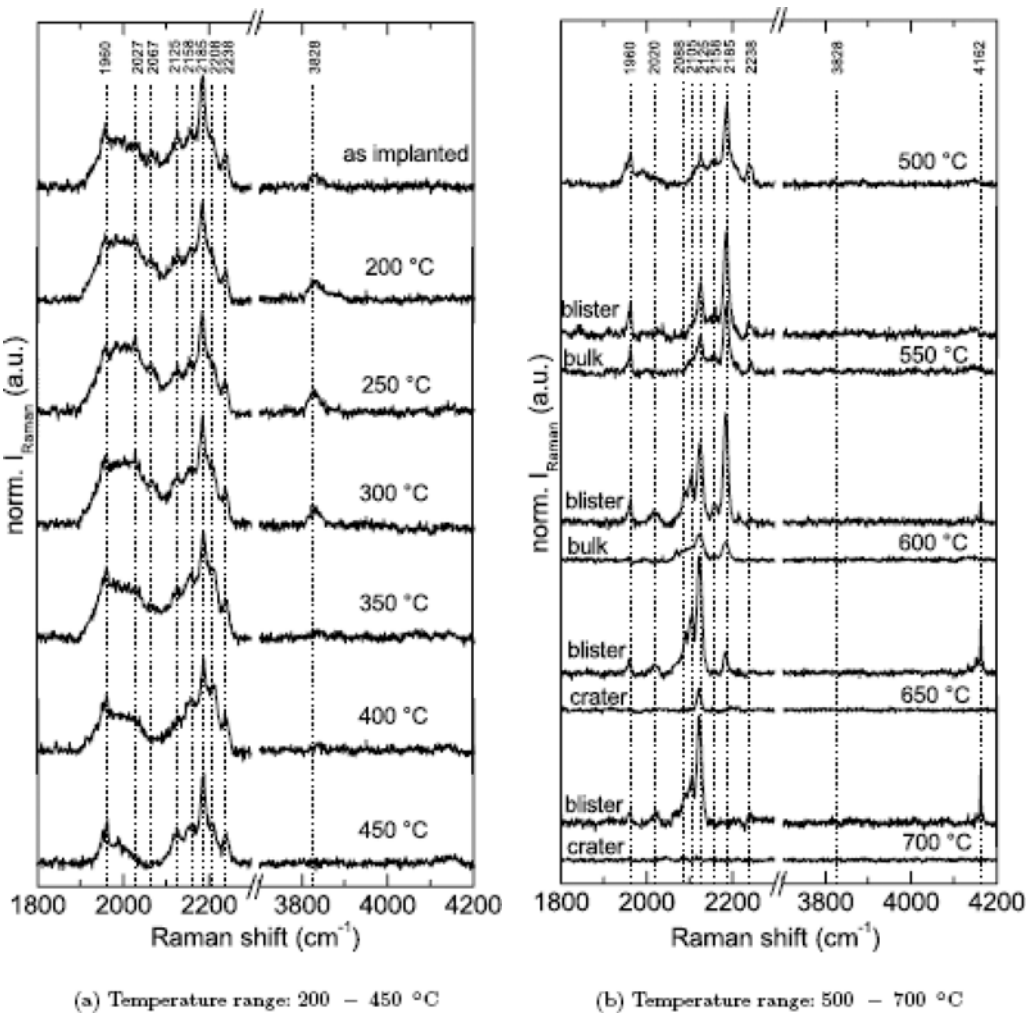

Fig. 27 Raman spectra in both the Si–H (1800–2300 cm^{-1}) and H_2 (3700–4200 cm^{-1}) stretch mode regions, at RT and after annealing at different temperatures for 10 min (from Düngen et al. [84]).

not show up until 600 °C when blistering is fully developed. Therefore, in the crucial phase from around 250–350 °C (depending on dose and annealing protocol), until blistering above ~450–550 °C, a large amount of hydrogen cannot be found, whether bound to Si or as H_2. It must exist in a Raman-invisible form. This is the mystery of the *elusive hydrogen*.

Two experimental artefacts could be invoked to explain away this paradox. First, all the reported IR measurements were carried out at RT, after cooling the samples down from whatever temperature they had been annealed at. But Ma et al. [94] have shown that some Si–H bonds (specifically Si–H on internal surfaces of {111} platelets) may reform upon cooling down. Therefore RT IR measurements are unreliable as a measure of the true state of annealed samples. However, if something similar has happened in the reported experiments, it will only make the discrepancy worse. (Actually, the results of Ma et al. may constitute an instance of *elusive hydrogen* because it is by no means clear that the H lost by Si–H modes is quantitatively accounted for by other modes.) The second possible explanation is that the "lost H" would have simply migrated beyond the depth accessible to the Raman laser beam. However, in the case of the 5 keV implantations [81], the mean H implant depth is only 75 nm whereas the laser

penetration depth is ~500 nm. As for the other cases, H migration in depth has never been observed at any temperature by IBA [42, 66] or SIMS, see next.

During the isothermal annealing experiment reported in Section 3.4.2, Personnic et al. [85] measured the H depth profiles by SIMS and found them to be also depleted (Fig. 17(b)), and at the same rate as the Si–H bonds measured by IRAS (Fig. 17(a)): After 10% of the annealing time, the H profiles are depleted not only on the surface side as found by IBA (Section 3.2), but are also depleted by a factor of ~1/2 at the peak. As annealing is pursued, they are further depleted uniformly. At no time is there a sign of migration in depth; this is important because SIMS is sensitive to very low H concentrations (<0.1 at%). The authors assume that dissociation of Si–H "results in the formation of H_2 that is not directly detectable by SIMS". The question arises whether the "lost H" could become visible using a beam ion (Ar^+, Cs^+, O_2^-?) and/or detected ion (H^+, H^-, H_2^+, H_2^-, SiH^+?) different from whatever unspecified ions were used in that work. If such a combination were found, it could give hints concerning the chemical state of the *elusive hydrogen*.

3.9 Temperature correlations; blistering scenarios

Figure 28 is intended to summarize the thermal evolution of the various quantities discussed above during either isochronal or isothermal annealing. The labels are explained in the caption. The so-called low-*k* and high-*k* IR modes are defined as those with $k < 2050$ cm^{-1} and $k > 2050$ cm^{-1}, respectively [4, 81]. The curves are taken from different real data but sometimes interpolated or smoothed. They are intentionally qualitative because: (i) the anneal times vary from ~20 min to 2 h; and (ii) the doses are variable, though all are relatively close (below or above) the blistering threshold. The curves are normalized to the maximum value reached by the corresponding quantity. A few generalizations can be made with reasonable certainty.

– At RT, most H is bound to Si dangling bonds and the majority of the defects are of the vacancy or cavity type including (001) platelets; there is also H_2 in large multivacancies. Atomic displacements and strain are already present at a level that implies major roles for H and H_2 in stabilizing the defects (certainly), and straining the crystal (probably), an effect at the source of the greater part of the displacement field.

– Between 200 and 300 °C (or in the first minutes in isochronal annealing), the various defects, especially those of the multivacancy type, start releasing H and H_2, the major part of which is retained in the sample but is curiously invisible by Raman scattering or SIMS. At the same time, the strain, the displacement field and the cavity volume start increasing, maybe not all at the same rate; however all three eventually reach similar levels of enhancement in comparison with their RT value: This is probably not a

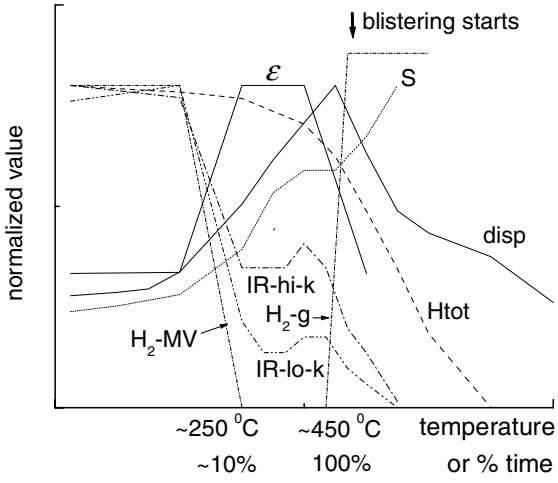

Fig. 28 Schematic evolution under annealing as a function of temperature or time (% of blistering time): total H retention (Htot), low-*k* and high-*k* Si–H IR modes (IR-lo-*k*, IR-hi-*k*), IR modes of H_2 in multivacancies (H_2-MV) or gaseous (H_2-g), atomic displacement density (disp), perpendicular strain (ε), and *S*-parameter (*S*).

coincidence. The circumstantial evidence therefore indicates that a vacancy-type defect (*S*-parameter) starts to grow; it involves hydrogen in a so far unknown form (IR), and this H presence causes a strong deformation of the lattice (ε), and strong backscattering (disp) and dechannelling.

– At 400 to 500 °C (typically), the low-*k* complexes disappear. Of the high-*k* complexes, only the internal (001) surfaces and V_2H_6 remain, but they contain no more than 20% of the H. Blisters appear, together with gaseous H_2, and the cavity volume keeps increasing as the blisters grow. The strain is relaxed and the displacement field weakens. H_2 starts to desorb out in abundance.

The nature of the complex that retains H and causes the strain at intermediate temperature is puzzling. Platelets are not likely culprits for two reasons. First, cavities do not by themselves cause hard collisions because no lattice atom is displaced into a channel; in addition, the TEM work shows little strain around the platelets. Second, their Ostwald-type growth at high temperature should reduce the strain in the implanted layer instead of increasing it (Eq. (3) in Section 3.1.2). The responsible complex must be hydrogen-related, must be so small that it is unrecognized by TEM, and must cause localized strain regions. Authors of TEM work speak of "heavily damaged regions" [4, 40, 68], faulted loops [11, 41, 66], or a high density (10^{12} cm^{-2}) of small (3 nm) defect clusters [58], but cannot be more specific. Cerofolini [61] has proposed assemblies of a few molecules trapped in vacancies or small vacancy clusters: they would certainly produce pressure and strain but why is the H_2 Raman- and SIMS-invisible? He further hypothesized that these structures are the blister precursors, rather than the platelets. However, the role of the platelets can hardly be denied in view of all the links between platelets and blisters, e.g. the coincidence between the peak in the platelet distribution and the depth of splitting, and also the obvious facilitating effect of the shape and orientation of the platelets.

4 Insights obtained using *hydrogen engineering*

4.1 Implantation temperature optimization

Implantation at LN_2 temperature [65] or –140 °C [70] strongly reduces both the displacement and the dechannelling damage observed afterwards at RT. Therefore annealing up to RT temperature after cryogenic implantation is not as effective in nucleating the relevant defect complexes as irradiating at RT, which clearly indicates the importance of "hot" defects (dynamic annealing). Frabboni [58] noted that no platelets were nucleated yet if the implantation was carried out at LN_2 temperature, but this did not change the final outcome after annealing. However, Lee et al. [70] noted a shallower and broader displacement profile with cryogenic implantation, and several other differences finally giving thinner and rougher transferred layers in ion-cutting. Moreover, implantation at –140 °C gave an IR spectrum that was shifted towards low-*k* values, i.e. having more H^*_2, multivacancy and interstitial defects, fewer VH_4 and V_2H_6, and no hint of Si(001):H [70]. In other words, low temperature implantation unsurprisingly has an effect that is the opposite of that of high temperature annealing, and its practical interest is thus limited.

It is then natural to surmise that implantation at higher than room temperature could be beneficial, but there have actually been few attempts at optimizing blistering or ion-cutting in this fashion. There is first the surprising result of Tong et al. [95]. They implanted the H ions at the high temperature of 400 °C, without causing any blistering, and then annealed the samples at different temperatures, including temperatures lower than 400 °C, until they blistered. True, blistering at 350 °C took ~25 hours, but at 400 °C it took only a modest ~100 minutes. It is unfortunate that the implantation time is not given in the paper. Another surprise is that the high temperature implantation did not speed up the rest of the process, the activation energy remained at a value of 2 eV for a dose of 7×10^{16} H/cm^2, in line with the results of Fig. 6.

Holland et al. [96] found for their part that the blistering dose could be minimized. By implanting at 350 °C and annealing at 450 °C, they only found a modest reduction in the threshold from 4.1×10^{16} H/cm^2 to 3.5×10^{16} H/cm^2. But they also discovered that, if they first carried out a high temperature implantation of a subthreshold dose, followed by a RT implantation, the total required dose

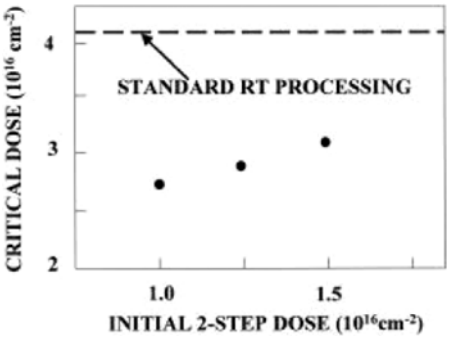

Fig. 29 Dose threshold (critical dose) for blistering under 30 min 450 °C annealling when the sample is implanted in two steps, first at 350 °C, then at RT, as a function of the initial dose (40 keV, from Holland et al. [96], by permission).

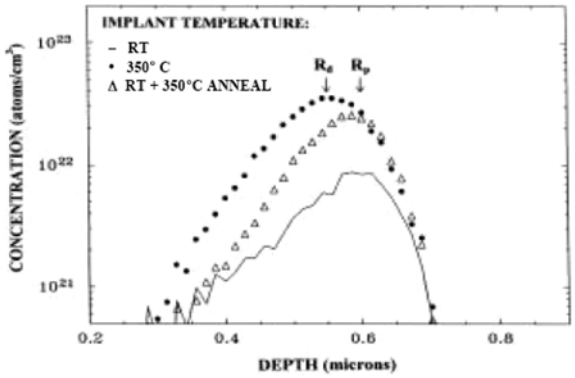

Fig. 30 Displacement concentration profiles (note the log scale) after a RT implant (line), a 350 °C implant (dots) and a 350 °C anneal of a RT implant (triangles) (from Holland et al. [96], by permission).

could be cut by as much as 1/3 (Fig. 29). One can suppose that the high temperature implantation "prepares the ground" by generating platelets or microcracks which efficiently trap the subsequently implanted H ions. This assumption is supported by RBS/C measurements (Fig. 30): They show a more intense displacement field at high temperature, consistent with the *reverse annealing* effect (Section 3.3.2), a well known forerunner of blistering. The backscattering yield is even higher than for RT implantation followed by annealing, a fact that is again consistent with the importance of dynamic annealing. The reason why a two step implantation is more effective than a single step high temperature one may be that the high temperature diffusivity of hydrogen is too high and results in premature H_2 release. One worry is that the higher RBS/C "damage" may result in poorer quality ion-cut wafers. The study of that question and further attempts at engineering the implantation temperature scheme are certainly warranted.

4.2 Effect of dopants

Hydrogen can react with dopants; the Fermi level determines the charge state of H in Si and strongly influences its diffusivity [20–22]. Therefore, it is of interest to elucidate the effects of doping on blistering, especially as heavy doping is used more and more in order to produce high conductivity regions. Concerning n-type doping, one can be brief, somewhat surprisingly it has no effect on blistering dose or temperature, except for a peculiar compensation effect that will be discussed below. On the other hand, boron doping has profound effects.

4.2.1 Boron facilitation of blistering

The presence of boron at high concentration reduces both the threshold dose and the minimum anneal temperature required for blistering, an attractive example of *hydrogen engineering*. Tong et al. [97] first reported that Si wafers uniformly doped at the level of 2×10^{20} B/cm^3 display 10 times faster blistering kinetics than undoped or n-type Si, but with the activation energy unchanged (E_a = 1.2 eV for 1×10^{17} H/cm^2). This is illustrated in Fig. 31. Alternatively, different B ion doses were implanted in undoped Si prior to H ion implantation. For B doses above 10^{15} B/cm^2, the blistering temperature was reduced from 340 °C to 280 °C. Very intriguingly, the effect was 50% weaker if the boron was electrically activated by high temperature annealing prior to H ion implantation. Similarly, in heavily B-doped

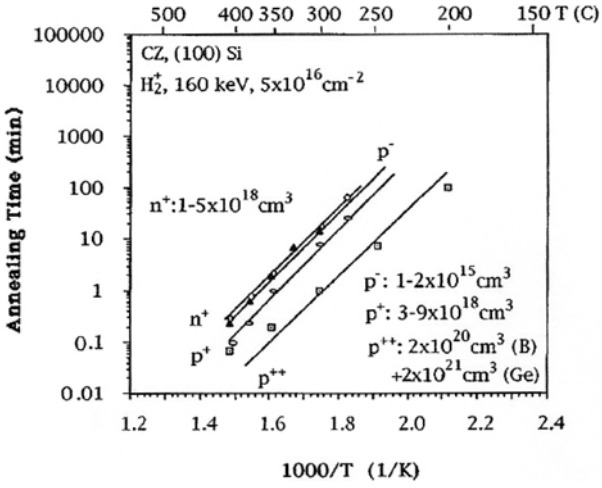

Fig. 31 Arrhenius plot of the blistering time vs. the inverse absolute temperature for uniformly doped Si wafers, with P or B concentrations as indicated (from Tong et al. [97], by permission).

Si (0.001–0.002 Ω cm), Desrosiers et al. [98] observed reductions in the blistering threshold from 1.75×10^{16} H/cm^2 to 1.0×10^{16} H/cm^2 and in the blistering temperature from 475 °C to 350 °C; consistent with the faster evolution of the implanted H, they found H_2 to start desorbing at as low a temperature as 225 °C. Kilanov et al. [79] carried out an innovative experiment: by epitaxy they deposited a B "delta layer" (6×10^{14} B/cm^2) on Si, followed by 500 nm of undoped Si on top. They then implanted H at 50 keV so that the H peak coincided with the B delta layer. They found a 100× faster blistering and a reduction in E_a from 1.3 to 0.8 eV (suggesting a switch from the "low temperature" to the "high temperature" regime, see Fig. 6). They also state that the blisters were smaller but more numerous, implying a higher density of nucleation sites and also a higher pressure (Eq. (2), Section 2.2). The Kilanov experiment shows that a highly localized B layer and/or an interface is particularly effective in blistering facilitation. A beginning of an explanation for the preceeding observations is a change in the mechanical strength of the implanted layer (Section 2.2), which starts to drop at ~200 °C with B doping, instead of ~280 °C without B [49]. In contrast, B ion implantation after H implantation leads to an exactly opposite effect on the strength, and an increase in the blistering temperature [99]. This last observation suggests that the defects generated by the passage of the B ions destroy the complexes of the "right" kind (described in Section 3) that are necessary for blistering.

4.2.2 Behaviour of H-related defects in B-doped Si

The presence of boron enhances platelet formation. Tong et al. [97] found by TEM more (001) platelets and fewer of the {111} type. Kilanov et al. [79] observed a quasi continuous narrow layer of microcracks at the B delta-layer depth after annealing for 2 h at 200 °C only, whereas without B-layer only a wide region of scattered microcracks was found. Several authors [49, 79, 100–103] reported that B doping reduced the atomic displacement density measured by RBS/C. An example is shown in Fig. 32 [101]. Here different B ion doses were implanted in p-type Si samples and diffused in at 1075 °C for 100 min, giving B doping concentrations in the range $1–9 \times 10^{19}$ B/cm^3. Then 4.5×10^{16} H/cm^2 was implanted. We observe that the number of displacements is reduced at the H implant depth for B concentrations $\geq 3 \times 10^{19}$ cm^{-3}. On the other hand, the RBS/C yield in the surface layer above the H-implanted region increases instead. Giving the usual interpretation to the RBS/C yield in that region, namely a macroscopic deformation of the lattice (Section 3.3.2), this demonstrates that B doping promotes the formation of blister precursors. The corresponding maximum strain is estimated as 0.7% [101]. Moreover, Lee et al. [103] showed that when the boron is not activated after implantation the reduction in backscattering is even more significant (and as we saw blistering is even more strongly favoured). Similar observations have been made by Henttinen [49]; in addition, they found there was no reduction in backscattering in

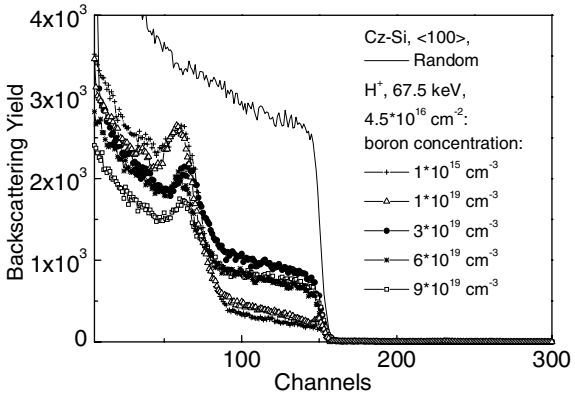

Fig. 32 Comparison of the backscattering spectra of H-implanted Si for different B concentrations: damage peak around channel 60 and near-surface deformation in channels 90–150 (from Popov et al. [101], by permission).

compensated samples heavily doped with both As and B. Finally, when B is implanted after H implantation, the damage profile is much more intense than with H alone or B alone [99]. The width of the profile looks like that of the boron primary defect production profile and indicates that an abnormally large fraction of the primary defects survive. This effect can only be due to the presence of the previously implanted H, which captures and stabilizes the B-ion-induced point defects. In the process, the blister-precursor complexes are destroyed.

Desrosiers et al. [98] found very different Raman spectra in heavily B-doped wafers, compared to undoped or Sb-doped Si, see Fig. 33. The low wave number modes, characteristic of multivacancies and interstitial defects, are much weaker in B-doped Si. Moreover, these low-k modes disappear at much lower temperature, i.e. ~200 °C instead of 300 °C with H alone, and the evolution towards the typical blistering configuration of dominance by Si(001):H and V_2H_6 is much more rapid. These results thus provide additional evidence that the important defects are those with a high ratio of H per vacancy. Another feature of the Raman spectrum that is equally noteworthy is the absence of any B–H line. This is in contrast with plasma-hydrogenated B-doped Si, in which there is a very conspicuous line at 1870 cm^{-1} [104], due to the stretch vibration of H trapped in a bond-middle site (slightly off the bond-center), between a Si atom and a substitutional B atom (B_{sub}). This absence in implanted B-doped Si indicates either that other traps are much more attractive or possibly that there are few substitutional B atoms available, see next.

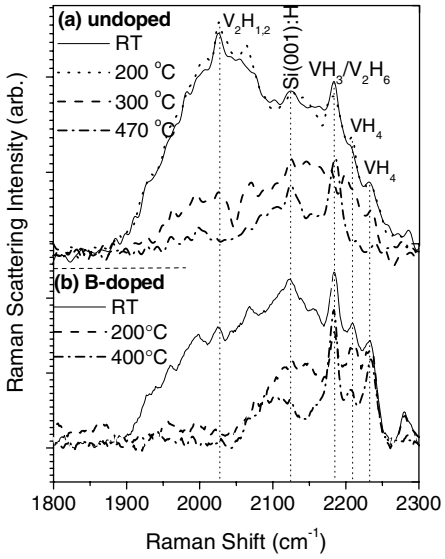

Fig. 33 Si–H stretch mode region of Raman spectra of Si after H ion implantation and annealing at the indicated temperatures: 2×10^{16} H/cm^2 in undoped Si (a); 1.5×10^{16} H/cm^2 in B-doped 10^{-3} Ω cm Si (b). (From Desrosiers et al. [98].)

4.2.3 B atom lattice location; the structure of irradiated B-doped Si

Some hints as to how boron can have such baffling effects on defect development and ultimately on blistering may be found in the atomic level structure of irradiated B-doped Si. The Catania group [105] has discovered a particular mechanism which operates in B-doped Si under any type of irradiation including H and B implantation. The excess self-interstitials (SI's) quickly latch onto the B_{sub} atoms with a binding energy of 0.9 eV (favoured by the small atomic radius of B, 0.117 nm, compared to Si, 0.146 nm). In this state, the B atom is mobile and upon encountering another B_{sub} (the distance between B atoms is only ~2 nm in highly doped Si), it forms a stable and immobile B–B complex. It has been determined that essentially all the B is incorporated into such structures as soon as the SI fluence reaches a few 10^{16} SI/cm^2. Since H ions of tens of keV produce ~10 SI/ion [43], the critical SI fluence is largely exceeded for blistering doses. It is important to note that this structure is also that of B-implanted Si before activation annealing. Thus H-implanted B-doped Si is deactivated and its structure not so different from that of B-implanted, non-activated Si.

Moreover, the lattice location of the B atoms in these complexes has been determined by measuring the yield of the $^{11}B(p,\alpha)^8Be$ reaction induced by protons channelled in ⟨001⟩ and ⟨110⟩ axial directions. Figure 34 [106] displays the channelling angular scans for both proton-irradiated B-doped Si (□) and for B-implanted Si (■). One can see, first, that both channels display considerably increased yields (□, ■) in the middle of the channels, compared to unirradiated activated B-doped Si (○) or to the silicon backscattering yield (◆). This demonstrates a strong presence of B interstitials in the channels; actually, essentially all the B atoms are so displaced. Secondly, there is little difference in yield between H ion irradiation of (previously activated) B-doped Si (□) and B implantation in undoped Si (■). Thirdly, the yields in the middle of the ⟨001⟩ and ⟨110⟩ channels reach ~65% and 50% respectively. Detailed analysis of the curves shows that they are consistent with the two B atoms being aligned along [100] directions in classic split-interstitial fashion. The 65% level (~2/3) indicates that those B–B pairs aligned along the ⟨001⟩ direction are shadowed by the ⟨001⟩ rows of Si atoms. The annealing behaviour of these complexes is interesting. In the case of H ion irradiation, the $^{11}B(p,\alpha)^8Be$ yield starts to decrease around 200 °C and is complete at 500 °C (although the full electrical activity is only recovered at 700 °C). In the case of B ion implantation, the yield first increases, between 400 °C and 700 °C, and only decreases at 900 °C (together with the recovery of the B activation); this is explained as due to the high level of SI oversaturation [106].

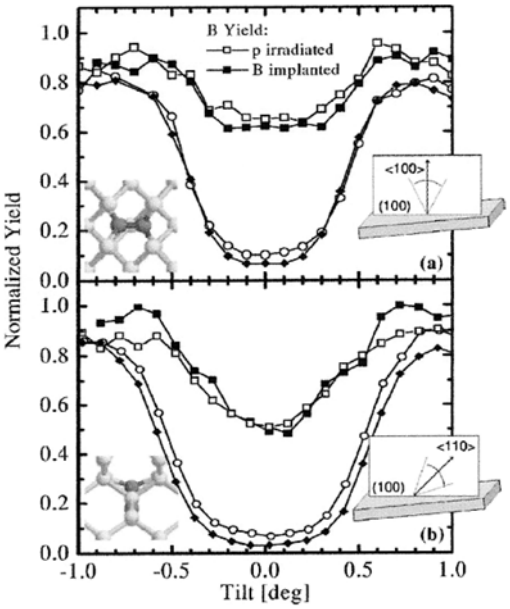

Fig. 34 Angular scans of the yields of $^{11}B(p,\alpha)^8Be$ reaction for protons channelled along the ⟨001⟩ (a) and ⟨110⟩ (b) axes; the elastic backscattering yields are also plotted. The symbols refer to H ion irradiated B-doped Si (□), B implanted Si (■), unimplanted activated B-doped Si (○) and backscattering (◆). (From Romano et al. [106], by permission.)

4.2.4 Discussion

The absence of B–H IR modes indicates that a form of chemical trapping of H by B is not likely involved in the blistering facilitation. Rather, the lattice location work suggests the hypothesis outlined in the following. The formation of each B–B pair eliminates one SI, which is henceforth unavailable for recombination or H atom trapping. The damage structure is thus modified, compared to undoped Si, witness the backscattering data (Fig. 32). Moreover, the presence of the B–B split interstitials necessarily produces a compressive stress; since the B atom concentration is $>10^{-3}$ in highly doped Si, the resulting strain is probably also of order 10^{-3}, in any case not negligible compared to the strain without B (fraction of %, Table 3 and Section 3.6). The depth distribution of the strain is also probably modified. In view of the demonstrated importance of the stress and strain for platelet nucleation, it is proposed that it is the strain field resulting from the presence of the B–B pairs that is particularly conducive to the formation of platelets, to the detriment of the weakly hydrogenated multivacancies, as seen in the Raman spectra (Fig. 33). This hypothesis could be tested by strain measurements.

This proposed mechanism brings the following remarks.

(1) The fact that the change in the damage structure outlined above modifies the backscattering yield (Fig. 32) is not surprising but it is not self-evident that the change should be a decrease in yield. For that purpose, one would have to understand first what is the exact source of the displacement damage in undoped Si. Then theory could perhaps be used to compute the respective RBS/C yields.

(2) If substantial effects are seen in properly activated B-doped wafers, it is because the subsequent proton bombardment actually deactivates the boron. And the significant difference in annealing behaviour between H-irradiated B-doped Si and B-implanted Si constitutes a natural explanation for the significant difference in blistering behaviour between activated and non-activated B-doped Si.

(3) The evolution of the Si–H stretch modes at considerably lower temperature with boron implies a lower stability for the low-*k* multivacancies. This is likely due to smaller clusters. If the hypothesis stated in Section 3.9 is correct, namely that the H released by the multivacancies is responsible for the huge rise in the backscattering yield at intermediate temperature, then a testable consequence follows: with B doping, the increase in displacements will occur at lower temperature (~200 °C) and it will be less impressive than without B doping.

(4) The apparent constancy of the blistering activation energy is more puzzling: The lower blistering temperature then implies a purely kinetic acceleration of the process. A possible explanation is as follows. Assume the rate-limiting process in blistering is H diffusion in the presence of traps (Sections 2.3.1 and 3.4.2). The lower backscattering yield with B suggests a lower trap density and then clearly the process will be accelerated. The possible weakness in this argument is that the precise nature of the defect that generates the displacement field is not known and it is not clear that it constitutes a trap for H.

(5) All IR studies show fewer H atoms bound to Si, and B–H bonds are not seen. Where is the missing H? Kilanov et al. assume that it is in the form of H_2. But we have seen that the H_2 appears to be bound in multivacancies at RT, which are precisely the defects that are depleted with B doping. However, the H_2 stretch region has not been studied by Raman scattering under B doping, and its quantification is in any case a difficult operation; it certainly deserves future work.

(6) When B is post-implanted in H-implanted undoped Si, the damage level is very high and blistering inhibited. It must be due to the capture of either the vacancies or the self-interstitials by some of the H-related defects present. If it is vacancy capture by vacancy clusters, that will give an observable enhancement in the low-*k* IR modes. If it is SI capture by the platelets, that would lead to a reduction in their size; that question would be studied best by TEM, and also by IR spectroscopy (Si(001):H peak).

(7) The compensation effect poses an interesting question. It would be worth finding out if the interstitial mechanism described in Section 4.2.3 does take place in that case, and whether the B–B pairs are formed or not in samples heavily co-doped with As and B.

Additional or alternate mechanisms have been proposed. One is the catalytic formation of H_2 by B interstitials [101]. It is argued that the B dangling bonds can capture not only free H atoms but also H from wandering IH_2 and VH_2 defects (presumably above 200 °C), and later release them as H_2. However,

we have seen that all the B is in the form of B–B pairs devoid of dangling bonds. Finally, the absence of IR lines due to B–H stretch modes and the compensation effect appear consistent with a direct effect of the Fermi level on the rate-limiting step [107]. So far, B-doping has been the only means of p-type doping studied. Therefore, modifying the Fermi level without using boron might be a way to settle that question.

4.3 Effect of He ion coimplantation

4.3.1 Threshold dose reduction; synergistic effect of He pressurizing of platelets

He ion implantation does not easily cause Si blistering, a dose on the order of $\sim 2 \times 10^{17}$ He/cm^2 is required for that purpose. It was then a surprise when Agarwal et al. [108] discovered that successive implantations (so-called coimplantation) of H and He ions allowed blistering at considerably lower total ion dose than H ions alone. This type of *hydrogen engineering* can of course save time and implies no unwanted doping since He is electrically inert. Helium can also be flushed out afterwards at ~800 °C. Figure 35 shows the threshold total ion doses obtained by Agarwal et al. as a function of the H ion fraction. The optimal H:He ratio is about 1:1, the minimum was obtained with 0.75×10^{16} H/cm^2 followed by 1×10^{16} He/cm^2; this compares to $\sim 4 \times 10^{16}$ H/cm^2 for H alone (Section 2.1) at the energy they used, namely 30 keV for H (and 33 keV for He). Intriguingly, implantation in the reverse order (He first) did not allow quite as low a total dose. Using 5 keV H and 8 keV He ions, Moutanabbir & Terreault [109] found that the He ions, rather than the H ions, had to be implanted first to get the lowest blistering threshold, i.e. 0.2×10^{16} He/cm^2 followed by 0.6×10^{16} H/cm^2. The reverse combination failed to give blisters for total doses as high as 3×10^{16} /cm^2.

The confusion about the implantation order for easy blistering was clarified by Lagahé-Blanchard et al. [110] who compared the kinetics of splitting for coimplantations of He ions of 32, 60 and 145 keV together with H ions of fixed energy, i.e. 32 keV, in both orders. For 32 keV He, for which the He implant depth is about 2/3 of the H implant depth, the splitting kinetics were faster with H first; for 60 and 145 keV He ions, which are implanted deeper that the H, the reverse was true. Note that the magnitudes of these effects, whether on the threshold dose or on the kinetics, are relatively modest when H is implanted deeper, but are quite dramatic when He is deeper. The deeper ion must therefore be implanted first to facilitate blistering: This indicates that if the second implant runs through the first implant, it will destroy some of the complexes that favour blistering, especially if it is a He ion. For the sake of brevity, the implantation order with the deeper implant first will be called "DF order" and the other one "DL order". An investigation [110] of the splitting kinetics in the DF order showed the following: (i) The kinetics are independent of the depth of the He implant, in other words He diffusion is not a rate-limiting factor. (ii) Splitting is faster at higher H and/or He doses, the activation energy varying between 1.8 and 2.5 eV. There is an exception: for a high He dose of 3×10^{16} He/cm^2, the He should not be implanted too

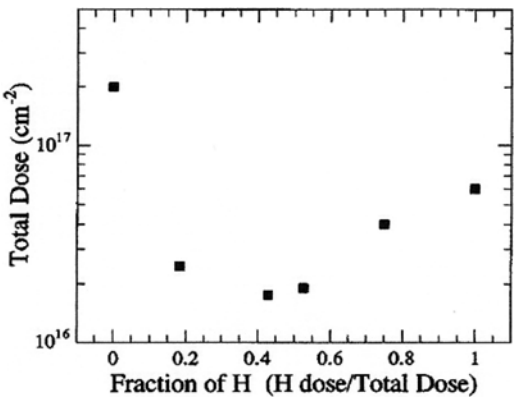

Fig. 35 Total (H + He) implantation dose necessary for blistering as a function of the H/(H + He) fraction (from Agarwal et al. [108], by permission).

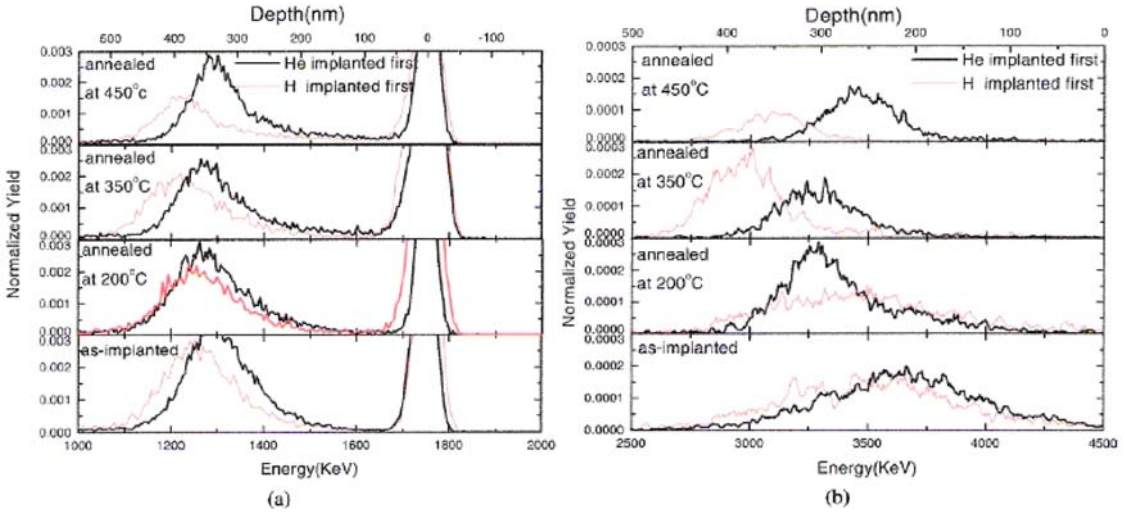

Fig. 36 (online colour at: www.pss-a.com) Normalized H (a) and He (b) depth distributions in coimplanted Si, as-implanted and after annealing at the indicated temperatures for 1 h. Solid (black) lines: He implanted first; dotted (pink) lines: H implanted first. In the H profiles the peak at ~1.75 MeV is due to surface contamination (from Duo et al. [113], by permission).

deep because in that case it forms very stable bubbles and fails to diffuse back to the H depth. On the other hand, if there is too much overlap between the H and He depth distributions, the ion-cut surfaces are rougher [111].

The He is actually observed to migrate to the H-rich (and platelet-rich) region during annealing, as shown by Weldon et al. [112] using SIMS and Duo et al. [113] using ERD. The last data are shown in Fig. 36. When the ions are implanted in the DF order (here H first since the H is deeper), upon annealing the He peak moves from ~220 nm to ~400 nm to match the H profile. If implanted in the DL order, the He only succeeds in moving half-way before being retrapped by some defects. The inverse motion of He from a large depth to a meet a shallow H implant was also observed [112]. Supposing the He to have been initially located in an interstitial site, it is obvious that its capture by a platelet will result in a large reduction in the free energy; and if it was trapped in nm-size bubbles, which is normal for He implantation, the driving force for capture by platelets must be a reduction in the strain energy (Eq. (3), Section 3.1.2). Once in the platelets, He is of course a formidable pressurizer since (i) it is not wall-adsorbed and (ii) it gives twice as much pressure as H_2, per atom. When the H and He are deliberately implanted at the same depth, the He still moves: its profile has been observed to sharpen by a remarkable factor of ~3 to coincide with the peak of the H profile [72].

4.3.2 Defect evolution

Coimplantation can have remarkable effects on the backscattering yield of as-implanted samples, compared with H-only implantation. With H (30 keV) implanted deeper and He (33 keV) shallower, Duo et al. [113] actually found little effect of implantation order on the RBS/C spectra. On the other hand, with H (5 keV) shallower and He (8 keV) slightly deeper, Moutanabbir et al. [71] observed very considerable differences. With He first (Fig. 37(a)), the damage level at RT or 200 °C is unmeasurably low (compare with, e.g., Fig. 13). This shows that the preimplanted He interacts with the "hot" defects produced during the H implantation to form preferentially the type of complexes giving blisters, probably He containing platelets, and to form less of those defects that cause backscattering. Upon annealing, the RBS/C yield rises remarkably strongly up to 600 °C. The shuttle motion of the peak (Section 3.3.2) is also visible, and at 600 °C in particular, the near-surface enhancement due to blisters [72] is clearly pre-

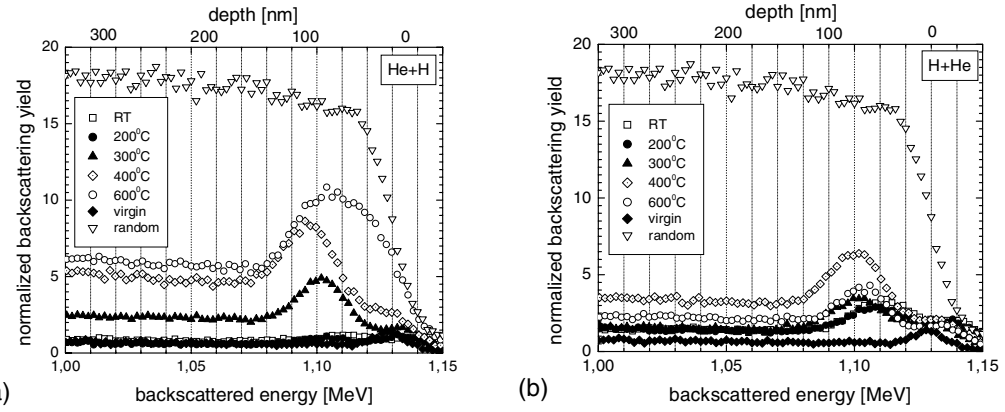

Fig. 37 Normalized RBS/C spectra for Si coimplanted with 0.7×10^{16} H/cm^2 at 5 keV and 0.25×10^{16} He/cm^2 at 8 keV, as-implanted and after ramp annealing at 0.33 K/s up to the indicated temperatures: (a) In DF order (He first); (b) in DL order (He last). (From Moutanabbir et al. [71].)

sent. When He is implanted last (Fig. 37(b)), the RT damage level is the same for 0.7×10^{16} H/cm^2 as for 2×10^{16} H/cm^2 alone. This indicates that some complexes, probably small vacancy and interstitial clusters, left over from the previous H irradiation, act as nuclei for the capture and stabilization of point defects generated during the subsequent He irradiation: this has the effect of generating larger clusters. Note that this mechanism is favoured by the fact that the peak in the distribution of He-ion-produced Frenkel defects is quite close to the peak in the H concentration, where one finds the H-stabilized defects. Contrary to the case of He first, annealing does not produce a very large increase in the peak yield, and above 400 °C the yield drops to a low value. This scheme proposed for He deeper turns out to be also consistent with the absence of order effect in the RBS/C spectra when He is shallower [113]. Indeed, in that case, the DL order is the one in which H ions go through the He implantation profile, but (i) there are fewer clusters left over from the He irradiation because they are not H-stabilized, and (ii) the passage of H ions produces much fewer Frenkel defects than He ions. This peculiar synergistic effect is thus not symmetric at all.

Weldon et al. [112] had remarked that the IRAS spectra for 1×10^{16} cm^{-2} each of He and H were already similar to those for 6×10^{16} H cm^{-2} (Fig. 16, Section 3.4.1), and much more "advanced", at the same temperature, than those for the same total dose of 2×10^{16} H cm^{-2} alone (Fig. 18). They also found that the integrated amount of Si–H bonds did not decrease until 500 °C, instead of 300 °C for H alone. This is consistent with the higher global gas retention found by thermal desorption spectroscopy [109]: He alone (at the low dose of 0.25×10^{16} He/cm^2) is released at ~200 °C, H alone and He in DL order at ~600 °C, and He in DF order at ~800 °C. For He deeper, Lagahé-Blanchard et al. [110] found in their IR spectra a profound difference between DF and DL implantation, as shown in Fig. 38. At RT, the basic difference is that, for the DL order (Fig. 38(b)), the sharp lines have practically all disappeared and in particular the ones at ~2160, ~2180 and ~2208 cm^{-1} (V_2H_6 and VH_4). The spectrum is more typical of amorphous silicon. Under annealing the spectrum does not evolve rapidly enough towards the elimination of low-k modes and the dominance of strong peaks around 2100–2120 cm^{-1} (internal surfaces) and 2160 cm^{-1} (V_2H_6), and the H is released before any platelet agglomeration can take place. Similar observations were made by Moutanabbir and Terreault [109] using RSS. For H deeper, on the other hand, the DL order has little effect on the IR spectra [112]. Roughly speaking, the synergistic effect is explained by He filling of platelets, provided platelets are given a chance to form. We see here in Fig. 38(a) that indeed the Si(001):H configuration (2100–2120 cm^{-1}) is present in abundance at high temperature for the DF implantation order.

Agarwal et al. [108] remarked that coimplantation in the DF order of a total dose of 2×10^{16} cm^{-2} produced as many platelets as 6×10^{16} H cm^{-2} alone. Tonini et al. [72] and Duo et al. [114] found these

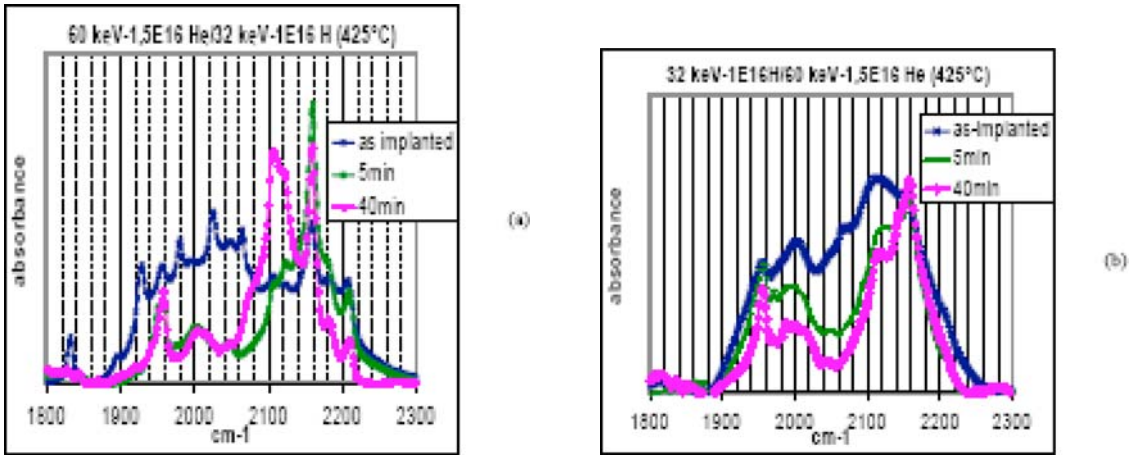

Fig. 38 (online colour at: www.pss-a.com) IRAS spectra of Si–H stretch mode region for Si coimplanted with H (32 keV) and He (60 keV), as-implanted and after annealing for the indicated times at 425 °C: (a) in "DF order" (He first); (b) in "DL order" (He last). (From Lagahé-Blanchard et al. [110], by permission.)

platelets to be surrounded by high strain contrast at high temperature, an indication of high pressure. In a comparative HRTEM study of the implanted layers for H only and for coimplantation in both orders, Nguyen et al. [111] found a higher density of microcracks for the DF implantation order, consistent with the ease of blistering. In the DL order, the damage zone was wider and denser and actually amorphous at higher dose, see Fig. 39. It can be seen that, if the dark regions retain crystalline order, the bright area is highly disordered. This is further demonstrated by the selected area Fourier transforms shown in the insets, where the c-Si diffraction pattern appears for the dark region but only diffuse scattering is seen for the bright area. These TEM observations of the RT damage are totally consistent with the results of

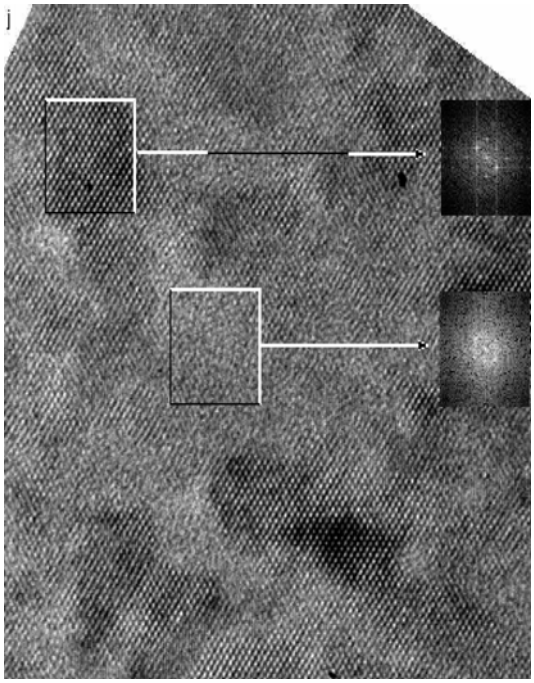

Fig. 39 Bright field HRTEM of Si coimplanted in DL order with H (30 keV) first and He (70 keV) next. The insets show selected area Fourier transforms: (top) from a dark area showing the diffraction pattern of c-Si, and (middle) from a bright area showing diffuse scattering from a-Si (from Nguyen et al. [111], by permission).

RBS/C (Fig. 37) and IRAS (Fig. 38) at RT. From the above observations, Nguyen et al. [111] elaborated a scenario for the inhibition of blistering in the DL order, compared to the DF order. The formation of platelets by the pre-implanted H ejects SI's, which are assumed to gather into small clusters. These would constitute the nuclei for the capture of the abundant SI's generated by the subsequent passage of the He ions, and these enlarged clusters in turn would be the embryos of the amorphous zones. It is well known that a-Si does not harbour platelets and does not blister. Therefore, platelets can only form deeper, past the amorphous layer, but necessarily at a higher dose.

4.4 Effect of isotope substitution

We have seen how the physical and chemical interactions between defects and hydrogen determine the evolution towards blistering. One can hardly modify the H–Si chemistry, but a conceivable way to influence, possibly control, and at least better understand blistering is to change the primary defect production rate by using deuterons (D) instead of protons. Because of more efficient collisional energy transfer, D ions indeed produce more than twice as many Frenkel pairs as H ions [28, 29].

4.4.1 Deuterium inhibition of blistering

The higher damage production rate of D ions could naively be expected to lead to better gas retention (just as He implantation does) and possibly to facilitate blistering. On the contrary, the threshold dose for D blistering was found by Moutanbbir et al. [3] to be more than twice that for H blistering, at least at the low energies (2–10 keV) investigated. This giant isotope effect is also present with boron doping [98] and with He coimplantation [109]. Figure 40 displays the minimum doses for blistering in the different cases. With n-type or lightly doped p-type Si, the doses are 1.75×10^{16} H cm^{-2}, 3.5×10^{16} D cm^{-2}, and 2.5×10^{16} (H + D) cm^{-2} for mixed implantation. With He pre-implantation, the minimum total dose is 0.8×10^{16} (He + H) cm^{-2} but at least 3×10^{16} (He + D) cm^{-2}. With 10^{-3} Ω cm B-doped Si, the numbers are 1×10^{16} H cm^{-2} and 2×10^{16} D cm^{-2}. At 100 keV, on the other hand, Bedell and Langford [42] report no significant H/D difference in the blistering thresholds. The main cause of the observed isotope effect is not "chemical" because the thermodynamics are not strongly affected: the blistering temperature is ~475 °C for H and ~500 °C for D in n-type or undoped Si. The TDS data also display only a small isotope effect, the release temperature is some 40 K higher for D_2 than for H_2. This ~5 % temperature difference corresponds to a 5% change in activation energy ($\Delta E_a \sim 0.1$ eV), consistent with the normal quantum zero-point energy effect.

4.4.2 Defect evolution

In Fig. 41 [71] is shown a comparison of the backscattering spectra from samples implanted with the same H and D doses (2×10^{16} cm^{-2}), either after RT implantation, or after annealing at the indicated

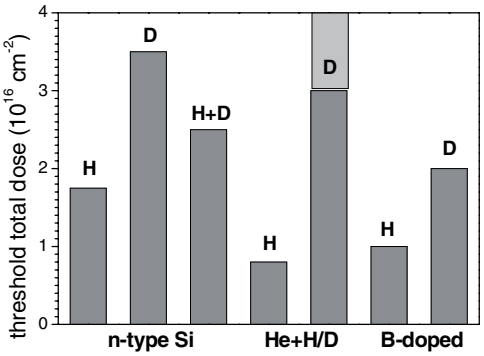

Fig. 40 Minimum total ion doses for blistering by 5 keV H and D and 8 keV He ions under different conditions: H alone, D alone, H + D, or He + H/D in n-type and low-doped Si; and in heavily B-doped Si (from Moutanabbir et al. [3, 109] and Desrosiers et al. [98]).

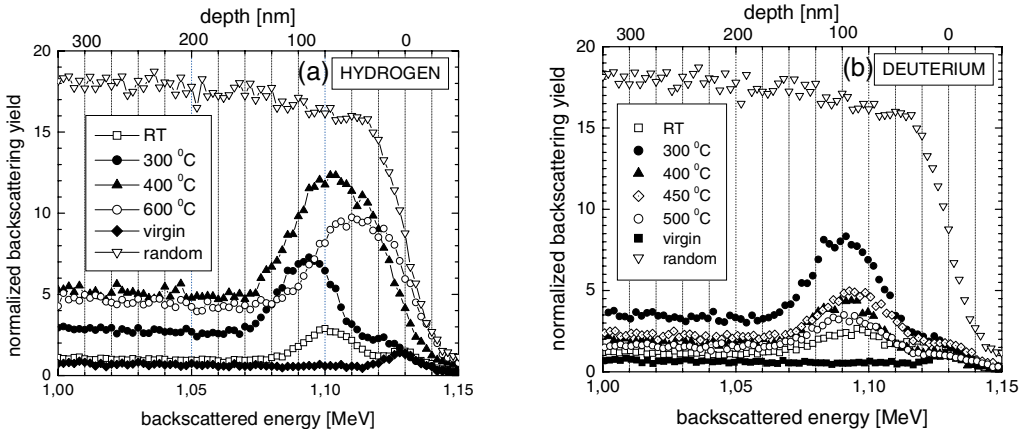

Fig. 41 ^{4}He backscattering spectra of samples implanted with 2×10^{16} H/cm^2 (a) or 2×10^{16} D/cm^2 (b), as-implanted and after ramp annealing up to the indicated temperatures (from Moutanabbir et al. [71].

temperatures. We first note that, at RT already, the peak yield for D is not anything like ~2.8 times higher than the peak yield for H, as would be expected from the defect creation rates at this energy [43], it is actually slightly lower. This indicates that it is not connected with the self-interstitials but that it is linked to the H or D atoms, which have comparable peak concentrations, with H having in fact the highest one [43]. The thermal evolution is similar for H and D up to 300 °C but diverges remarkably afterwards. While, for H, the reverse annealing process continues up to 400 °C, for D, it aborts above 300 °C – and there is no blistering. Both the peak yield and the dechannelling yield decrease above 300 °C for D. As we saw, the backscattering enhancement (for H) is connected with an increase in strain and with the transformations in Si–H and H–H bonding taking place at intermediate temperature. The back and forth motion of the peak is barely present for D; the near-surface enhancement, seen at 30–60 nm at the highest temperature for H, is absent for D. We recall that the shift in depth at intermediate temperature appears connected with a move between the damage peak R_d and the concentration peak R_p, while the shift towards the surface is due to blistering.

In Fig. 42 [115] is presented a comparison between the Raman spectra for samples implanted with H and D, for six particularly critical temperatures. A considerable difference between the Si–H and Si–D data is manifest at RT already. This difference therefore arises during the implantation: D atoms somehow interact in a different way than H atoms with the defects that are being continuously created. The D spectrum is bunched at low k values (multivacancies V_nD_m, and interstitial defects like ID_2). In contrast, the H spectrum has a balance of low-k and high-k modes; the latter are due to VH_4, V_2H_6 and Si(001):H. This difference in H vs. D can be understood by comparing the defect production rates during implantation: Since D produces ~2.8 times more vacancies per implanted ion than does H [43], we should expect to see a higher proportion of saturated vacancies for H than for D.

The differences become even more apparent after annealing. At 300 °C, while, for H, the low-k modes are strongly attenuated and the high-k modes clearly dominate, for D, the low-k modes are still the strongest. The higher stability of the V_nD_m compared to the V_nH_m suggests that they are made up of larger clusters. At 400 °C, the V_2H_6 mode at ~2180 cm^{-1} seems to have actually increased. During that time, the D sample has evolved only moderately. At 470 and 500 °C, blistering is well developed on H-implanted Si and the H spectrum is entirely dominated by the Si(100):H and the V_2H_6. The V_2D_6 have also finally emerged to some extent but not Si(100):D. At 550 °C, practically all the bound H has disappeared. Since the H is not all desorbed by far [44], it probably resides in the blisters. Another difference is the striking persistence of the low-k modes for D; they can only be due to weakly deuterated but particularly large and stable clusters of vacancies and interstitials. A higher average cluster size is consistent with radiation

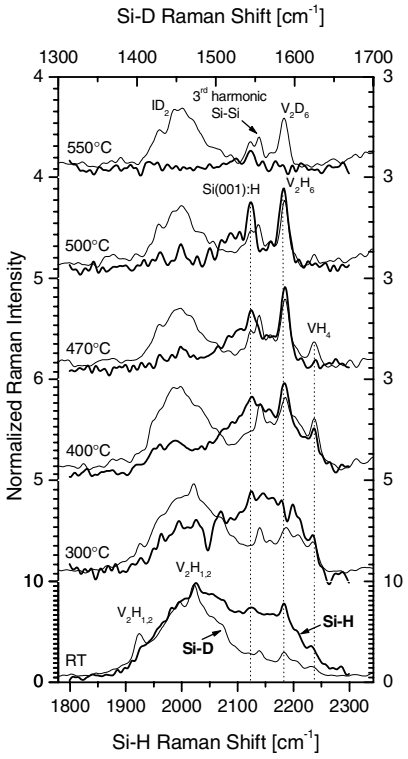

Fig. 42 Si–H (thick lines) and Si–D (thin lines) Raman spectra of samples implanted with 2×10^{16} H or D cm^{-2}, as-implanted and after ramp annealing up to the indicated temperatures (from Moutanabbir et al. [115]).

damage theory [28] since the primary defect production rate is higher. Their failure to release their D may be partly responsible for the absence of blistering.

But the main cause of that absence is probably the lack of high-*k* complexes at the very beginning, i.e. after implantation. Positron annihilation data actually suggest that large void volumes do appear around 475 °C in D-implanted samples but soon collapse without giving blisters for lack of sufficient gas pressure [71]. This may be a consequence of the greater rate of vacancy production for D vs. H: the great number of vacancies leads to void formation, but without sufficient gas available to stabilize them against annealing, whereas the smaller quantity of voids formed with H, with more gas available per void, survive to lead to blistering. It was suggested in Section 3.4.3 that, based on the high dose data in particular (Fig. 19), much of the "background" at high k was made up of imperfect but well hydrogenated platelet-like structures that eventually evolve or coalesce into "real" platelets. Indeed the Raman spectra for high D doses giving blistering (6×10^{16} D cm^{-2}) show relatively more high-*k* modes than at lower dose [81]. The H/D differences are also manifest in the H_2/D_2 stretch modes: while the 3820 cm^{-1} H_2 mode anneals out between 200 and 300 °C, the corresponding 2770 cm^{-1} D_2 mode only anneals between 300 and 325 °C [71]. This indicates a higher stability of the D-related multivacancy defects, in agreement with the Si–H/D data.

4.4.3 Discussion

The qualitative resemblance in the evolution, but not in the initial (RT) conditions, between all the Raman spectra – H or D [81], low or high dose [44, 81], with and without boron [98], with or without He [109] – suggests that eventual blistering is essentially a question of quantity: namely already having after RT implantation a sufficient amount of platelet-type complexes. A comparative TEM study of platelet production by H and D ions would constitute a good test of this hypothesis. The absence of significant isotopic difference in the blistering thresholds at 100 keV makes it imperative that the question be inves-

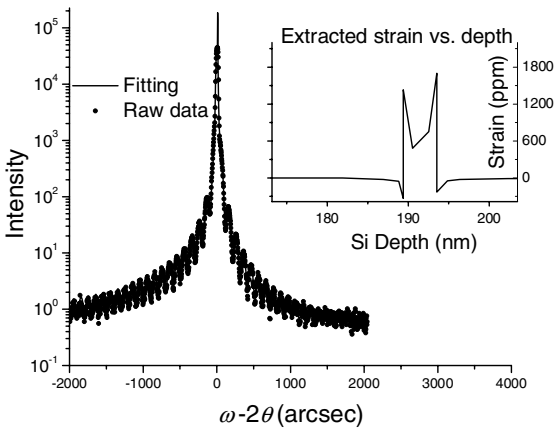

Fig. 43 X-ray $\omega-2\theta$ scans around the ⟨004⟩ diffraction peak on a MBE-Si/SiGe/Si structure. The inset shows the depth profile of the perpendicular strain extracted from the diffraction peak (from Shao et al. [121], by permission).

tigated at intermediate energies. If confirmed, a strong dependence on ion energy would imply that the type of RT-stable defects produced, and their eventual thermal evolution, depend sensitively on the characteristics of the collision cascade.

4.5 Plasma hydrogenation and artificially imposed strain

4.5.1 Trap creation by ion implantation and plasma hydrogenation

Usenko and Ulyashin [5] discovered in 2002 that, if a wafer was first pre-implanted to a definite depth with a small dose ($\leq 5 \times 10^{15}$ cm^{-2}) of Ar, He or H, and then hydrogenated at a few hundred degree C using a plasma at moderate bias (≤2 kV), blistering resulted. The depth of the craters indicated that the hydrogen was trapped somewhere between the peak in damage and the peak in concentration of the pre-implanted ions, depending on dose. The plasma hydrogenation can also be performed at somewhat lower temperature and followed by a high temperature anneal [116]. The study of the Raman spectra revealed interesting differences with conventional H ion implantation [116, 117]. After plasma hydrogenation the low-k modes due to multivacancies are practically absent, the high-k Si–H region is prominent though devoid of narrow peaks (somewhat like high dose implantation, Fig. 19), and H_2, both in multivacancies (3820 cm^{-1}) and gaseous (4160 cm^{-1}), is clearly seen. High temperature annealing leaves as usual only Si(001):H and V_2H_6. In a slightly different approach Chen et al. [118, 119] carried out a pre-implantation of boron instead of a gas and used (111) wafers. They showed by ERD that a H dose of 7×10^{15} cm^{-2} was trapped on the shallow side of the B peak (at ~0.8 R_p). This shows indeed that only really small H doses are necessary for blistering.

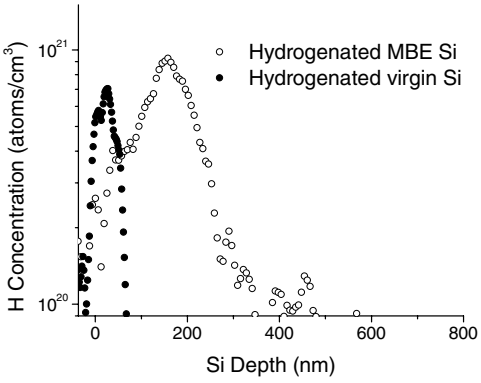

Fig. 44 Comparison between the H depth profiles in plasma hydrogenated MBE-Si/SiGe/Si structure and virgin Si (from Shao et al. [121], by permission).

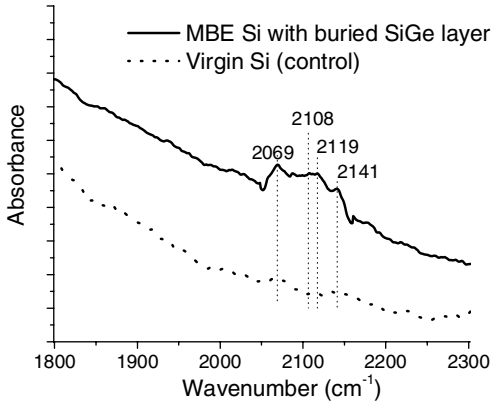

Fig. 45 Comparison between IRAS spectra in plasma hydrogenated MBE-Si/SiGe/Si structure and virgin Si (from Shao et al. [121], by permission).

4.5.2 Strained layer creation and plasma hydrogenation

The already cited work of Kilanov et al. [79] and that of Shao et al. [120] have shown that an interface such as a boron δ-layer [79], or a c-Si/epi-Si boundary [120], facilitated blistering, when H ions were subsequently implanted so as to peak at the interface depth. Interfaces create localized strain. In a series of reports, Shao and co-workers took this idea further. They fabricated a variety of structures by molecular beam epitaxy (MBE), consisting of MBE-Si on strained GeSi on Si [121], or MBE-Si on Sb-doped Si on Si [122], or MBE-Si on B-doped Si on Si [123]. In all cases, after plasma hydrogenation, H was trapped at the interface and produced microcracking and blistering or ion-cutting. The physics of the process will be illustrated by the case of Si/SiGe/Si [121]. The structure used had 190 nm of MBE-Si on 5 nm of SiGe. Figure 43 displays the X-ray measurement of the induced strain; the inset shows the depth distribution of the perpendicular strain extracted from the diffraction peak: a tensile strain of 0.12% appears on both faces of the SiGe layer. This strain value is definitely less than that obtained by ion implantation (0.3–1%), though its gradient is definitely very strong. When the wafer is exposed at 300–350 °C to a H plasma, the GeSi layer becomes a trapping center, as shown in Fig. 44. After 3 h of plasma exposure, the integrated trapped dose measured by ERD is $\sim 10^{16}$ cm^{-2}. This is several times less than required using H implantation, and smaller by a factor of ~2 compared to H implantation combined with heavy boron doping or He coimplantation. The IRAS spectrum (Fig. 45) comprises only LVM's due to H bound on extended internal surfaces (2060–2120 cm^{-1}) and a peak around 2141 cm^{-1} (presumed to be VH_2, see Table 1). The hydrogen is thus used very efficiently to generate the type of complexes that are essential for blistering, at the exclusion of low-k defects and even V_2H_6. In Fig. 46 are shown the XTEM micrographs of similarly plasma hydrogenated virgin Si (a) and the Si/SiGe/Si stucture (b). While in

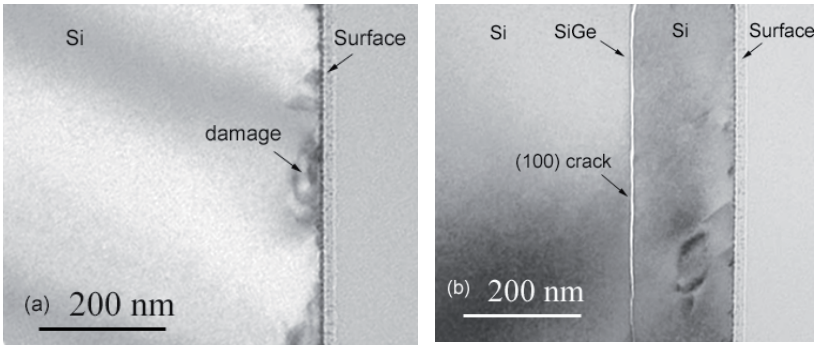

Fig. 46 Comparison between XTEM micrographs of plasma hydrogenated virgin Si (a) and MBE-Si/SiGe/Si structure (b) (from Shao et al. [121], by permission).

virgin Si only subsurface damage can be detected, in the Si/SiGe/Si stucture neat microcracking parallel to the surface has taken place at the depth of the SiGe layer.

5 Models and theories

The theoretical literature directly motivated by the blistering question is not abundant. It is of course a "messy" problem in which several steps are involved. There is no lack of theoretical work on hydrogen behaviour in silicon, but it does not frequently apply to blistering because the hydrogen is assumed to be dilute and/or to have been introduced in a "soft" manner with little or no radiation damage. For completeness sake, this background literature on H in Si will be very briefly recalled. Afterwards, theoretical and modelling work on different steps in blistering will be reviewed: H-defect interactions during RT implantation, platelet nucleation, and platelet evolution into blisters.

5.1 Background on hydrogen in silicon

A classic work is the set of first-principles calculations by Van de Walle [60] of the ground state energies of a number of hydrogen configurations in silicon, including H_2 molecules and H bound on the {111} surface or in some defect sites. His results are summarized in Table 5. The ranking is in general agreement with observations and confirms that vacancies and platelets are the most stable sites for H in irradiated Si. In the absence of defects, only H_{BC} (mobile at RT) and the two forms of H_2 can exist. Dopants such as B and P can also trap H. The values for Si–H on Si {111} are in a way misleading because the activation barrier to form internal surfaces is not included. Conspicuously absent from our point of view is H on {100} surfaces: the existence of (001) platelets, only seen after ion implantation, was barely acknowledged in 1994 because the {111} surface has in principle lower energy. One could also wish to see performed *ab initio* calculations of the differences in energy (per H atom) of the various vacancy complexes VH_n ($n = 1–4$) and V_2H_6, even if they are presumed to be small; even more ambitious would be energy calculations for the other relevant defects, multivacancies of various sizes and IH_2.

Several years later Jones et al. [21] reviewed the theoretical situation, this time with more emphasis on interstitial and vacancy defects and especially on the calculation of LVM frequencies for VH_n and V_2H_6. The calculated values of the mode wavenumbers are greater than the experimental values by 100–200 cm^{-1} in all cases. One pertinent new energy calculation is reported: the dissociation energy of VH_2 into V and H_2 would be 2 eV/H. Most interestingly, theory confirms the higher stability of V_2H_6 compared to VH_4 (and *a fortiori* VH_3), which was conjectured in Section 3.4.1, based on the annealing behaviour.

Table 5 Calculated values of different configurational energies for H in Si, per H atom, with respect to free H (adapted from Ref. [60]).

configuration	energy (eV)
neutral H in free space	0
H at BC site	−1.05
H_2^*	−1.65
H_2 at T_d site	−1.92
H–P	−2.04
H–B	−2.14
Si–H on {111}	−2.14
Si–H at isolated dangling bond (d.b.)	−2.17
H_2 in free space (or blisters)	−2.31
Si–H bound in preexisting vacancy	−3.15
Si–H at preexisting d.b.	−3.55
Si–H on preexisting {111}	−3.60

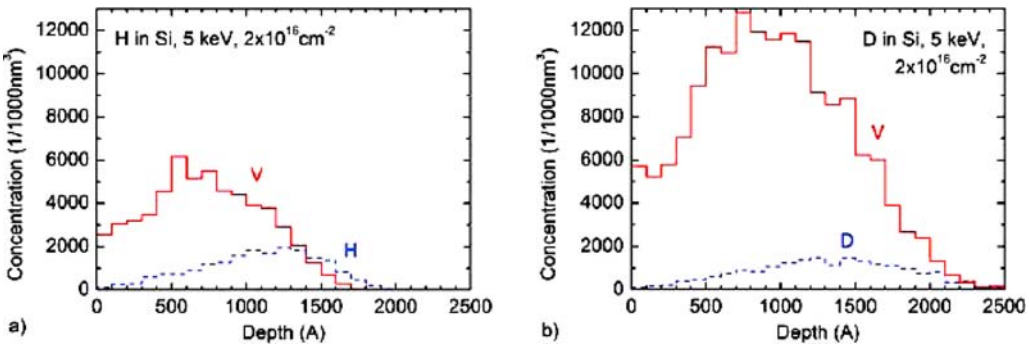

Fig. 47 (online colour at: www.pss-a.com) Compared H (a) and D (b) implantations at 5 keV in Si, as simulated by the binary collision code: depth profiles of ions (dashed lines) and generated vacancies (solid lines); the ion dose is 2×10^{16} cm^{-2} (from Zahel et al. [125], by permission).

5.2 Dynamic interaction of hydrogen with mobile defects during implantation

We have seen how the evolution of the defect structure under annealing depends on the initial mix of defects seen for example by IR spectroscopy. The initial RT defects result from (i) the creation of Frenkel pairs by the incident ion, and (ii) the interaction of all these "hot" species (H, V, I) with each other. Therefore theoretical calculations must treat these two phenomena simultaneously while the species are hot. The approach adopted by Hobler's group [124, 125] comprises binary collision simulation of the collision cascade and kinetic lattice Monte-Carlo (KLMC) simulation of H and defect diffusion and reactions. The term "lattice" means that atoms diffuse by hops between neighbouring sites in a real Si lattice. The time between two ion impacts is determined by the actual dose rate in the experiment to be simulated. The binary collision simulation yields the atomic positions of the implanted ion and the generated point defects, which are added to the defects from previous impacts. During the KLMC simulation the hot species migrate, form clusters or complexes or recombine. The different parameters such as the diffusivities are taken from *ab initio* calculations (e.g. [126, 127]).

Using this code, Zahel et al. [125] simulated the effect of the implantation of 5 keV H or D ions to a dose of 2×10^{16} cm^{-2}. Figure 47 shows the depth profiles of the H or D ions (dashed lines) and generated vacancies (solid lines) computed by the binary collision part of the code. We emphasize that these profiles are not those that would be observed following the RT implantation (though they would be at 0 K): they just indicate the concentrations and locations of these species before they start to migrate and react. We see that deuterons produce many more vacancies than protons. Now, in Fig. 48 is illustrated the temporal evolution of the different vacancy defects, as a function of the cumulative dose. (The assumed current density is 2 μA/cm^2 and the ions are incident along the ⟨001⟩ axis.) The actual quantities plotted are the numbers of H or D atoms bound in either mono- or multi-vacancies. First we see that a much smaller fraction of the generated vacancies survive when D is implanted than when H is. Even more interestingly, H atoms tend to be trapped in monovacancies whereas D atoms are mostly trapped in multivacancies. This is precisely what is observed experimentally, see Fig. 42. Another interesting point is that slightly more H atoms than D atoms are bound to vacancies of all types while more D atoms than H atoms are bound to intersitital defects (not shown). These facts are qualitatively consistent with the Raman spectra. The code also predicts the migration of vacancies towards the maximum in H concentration. There is no magic in these results, H and D have the same diffusion coefficients, binding energies, etc., it is simply the result of the high number of defects per ion for deuterium, which causes the hot defects to preferentially react with each other (clustering or annihilating) than with D atoms.

The simulation of platelet formation would constitute the next stage in the development of the code; this requires first principles information on the structure and configuration energy of platelets or platelet precursors, and a scenario for their nucleation. There is yet no consensus on these questions but they will

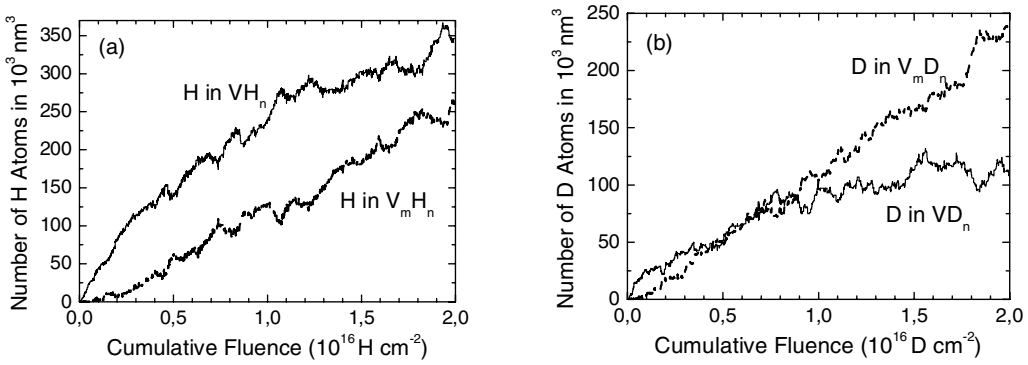

Fig. 48 Compared evolutions of vacancy complexes during implantation of 5 keV H (a) and D (b) ions in Si, as simulated by the full binary collision plus kinetic lattice Monte-Carlo approach. The numbers of H and D atoms bound to mono- or multi-vacancies are plotted as a function of the cumulative dose (from Zahel et al. [125], by permission).

be discussed in the next section. In view of the previous considerations (in Sections 3.6, 3.9 and 4.5), it is doubtful (001) platelets would spontaneously arise: the presence of strain has to be taken into account to favour nucleation in (001) planes. The fact that the simulation agrees semiquantitatively with experiment and provides an explanation for the giant isotope effect gives confidence in the validity of the approach. It is comforting to think that a reliable simulation tool, probably applicable to a host of problems, is available in order to predict the defect configuration resulting from RT implantation. The approach is in principle applicable to high temperature annealing but is presently hampered by the paucity of first principles data on the dissociation energies and rates for the various complexes.

5.3 Platelet nucleation mechanisms

Until recently one often referred to the theoretical work on {111} platelets (e.g. [128]) in discussing (001) platelets. However, it was difficult to see how the nucleation mechanisms proposed for the former applied to the latter. The many differences between these two types, for example the role of strain and the totally different behaviour of H_2 (appearing under annealing for {111} [129], disappearing [71, 84] and reappearing [11, 84] for (001)), have led some researchers to put forth specific scenarios and theoretical models for the (001) platelets.

5.3.1 VH_4 agregation mechanism

Reboredo et al. [130] proposed a platelet structure and a nucleation scenario based on calculations of configuration energies using density functional theory. It is assumed that the pre-platelet species present are the highly stable VH_4 and mobile H_2. The platelets grow progressively through the reactions:

$$VH_4 + H_2 + 2.5\ \text{eV} \rightarrow V_2H_6 + \text{SI}\ , \tag{4}$$

$$V_2H_6 + H_2 \rightarrow VH_4©VH_4 + 0.1\ \text{eV}\ , \tag{5}$$

$$VH_4©VH_4 + H_2 + 2.5\ \text{eV} \rightarrow VH_4©V_2H_6 + \text{SI}\ , \tag{6}$$

$$VH_4©V_2H_6 + H_2 \rightarrow VH_4©VH_4©VH_4 + 0.1\ \text{eV}\ , \tag{7}$$

and so on. Here the symbol "©" means that the hydrogenated vacancies are coordinated in the sense that they are next-nearest neighbours, as illustrated in Fig. 49. Note that the SI ejection steps of Eqs. (4) and (6) and higher order ones require an energy input. The calculations showed that: (i) the stablest configu-

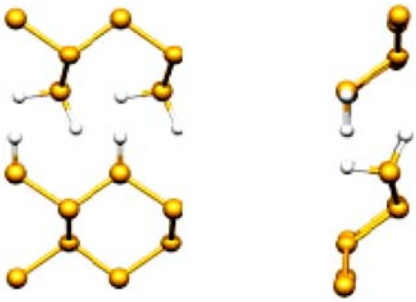

Fig. 49 (online colour at: www.pss-a.com) Structure of the $n[VH_4©]$ model of the {001} platelet (large yellow balls = Si, small white balls = H). On the right is an isolated VH_4, on the left a "canted" $VH_4©VH_4$ (adapted from Martsinovich et al. [133], with permission.)

rations for large arrays of ($nVH_4©$) are those with all the $VH_4©$ in a single {001} plane, and (ii) as the number of $VH_4©$ increases the total energy decreases. So, the $nVH_4©$ arrays were proposed as likely platelet precursors.

An objection to this model is the high activation energy (2.5 eV) required by Eqs. (4), (6), etc. In particular, it is difficult to explain the well attested presence of platelets at RT (Section 3.1.1) in this nucleation scenario. A second difficulty is that H_2 is not extremely mobile at RT, having a diffusion coefficient on the order of 10^{-16} cm^2/s [131], which translates into a diffusion time of 100 s for a distance of 1 nm. Atomic H is somewhat less sluggish, with a RT diffusion coefficient of 10^{-12} cm^2/s [126], but then two atoms would be required simultaneously. Finally, the rather early disappearance of VH_4 under annealing while V_2H_6 remains very strong (Figs. 16, 18, 33, 38, 42) is hard to explain in the scheme implied by Eqs. (4)–(7) in which, as the $nVH_4©$ arrays grow, the VH_4 become the dominant vacancy complexes, unless, possibly, the IR signature becomes that of Si(001):H quite early in the process. All this is very speculative. One thing is clear however, it is that the ejection of SI's will result in a compressive stress.

5.3.2 Role of the tensile strain

The facilitating role of the tensile strain has been emphasized earlier in Sections 3.6, 3.9 and 4.5. Lee et al. [91], following their earlier lines of thought [90], take the tensile strain for "granted" (caused by some unspecified defects). Upon annealing, the vacancies will regroup in dislocation loops with a gain in strain energy if the loop Burger's vector is parallel to the strain. Hydrogen will condense exothermally in the dislocations, thus giving 2-dimensional hydrogenated cavities. This mechanism depends on a net influx of vacancies into a narrow layer (where the blisters will appear). This layer being itself at the peak in damage, the concentration gradient will tend to drive vacancies away. Using measured values of the strain distribution, Lee et al. [91] calculated that the strain driven flux $[(DC/kT)\,(Y/1-\nu)\,\Omega(\mathrm{d}\varepsilon/\mathrm{d}x)]$ could overcome the concentration gradient flux $[-D(\mathrm{d}C/\mathrm{d}x)]$. (In these expressions D and C are the vacancy diffusion coefficient and concentration, T the absolute temperature, k Boltzmann's constant, Y, ν and Ω the Young modulus, Poisson ratio and atomic volume of Si, and ε the strain.) Both fluxes being linear in D and C, this could be done without knowledge of D and C, therefore only relative values are given. The necessary flux of H is not modelled either.

Swadener et al. [132] carried out a molecular dynamics study of the effect of strain on vacancy clusters. They compared the formation energies of planar {100} cavities with those of {111} and spherical cavities, with and without strain. Their most interesting result is shown in Fig. 50. The quantity plotted is the difference in energy between a {100} cavity and a spherical cavity, with strain present. (The strain was simulated by applying a 1% in-plane compressive strain and allowing the structure to relax.) It can be seen that, for cavities with 20 vacancies or less, planar {100} cavities are favoured. Since platelets are much larger than this (~10^3 vacancies), the authors propose the following scenario for their formation: (1) Small planar vacancy clusters are formed. (2) Hydrogen diffuses in and satisfies the dangling bonds; once this is done, the cavities are very stable and there is no more driving force to change to a spherical shape. In this respect, {100} arrays are favoured over {111} arrays because they have two dangling bonds per Si atom. (3) The cavities can now grow by Ostwald ripening and/or addition of free vacancies

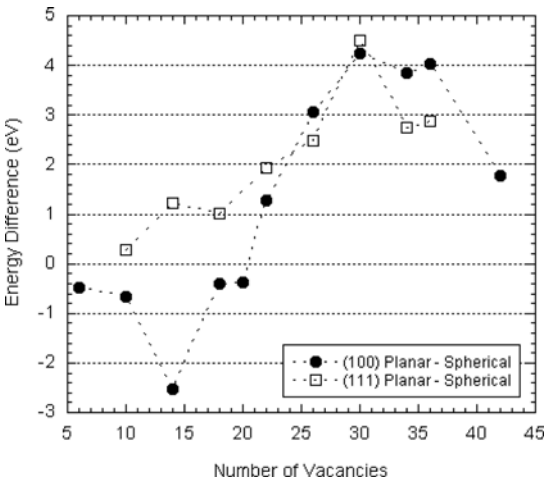

Fig. 50 Differences in total energy of formation between planar {100} and spherical vacancy clusters, and between planar {111} and spherical vacancy clusters, under a biaxial compressive stress in the {100} plane (from Swadener et al. [132], by permission).

together with H atoms. There is possible evidence for these small to medium-size hydrogenated cavities in the IR spectra (Figs. 16, 18, 33, 38, 42), both in the aptly called multivacancy hump centered on ~2000 cm^{-1} and in the "background" at $k > 2050$ cm^{-1} which possibly evolves into Si(001):H. On the other hand, the KLMC simulations (Section 5.2) do not predict the formation of many clusters larger than a few vacancies at RT. Taken together, the work of Lee et al. above and the last one offer a possible low activation energy scenario for platelet nucleation, but the origin of the strain is still nebulous.

5.3.3 Vacancy-less formation of hydrogenated internal surfaces

Martsinovich et al. [133] proposed hydrogen passivated {100} platelet structures that do not require vacancies or stress for their formation. Using density functional total energy calculations, they were able to show that several such structures are just as stable as {111} platelets, and deduced the most stable ones. The reason for their stability is the H passivation whose effect is included in the calculations, contrary to the preceding ones. The basic structures are shown in Fig. 51 and simply consist of Si–H or $Si–H_2$ decorated {100} planes that are separated by a dilation. What is necessary for their formation is breaking of Si–Si bonds by H insertion. In implanted material, many broken bonds are already present, which facilitates the process by minimizing the activation energy. Even more important, calculations showed that these structures can accommodate H_2 molecules exothermally in the interstices, in definite

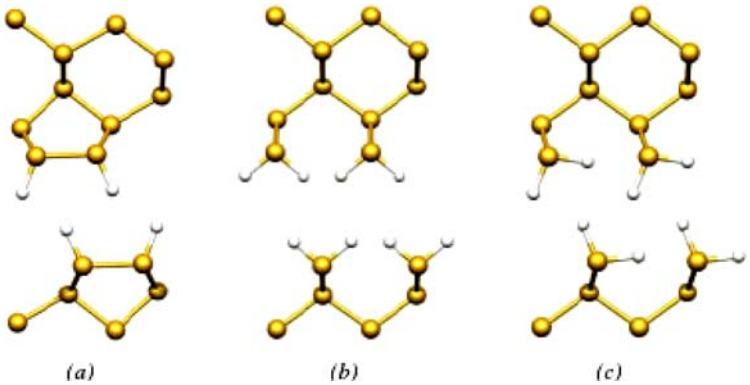

Fig. 51 (online colour at: www.pss-a.com) Structures of three different hydrogenated Si{001} surfaces: monohydride (a), symmetric dihydride (b), and canted dihydride (c) (adapted from Martsinovich et al. [133], by permission).

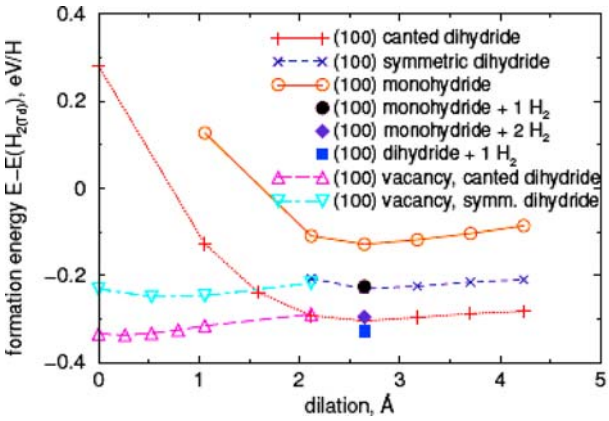

Fig. 52 (online colour at: www.pss-a.com) Energies, as a function of dilation, of hydrogenated Si{001} surfaces having various structures described in the text. The energies per H atom are referred to that of H_2 in the T_d site (adapted from Martsinovich et al. [133], by permission).

configurations that minimize steric hindrance. Finally, the authors also repeated, with a claimed higher precision, the calculations of Reboredo et al. (Section 5.3.1) of the energies of VH_4© agregates. The ensemble of their results are shown in Fig. 52. First, one can see that, with an optimal dilation of around 0.27 nm, stable structures are obtained; the most stable one is the dihydride with the canted structure (Fig. 51(c)) which minimizes the steric hindrance between H atoms. Second, H_2 molecules can be absorbed in all three structures without destabilizing them. Third, concerning the vacancy models, the new calculations show that they have energies very similar to those of the optimized vacancy-less structures, and that a canted structure (not considered by Reboredo et al.) has the lowest energy.

On stability grounds, one then cannot prefer vacancy or vacancy-less models; however the latter have the great advantage of not requiring the high activation energies implied by Eqs. (4) and (6). The vacancy-less models also face some objections. The TEM studies show no strain contrast around platelets: is this compatible with the strong dilation? Both types of models also result in platelet thicknesses ≤0.41 nm, compared to a measured value of ~1 nm. An interesting question for future work would be the calculation of the IR signatures of these structures. In view of the proximity of the two internal surfaces, how precisely will the Si(001):H IR lines be distorted? How about the Raman signature of H_2 trapped in such thin platelets? These calculations could presumably be carried out by the same approach employed by Lavrov and Weber [27] in the case of {111} platelets.

5.4 Final step: from platelets to blisters

There are no first principles calculations or simulation works yet on the intermediate steps of Si–H dissociation and reconfiguration, strain build-up, and platelet growth. There have been some attempts [134–137] at modelling the final steps of crack propagation and surface deformation, beyond Huang's [39] Eq. (2) in Section 2.2. These works have identified some relevant physical processes and parameters and refined oversimplified previous approximations; the most complete is Yang's paper [137]. Some of the predictions in these papers disagree with experiment and others are not verifiable because they involve not directly measurable quantities. When in qualitative agreement with experiment, the calculated trends were already predicted by simple physical intuition. In truth, the problem is too complex for analytic calculations. Some of the most obvious oversimplifications are the following. (i) The fraction of the implanted atoms that actually end up in blisters is not calculated: we know it is relatively small in most cases. (ii) Modification of the mechanical properties under irradiation is not taken into account. (iii) At the tip of the crack, molecular dynamics rather than continuum mechanics should be used and include the effect of hydrogen on Si–Si bonds. (iv) A suitable equation of state for H_2 at kilobar pressures has to be used instead of the ideal gas law, and its equilibrium with H chemisorbed on the walls and in the bulk modelled (as was done by Cerofolini [61] for He). (v) H_2 and/or H detrapping and diffusion has to be modelled.

6 Conclusions

The understanding of hydrogen blistering of silicon has progressed at a steady pace since 1990 and the last years have seen several scattered informations crystallize into solid science. The threshold dose is not fundamental because the actual useful gas amount can be as small as a few equivalent monolayers of H_2: all depends on how cleverly the gas is used. The upper dose is not basic either because one can have blistering, ion-cutting or swelling depending on the boundary conditions. The blister size and morphology indicate that the proto-blisters are nucleated at random points on the surface, from which point they expand in a roughly circular disc, without long-range interactions between them, until the gas pressure drives catastrophic microcracking. The phenomenological activation energy appears to be related to the scission of Si–H bonds but the evidence is not unquestionable: the dose dependence is still not satisfactorily explained.

Let us consider each step in the blistering process in succession.

Implantation step. – The implantations carried out at room or higher temperature and at cryogenic temperature demonstrate that both the point defects and the implanted H atoms are extremely active during or after the implantation (depending on the case). An abundance of Si–H complexes and also H_2 molecules are formed and, at RT and above, ~10 nm size platelets are already present. A significant part of this process, i.e. the formation of I_nH_m and V_nH_m complexes and H_2, can now be simulated with reasonable accuracy by kinetic lattice Monte-Carlo computations using only *ab initio* parameters, and can thus be considered understood. However, the simulation of platelet nucleation and growth has not been attempted yet, because only very recently have theoretical calculations of the properties of platelets with well-defined configurations become available. The implementation of a platelet nucleation scenario in a KLMC code (or in molecular dynamics?) would be highly valuable and is certainly a challenge.

Also not understood is the origin of the strain and of the displacement field measured by RBS/C, which is probably related to it. We do know from TEM and IR work the nature of some of the defects present, and theorists would probably be able to compute their contribution to the strain and the backscattering yield with the present tools. However, the defects corresponding to the "background" in the IR spectra are not well identified and the defects not related to H even less. Only meticulous and quantitative HRTEM and atom lattice location work using channelling appear possibly capable of giving a description of the configurations of these defects, from which the strain and the displacement field could be computed. Is this effort worth it? Indeed we do not really know how important the strain is for blistering. Sound physical arguments tell us that the out-of-plane strain must favour platelet formation. However, the causal relation is certainly not straightforward since the RBS/C yield at RT is lower in situations that are highly favourable to blistering like He coimplantation and B doping.

Multivacancy disappearance and the elusive hydrogen. – This step starts somewhere between 250 and 300 °C (or in the first minutes in high temperature isothermal annealing). It may not be essential for blistering (the RT platelets may already contain enough H); it could be only a sign of what is going on. Essential or not, multivacancy dissociation is in principle amenable to KLMC calculations, but not enough of the activation energies and kinetic factors are yet available for that. Worse, we do not know into what elusive form the liberated H is transformed. The techniques used so far provide no hint on the nature of the *elusive H*, therefore it would be worth trying H atom lattice location using axial channelling. Unfortunately, the (001) crystal only allows ⟨111⟩ and ⟨121⟩ channelling in the ERD geometry [138]; alternatively, NRA could be used allowing also ⟨001⟩ and ⟨110⟩ channelling. Or else, one could study the phenomenon by [100], [111] and [110] channelling in (111) crystals. Any argument or calculation that would explain the insensitivity of some particular H configuration to RSS and SIMS would of course be welcome, and would provide a target for the experimentalists to zero on.

Strain and displacement field buildup. – The coincidence in time or temperature suggests that the *reverse annealing* ensues from the H release just described. It may only be a "parasitic" phenomenon, or the generated strain may be crucial for platelet growth: although He coimplantation and B-doping give low RT RBS/C yields, they display high yield increases at high temperature. This should be confirmed by high temperature strain measurements. Understanding the *reverse annealing* requires identifying the

precise atomic configuration of damage at that stage, possibly including the *elusive H*, utilizing again HRTEM and lattice location techniques; so far, the single high temperature strain measurement only suggests that it is due to a defect with a relaxation volume of the order of 10 atomic volumes.

Ostwald ripening. – Complete thermodynamic characterization of that step should be an essential objective because in all probability it is the rate-limiting step. Fortunately, enough phenomenology is now known so that this step can be studied in isolation: it takes place in a definite time/temperature window while other processes are more or less frozen. In correlation with the strain and RBS/C data, that information may help in identifying the respective roles of the surface, strain and chemical energies in driving platelet growth. Unfortunately, it requires painstaking TEM work, but happily again, this technique allows much information about the precise, atomic level platelet geometry to be obtained at the same time. This can provide focus for the theoretical work: The proposed platelet models could be compared and possibly refined. In addition, it would be highly valuable to try and compute the IR signature of H_2 molecules trapped in such structures.

Microcracking and blistering. – This last step is considered "understood" because it involves almost only classical macroscopic physics, except for the desorption of H_2 in the cavities. However its detailed simulation must await a good atomic level description of the platelets and the other defects that can alter the mechanical properties of the substrate.

Let us now consider our understanding of special working conditions.

Crystal orientation effects. – These are understood in terms of the relative tendencies to generate platelets resulting from (i) surface energy effects, including H passivation, and (ii) the out-of-plane strain.

High dose effects. – The reasons for the high frequency shift of the IR spectrum, as well as the saturation of the RBS/C yield (and possibly the stress), all without amorphization, are not clear. TEM may allow testing the hypothesis that imperfect (and difficult to identify) platelet-like structures evolve into real platelets under annealing.

Implant temperature effects. – Higher temperature implantation does appear to facilitate blistering at lower dose, by promoting the evolution of the defect structures even more efficiently than annealing, at least as measured by RBS/C. This approach deserves more practical optimization work and better characterization by IR spectroscopy and other methods.

Boron doping. – An explanation for the facilitation of blistering is proposed in terms of the strain generated by the peculiar structure of the B interstitial defect in irradiated Si. It accounts for the enhancement in platelet formation, the reduction in RBS/C yield and the activation/non activation effects. It may also explain the effects of compensation and implantation in reversed order: this is testable using channelling by verifying whether the B–B split interstitial is formed or not. A direct electronic influence could be tested by modifying the Fermi level by other means than boron doping.

Helium coimplantation. – Blistering facilitation is understood as due to helium capture by platelets. The more subtle implantation order effect is also basically elucidated, except for a detailed description of how deep He post-implantation after shallow H implantation causes amorphization.

Deuterium implantation. – Blistering inhibition is understood through the excessive point defect creation rate which results in larger defect clusters and poorer passivation of the defects.

In all the above cases, comparative strain measurements at room and high temperature are highly desirable to establish the true role of the strain and confirm the above explanations or hypotheses.

Acknowledgements I would like to acknowledge first my INRS colleagues and students: Nicholas Desrosiers, Alexandre Giguère, Oussama Moutanabbir, Chao Qian and Guy Ross, and collaborators in other institutions: Martin Chicoine and François Schiettekatte (Université de Montréal), Peter Simpson (University of Western Ontario), Gerhard Hobler and Thomas Zahel (Technische Universität Wien). Many people have kindly responded to my precise enquiries and/or shared over the years their insights in sometimes lengthy discussions: Bernard Aspar, Konstantin Bourdelle, Michel Bruel, George Celler, Gianfranco Cerofolini, Yves Chabal, Alain Claverie, Ulrich Gösele, Tobias Höchbauer, Chrystelle Lagahé, Jung Kun Lee, Natalia Martsinovich, Michael Nastasi, Phuong Nguyen, Sandrine Rivillon, Lin Shao and particularly Aurélie Tauzin. And I omit several enlightening conference discus-

sions. I finally thank the numerous authors for their permission to reproduce figures and for kindly forwarding good quality graphic files for these figures.

References

[1] E. Ligeon and A. Guivarc'h, Radiat. Eff. **27**, 129 (1976).
[2] A. Giguère, J. Beerens, and B. Terreault, Nanotechnology **17**, 600 (2006).
[3] O. Moutanabbir, A. Giguère, and B. Terreault, Appl. Phys. Lett. **84**, 3286 (2004).
[4] M. K. Weldon, V. E. Marsico, Y. J. Chabal, A. Agarwal, D. J. Eaglesham, J. Sapjeta, W. L. Brown, D. C. Jacobson, Y. Caudano, S. B. Christman, and E. E. Chaban, J. Vac. Sci. Technol. B **15**, 1065 (1997).
[5] A. Y. Usenko and A. G. Ulyashin, Jpn. J. Appl. Phys. **41**, 5021 (2002).
[6] U. Gösele and Q.-Y. Tong, Annu. Rev. Mater. Sci. **28**, 215 (1998).
[7] A. Giguère and B. Terreault, Surf. Coat. Technol. (in press).
[8] L. Di Cioccio, Y. Letiec, F. Letertre, C. Jaussaud, and M. Bruel, Electron. Lett. **32**, 1144 (1996).
[9] I. Radu, I. Szafraniak, R. Sholz, M. Alexe, and U. Gösele, J. Appl. Phys. **94**, 7820 (2003).
[10] E. Jalaguier, B. Aspar, S. Pocas, J. F. Michaud, M. Zussy, A. M. Papon, and M. Bruel, Electron. Lett. **34**, 408 (1998).
[11] B. Aspar, H. Moriceau, E. Jalaguier, C. Lagahé, A. Soubie, B. Biasse, A. M. Papon, A. Claverie, J. Grisolia, G. Benassayag, F. Letertre, O. Rayssac, T. Barge, C. Maleville, and B. Ghyselen, J. Electron. Mater. **90**, 834 (2001).
[12] F. J. Kub, K. D. Hobart, J. M. Pond, and S. W. Kirchoefer, Electron. Lett. **35**, 477 (1999).
[13] L. J. Huang, Q. Y. Tong, and U. Gösele, Electrochem. Solid State Lett. **2**, 238 (1999).
[14] S. K. Das and M. Kaminsky, in: Radiation Effects on Solid Surfaces, edited by M. Kaminsky, Advances in Chemistry Vol. 158 (American Chemical Society, Washington, DC, 1976), p. 112.
[15] B. M. U. Sherzer, in: Sputtering by Particle Bombardment II, edited by R. Behrisch, Topics in Applied Physics, Vol. 52 (Springer, Berlin, 1983), p. 271.
[16] A. Giguère, N. Desrosiers, and B. Terreault, Appl. Phys. Lett. **87**, 211911 (2005).
[17] S. Romani and J. H. Evans, Nucl. Instrum. Methods B **44**, 313 (1990).
[18] S. J. Pearton, J. W. Corbett, and M. Stavola, Hydrogen in Crystalline Semiconductors (Springer-Verlag, Heidelberg, 1992).
[19] S. M. Myers, M. I. Baskes, H. K. Birnbaum, J. W. Corbett, G. G. DeLeo, S. K. Estreicher, E. E. Haller, P. Jena, N. M. Johnson, R. Kirchheim, S. J. Pearton, and M. J. Stavola, Rev. Mod. Phys. **64**, 559 (1992).
[20] S. K. Estreicher, Mater. Sci. Eng. R **14**, 319 (1995).
[21] R. Jones, B. J. Coomer, J. P. Goss, B. Hourahine, and A. Resende, Solid State Phenom. **71**, 173 (2000).
[22] C. Herring, N. M. Johnson, and C. G. Van de Walle, Phys. Rev. B **64**, 125209 (2001).
[23] R. E. Pritchard, M. J. Ashwin, J. H. Tucker, and R. C. Newman, Phys. Rev. B **57**, R15048 (1998).
[24] N. M. Johnson, F. A. Ponce, R. A. Street, and R. J. Nemanich, Phys. Rev. B **35**, 4166 (1987).
[25] J. N. Heyman, J. W. Ager III, E. E. Haller, N. M. Johnson, J. Walker, and C. M. Doland, Phys. Rev. B **45**, 13363 (1992).
[26] S. Muto, S. Takeda, and M. Hirata, Philos. Mag. A **72**, 1057 (1995).
[27] E. V. Lavrov and J. Weber, Phys. Rev. Lett. **87**, 185502 (2001).
[28] M. W. Thompson, Defects and Radiation Damage in Metals (University Press, Cambridge, 1969).
[29] M. Nastasi, J. W. Mayer, and J. K. Hirvonen, Ion-Solid Interactions: Fundamentals and Applications (University Press, Cambridge, 1996).
[30] M. Bruel, Electron. Lett. **31**, 1201 (1995).
[31] M. Bruel, Mater. Res. Soc. Bull. **23**, 35 (1998).
[32] G. K. Celler and Sorin Cristoloveanu, J. Appl. Phys. **93**, 4955 (2003).
[33] G. K. Celler (ed.), Silicon-on-Insulator Technology and Devices XII, ECS Proc., Vol. 2005-03 (The Electrochemical Society, Pennington, NJ, 2005).
[34] Q.-Y. Tong and U. M. Gösele, Adv. Mater. **17**, 1409 (1999).
[35] J. B. Boyce and M. Stutzmann, Phys. Rev. Lett. **54**, 562 (1985).
[36] Y. J. Chabal and C. K. N. Patel, Phys. Rev. Lett. **53**, 210 (1984).
[37] S. Agarwal, B. Hoex, M. C. M. van de Sanden, D. Maroudas, and E. S. Aydil, J. Vac. Sci. Technol. B **22**, 2719 (2004).
[38] X. Liu, N. W. Cheung, M. D. Strathman, P. K. Chu, and B. Doyle, Appl. Phys. Lett. **71**, 1804 (1997).

[39] L.-J. Huang, Q.-Y. Tong, Y.-L. Chao, T.-H. Lee, T. Martini, and U. Gösele, Appl. Phys. Lett. **74**, 982 (1999).
[40] T. Höchbauer, A. Misra, M. Nastasi, and J. W. Mayer, J. Appl. Phys. **92**, 2335 (2002).
[41] B. Aspar, C. Lagahé, H. Moriceau, A. Soubié, M. Bruel, A. J. Auberton-Hervé, T. Barge, and C. Maleville, Mater. Res. Soc. Symp. Proc. **510**, 381 (1998).
[42] S. W. Bedell and W. A. Lanford, J. Appl. Phys. **90**, 1138 (2001).
[43] J. F. Ziegler and J. P. Biersack, SRIM-2003 (www.srim.org).
[44] O. Moutanabbir, B. Terreault, M. Chicoine, and F. Schiettekatte, Appl. Phys. A **80**, 1455 (2005).
[45] A. Tauzin (CEA-LETI, Grenoble, France), private communication.
[46] O. Moutanabbir, B. Terreault, and G. G. Ross, Appl. Phys. Lett. **82**, 4675 (2003).
[47] W. Primak and J. Luthra, J. Appl. Phys. **37**, 2287 (1966).
[48] S. K. Das and M. Kaminsky, J. Appl. Phys. **44**, 25 (1973).
[49] K. Henttinen, T. Suni, A. Nurmela, I. Suni, S. S. Lau, T. Höchbauer, M. Nastasi, and V.-M. Airaksinen, Nucl. Instrum. Methods B **190**, 761 (2002).
[50] Q.-Y. Tong, K. Gutjahr, S. Höpfe, U. Gösele, and T.-H. Lee, Appl. Phys. Lett. **70**, 1390 (1997).
[51] K. K. Bourdelle, Ref. [33], p. 167.
[52] Y. Zheng, S. S. Lau, T. Höchbauer, A. Misra, R. Verda, X.-M. He, M. Nastasi, and J. W. Mayer, J. Appl. Phys. **89**, 2972 (2001).
[53] G. F. Cerofolini, R. Balboni, D. Bisero, F. Corni, S. Frabboni, G. Ottaviani, R. Tonini, R. S. Bruza, A. Zecca, M. Ceschini, G. Giebel, and L. Pavesi, phys. stat. sol. (a) **150**, 539 (1995).
[54] Nicholas Desrosiers and Bernard Terreault, Appl. Phys. Lett. **89**, 151922 (2006).
[55] G. F. Cerofolini, L. Meda, R. Balboni, F. Corni, S. Frabboni, G. Ottaviani, R. Tonini, M. Anderle, and R. Canteri, Phys. Rev. B **46**, 2061 (1992).
[56] B. Aspar, M. Bruel, H. Moriceau, C. Maleville, T. Poumeyrol, A. M. Papon, A. Claverie, G. Benassayag, A. J. Auberon-Hervé, and T. Barge, Microelectron. Eng. **36**, 233 (1997).
[57] M. Bruel, Mater. Res. Innovat. **3**, 9 (1999).
[58] S. Frabboni, Phys. Rev. B **65**, 165436 (2002).
[59] T. Akatsu, K. K. Bourdelle, C. Richtarch, B. Faure, and F. Letertre, Appl. Phys. Lett. **86**, 181910 (2005).
[60] C. G. Van de Walle, Phys. Rev. B **49**, 4579 (1994).
[61] G. F. Cerofolini, F. Corni, S. Frabboni, C. Nobili, G. Ottaviani, and R. Tonini, Mater. Sci. Eng. **27**, 1 (2000).
[62] J. Grisolia, G. Ben Assayag, A. Claverie, B. Aspar, C. Lagahé, and L. Laanab, Appl. Phys. Lett. **76**, 852 (2000).
[63] M. Bruel, Nucl. Instrum. Methods B **108**, 313 (1996).
[64] J. Weber, T. Fisher, E. Hieckmann, M. Hiller, and E. V. Lavrov, J. Phys.: Condens. Matter **17**, S2303 (2005).
[65] G. F. Cerofolini, L. Meda, C. Volpones, G. Ottaviani, J. DeFayette, R. Dierckx, D. Donelli, M. Orlandini, M. Anderle, R. Canteri, C. Claeys, and J. Vanhellemont, Phys. Rev. B **41**, 12607 (1990).
[66] T. Höchbauer, A. Misra, M. Nastasi, J. W. Mayer, and W. Ensinger, Nucl. Instrum. Methods B **242**, 623 (2006).
[67] T. Höchbauer, A. Misra, M. Nastasi, and J. W. Mayer, J. Appl. Phys. **89**, 5980 (2001).
[68] T. Höchbauer, A. Misra, M. Nastasi, K. Henttinen, T. Suni, I. Suni, S. S. Lau, and W. Ensinger, Nucl. Instrum. Methods B **216**, 257 (2004).
[69] D. Kovač and G. Hobler, Nucl. Instrum. Methods B **249**, 776 (2006).
[70] J. K. Lee, M. Nastasi, N. David Theodore, A. Smalley, T. L. Alford, J. W. Mayer, M. Cai, and S. S. Lau, J. Appl. Phys. **96**, 280 (2004).
[71] O. Moutanabbir, B. Terreault, M. Chicoine, F. Schiettekatte, and P. J. Simpson, Phys. Rev. B **75**, 075201 (2007).
[72] R. Tonini, F. Corni, C. Nobili, G. Ottaviani, F. Cazzaniga, and G. Queirolo, Solid State Phenom. **82–84**, 291 (2002).
[73] J. D. Holbech, B. Bech Nielsen, R. Jones, P. Stich, and S. Öberg, Phys. Rev. Lett. **71**, 875 (1993).
[74] B. Bech Nielsen, L. Hoffmann, and M. Budde, Mater. Sci. Eng. B **36**, 259 (1996).
[75] M. Budde, B. Bech Nielsen, P. Leary, J. Goss, R. Jones, P. R. Briddon, S. Öberg, and S. J. Breuer, Phys. Rev. B **57**, 4397 (1998).
[76] Y. J. Chabal, M. K. Weldon, Y. Caudano, B. B. Stefanov, and K. Raghavachari, Physica B **273/274**, 152 (1999).
[77] M. Budde, C. Parkes Cheney, G. Lüpke, N. H. Tolk, and L. C. Feldman, Phys. Rev. B **63**, 195203 (2001).
[78] E. V. Lavrov, J. Weber, L. Huang, and B. Bech Nielsen, Phys. Rev. B **64**, 035204 (2001).

[79] D. V. Kilanov, V. P. Popov, L. N. Safranov, A. I. Nikiforov, and R. Sholz, Semiconductors **37**, 620 (2003); translated from Fiz. Tekh. Poluprovodn. **37**, 644 (2003).
[80] C. Lagahé, B. Aspar, H. Moriceau, A. Sousbie, and T. Barge, 2001 IEEE Int. SOI Conf. Proc. (IEEE, 2001), p. 69.
[81] O. Moutanabbir and B. Terreault, J. Chem. Phys. **121**, 7973 (2004).
[82] K. Ishioka, M. Kitajima, S. Tateishi, K. Nakanoya, N. Fukata, T. Mori, K. Murakami, and S. Hishita, Phys. Rev. B **60**, 10852 (1999).
[83] T. Mori, K. Otsuka, N. Umehara, K. Ishioka, M. Kitajima, S. Hishita, and K. Murakami, Physica B **302/303**, 239 (2001).
[84] W. Düngen, R. Job, Y. Ma, Y. L. Huang, T. Mueller, W. R. Fahrner, L. O. Keller, J. T. Horstmann, and H. Fiedler, J. Appl. Phys. **100**, 034911 (2006).
[85] S. Personnic, A. Tauzin, K. K. Bourdelle, F. Letertre, N. Kernevez, F. Laugier, N. Cherkashin, A. Claverie, and R. Fortunier, Paper O601, 16th Int. Conf. on Ion Implantation Technology, AIP Conf. Proc., Vol. 866 (AIP, 2006), p. 65.
[86] A. W. R. Leitch, V. Alex, and J. Weber, Phys. Rev. Lett. **81**, 421 (1998).
[87] M. Hakala, M. J. Puska, and R. M. Nieminen, Phys. Rev. B **57**, 7621 (1998).
[88] R. S. Brusa, M. Duarte Naia, A. Zecca, C. Nobili, G. Ottaviani, R. Tonini, and A. Dupasquier, Phys. Rev. B **49**, 7271 (1994).
[89] M. Fujinami, R. Suzuki, T. Ohdaira, and T. Mikado, Phys. Rev. B **58**, 12559 (1998).
[90] M. Nastasi, T. Höchbauer, J.-K. Lee, J. P. Hirth, M. Ridgway, and T. Lafford, Appl. Phys. Lett. **86**, 154102 (2005).
[91] J.-K. Lee, Y. Lin, Q. X. Jia, T. Höchbauer, H. S. Jung, L. Shao, A. Misra, and M. Nastasi, Appl. Phys. Lett. **89**, 101901 (2006).
[92] N. Sousbie, L. Capello, J. Eymery, F. Rieutord, and C. Lagahé, J. Appl. Phys. **99**, 103509 (2006).
[93] A. L. Bement, Jr., R. G. Hoagland, and F. A. Smith, Jr., in Fracture: An Advanced Treatise, edited by H. Liebowitz, Vol. III (Academic, New York, 1971), p. 536.
[94] Y. Ma, Y. L. Huang, R. Job, and W. T. Fahrner, Phys. Rev. B **71**, 045206 (2005).
[95] Q.-Y. Tong, T.-H. Lee, L.-J. Huang, Y. L. Chao, and U. Gösele, Electron. Lett. **34**, 407 (1998).
[96] O. W. Holland, D. K. Thomas, and R. B. Gregory, Mater. Res. Soc. Symp. Proc. **647**, O6.1 (2000).
[97] Q.-Y. Tong, R. Scholz, U. Gösele, T.-H. Lee, L.-J. Huang, Y.-L. Chao, and T. Y. Tan, Appl. Phys. Lett. **72**, 49 (1998).
[98] N. Desrosiers, A. Giguère, O. Moutanabbir, and B. Terreault, Appl. Phys. Lett. **87**, 231908 (2005).
[99] A. Nurmela, K. Henttinen, T. Suni, A. Tolkki, and I. Suni, Nucl. Instrum. Methods B **219/220**, 747 (2004).
[100] T. Höchbauer, K. C. Walter, R. B. Schwartz, M. Nastasi, R. W. Bower, and W. Ensinger, J. Appl. Phys. **86**, 4176 (1999).
[101] V. P. Popov, V. F. Stas, and I. V. Antonova, Mater. Res. Soc. Symp. Proc. **540**, 109 (1999).
[102] J. K. Lee, T. Höchbauer, R. D. Averitt, and M. Nastasi, Appl. Phys. Lett. **83**, 3042 (2003).
[103] J. K. Lee, T. Höchbauer, R. D. Averitt, and M. Nastasi, Nucl. Instrum. Methods B **219/220**, 662 (2006).
[104] M. Stutzmann, Phys. Rev. B **35**, 5921 (1987).
C. P. Herrero, M. Stutzmann, and A. Breitschwerdt, Phys. Rev. B **43**, 1555 (1991).
[105] A. M. Piro, L. Romano, S. Mirabella, and M. G. Grimaldi, Appl. Phys. Lett. **86**, 081906 (2005).
[106] L. Romano, A. M. Piro, S. Mirabella, M. G. Grimaldi, and E. Rimini, Appl. Phys. Lett. **87**, 201905 (2005).
[107] U. Gösele (MPI, Halle, Germany), private communication.
[108] Aditya Agarwal, T. E. Haynes, V. C. Venezia, O. W. Holland, and D. J. Eaglesham, Appl. Phys. Lett. **72**, 1086 (1998).
[109] O. Moutanabbir and B. Terreault, Appl. Phys. Lett. **86**, 051906 (2005).
[110] C. Lagahé-Blanchard, N. Sousbie, S. Sartori, H. Moriceau, A. Sousbie, B. Aspar, P. Nguyen, and B. Blondeau, ECS Proc. **2003-19**, 346 (2003).
[111] Phuong Nguyen, I. Cayrefourcq, K. K. Bourdelle, A. Boussagol, E. Guiot, N. Ben Mohammed, N. Sousbie, and T. Akatsu, J. Appl. Phys. **97**, 083527 (2005).
Phuong Nguyen, K. K. Bourdelle, T. Maurice, N. Sousbie, A. Boussagol, X. Hebras, L. Portigliatti, and F. Letertre, J. Appl. Phys. **101**, 033506 (2007).
[112] M. K. Weldon, M. Collot, Y. J. Chabal, V. C. Venezia, A. Agarwal, T. E. Haynes, D. J. Eaglesham, S. B. Christman, and E. E. Chaban, Appl. Phys. Lett. **73**, 3721 (1998).
[113] Xinzhong Duo, Weili Liu, Miao Zhang, Lianwei Wang, Chenglu Lin, M. Okuyama, M. Noda, Wing-Yiu Cheung, Paul K. Chu, Peigang Hu, S. X. Wang, and L. M. Wang, J. Phys. D, Appl. Phys. **34**, 477 (2001).

[114] Xinzhong Duo, Weili Liu, Miao Zhang, Lianwei Wang, Chenglu Lin, M. Okuyama, M. Noda, Wing-Yiu Cheung, S. P. Wong, Paul K. Chu, S. X. Wang, and L. M. Wang, J. Appl. Phys. **90**, 3780 (2001).
[115] O. Moutanabbir, B. Terreault, M. Chicoine, P. J. Simpson, T. Zahel, and G. Hobler, Physica B **376/377**, 36 (2006).
[116] R. Job, W. Düngen, Y. Ma, Y. L. Huang, and J. T. Horstmann, Mater. Res. Soc. Symp. Proc. **864**, E10.2.1 (2005).
[117] Y. Ma, R. Job, W. Düngen, Y. L. Huang, W. R. Farmer, M.-F. Beaufort, S. Rousselet, and J. T. Horstmann, Appl. Phys. Lett. **86**, 252109 (2005).
[118] Peng Chen, Paul K. Chu, T. Höchbauer, J.-K. Lee, M. Nastasi, D. Buca, S. Mantl, R. Loo, M. Caymax, T. Alford, J. W. Mayer, N. Davis Theodore, M. Cai, B. Schmidt, and S. S. Lau, Appl. Phys. Lett. **86**, 031904 (2005).
[119] Peng Chen, S. S. Lau, Paul K. Chu, K. Henttinien, T. Suni, I. Suni, N. David Theodore, T. L. Alford, J. W. Mayer, Lin Shao, and M. Nastasi, Appl. Phys. Lett. **87**, 111910 (2005).
[120] Lin Shao, J. K. Lee, T. Höchbauer, M. Nastasi, Phillip E. Thompson, I. Rukasova, H. W. Seo, Q. Y. Chen, J. R. Liu, and Wie-Kan Chu, Nucl. Instrum. Methods B **242**, 509 (2006).
[121] Lin Shao, Yuan Li, J. K. Lee, Q. X. Lia, Yongqiang Wang, M. Nastasi, Phillip E. Thompson, N. David Theodore, Paul K. Chu, T. L. Alford, J. W. Mayer, Peng Chen, and S. S. Lau, Appl. Phys. Lett. **87**, 091902 (2005).
[122] Lin Shao, Yuan Lin, J. G. Swadener, J. K. Lee, Q. X. Jia, Y. Q. Wang, M. Nastasi, Phillip E. Thompson, N. David Theodore, T. L. Alford, J. W. Mayer, Peng Chen, and S. S. Lau, Appl. Phys. Lett. **87**, 251907 (2005).
[123] Lin Shao, Yuan Lin, J. G. Swadener, J. K. Lee, Q. X. Jia, Y. Q. Wang, M. Nastasi, Phillip E. Thompson, N. David Theodore, T. L. Alford, J. W. Mayer, Peng Chen, and S. S. Lau, Appl. Phys. Lett. **88**, 021901 (2006).
[124] G. Hobler and G. Otto, Mater. Sci. Semicond. Process. **6**, 1 (2003).
[125] T. Zahel, G. Otto, and G. Hobler, Ref. [33], p. 179.
[126] S. Bédard and L. J. Lewis, Phys. Rev. B **61**, 9895 (2000).
[127] S. Libertino, S. Coffa, A. La Magna, and V. Privitera, Nucl. Instrum. Methods B **178**, 25 (2001).
[128] S. B. Zhang and W. B. Jackson, Phys. Rev. B **43**, 12142 (1991).
[129] A. W. R. Leitch, V. Alex, and J. Weber, Solid State Commun. **105**, 215 (1998).
[130] F. A. Reboredo, M. Ferconi, and S. T. Pantelides, Phys. Rev. Lett. **82**, 4870 (1999).
[131] V. P. Markevich and M. Suezawa, J. Appl. Phys. **83**, 2988 (1998).
[132] J. G. Swadener, M. I. Baskes, and M. Nastasi, Phys. Rev. B **72**, 201202 (2005).
[133] N. Martsinovich, I. Suarez Martinez, and M. Heggie, phys. stat. sol. (c) **2**, 1771 (2005).
[134] L. B. Freund, Appl. Phys. Lett. **70**, 3519 (1997).
[135] C. M. Varma, Appl. Phys. Lett. **71**, 3519 (1997).
[136] W. Han and J. Yu, J. Appl. Phys. **89**, 6551 (2001).
[137] F. Yang, J. Appl. Phys. **94**, 1454 (2003).
[138] Lin Shao, Y. Q. Wang, M. Nastasi, and J. W. Mayer, Nucl. Instrum. Methods B **249**, 230 (2006).

After a Ph.D. and a few years of research in elementary particle physics, the author joined in 1972 the Institut national de la recherche scientifique (INRS) – Énergie in Québec, Canada, an institute devoted to energy-related research and graduate teaching. He first focussed on basic studies of the processes involved in plasma–surface interactions, relevant to thermonuclear fusion research, and particularly on helium blistering of metals. In the 1980s and 1990s, he was group leader for plasma–wall interactions, materials, and nuclear studies within the Centre Canadien de Fusion Magnétique (CCFM) consortium operating the Tokamak de Varennes (TdeV). After the demise of the Canadian Fusion Program, he turned to plasma and ion beam processing of materials, and most recently to the study of ion blistering as applied to microelectronic and photonic device fabrication. He is now an Honorary retired Professor at INRS.

